Study of periodic and standing waves for the nonlinear Schrödinger equation

Perla Kfoury

THÈSE

En vue de l'obtention du
DOCTORAT DE L'UNIVERSITÉ DE TOULOUSE

Délivré par l'Université Toulouse 3 - Paul Sabatier

Présentée et soutenue par

Perla KFOURY

Le 2 juin 2023

Etude des ondes périodiques et stationnaires pour l'équation de Schrödinger non linéaire

Ecole doctorale : **EDMITT - Ecole Doctorale Mathématiques, Informatique et Télécommunications de Toulouse**

Spécialité : **Mathématiques et Applications**

Unité de recherche :
IMT : Institut de Mathématiques de Toulouse

Thèse dirigée par
Stefan LE COZ et Tai-Peng TSAI

Jury

M. Mathieu COLIN, Rapporteur
M. Nabile BOUSSAïD, Rapporteur
Mme Hajer BAHOURI, Examinatrice
M. Stefan LE COZ, Directeur de thèse
M. Tai-Peng TSAI, Co-directeur de thèse
M. Mihai MARIS, Président

À ma mère, dont l'amour et les sacrifices
ont rendu cette réussite possible.
À mon père, dont la mémoire m'inspirera
toujours à viser les étoiles.

Remerciements

J'exprime tout d'abord ma profonde gratitude à mon directeur de thèse Stefan Le Coz et mon co-directeur Tai-Peng Tsai, pour leur accompagnement tout au long de cette thèse.

Stefan, tu m'as encouragé et guidé avec patience, tout en faisant preuve de qualités humaines et scientifiques exceptionnelles. Ta présence bienveillante a été une source d'inspiration constante pour moi, et tes connaissances approfondies ont grandement contribué à l'enrichissement de mon travail. Ton soutien m'a permis de surmonter les difficultés et de repousser mes limites. Je te suis profondément reconnaissante d'avoir assumé la direction de mon doctorat ainsi que pour tout le savoir que tu m'as transmis et pour tout ce que j'ai appris grâce à toi.

Tai-Peng, your remarkable scientific expertise, valuable recommendations, and support have greatly contributed to the quality of my work. I want to offer my heartfelt thanks for the knowledge and insights that I gained during my time in Vancouver under your guidance. Moreover, I sincerely thank you for your commitment and dedication during this thesis.

J'exprime mes sincères remerciements à Mathieu Colin et Nabile Boussaïd pour avoir consacré leur temps à la lecture de mon manuscrit et à l'évaluation de mon travail. Je tiens également à remercier chaleureusement Hajer Bahouri et Mihai Maris d'avoir accepté de faire partie de mon jury.

Je remercie également le personnel administratif, les agents d'entretien ainsi que les chercheurs et enseignants-chercheurs de l'Institut de Mathématiques de Toulouse.

Pendant ces 4 années passées au laboratoire, la présence des doctorants a été une véritable source de joie et de plaisir. Je tiens à vous remercier du fond du cœur pour le temps que nous avons partagé ensemble. Votre compagnie a fait de ces années parmi les plus merveilleuses de ma vie. Je suis infiniment reconnaissante pour les rires partagés, les discussions enrichissantes, votre humour, votre intelligence, votre soutien et votre gentillesse. Merci sincèrement pour toutes les expériences, les voyages, les soirées et tous les autres moments précieux que nous avons partagés.

J'adresse mes plus affectueux remerciements à Paola d'avoir été une amie précieuse et véritable, je ne pourrai jamais te remercier assez, Corentin d'être celui sur qui je peux toujours compter, tu es le meilleur, Javi qui apporte une dose de joie et de folie à chaque instant, Alain le plus sympa et toujours souriant. Votre amitié m'a apporté tellement.

Merci à Alexandre (et sa passion pour les jeux), Anthony (et ses blagues), Maxime (qui surveille mon heure d'arrivée), Nicolas O, Etienne, Armand, Joachim, Nicolas E, Sophia (qui me met la pression pour m'habiller aussi bien

qu'elle), pour tous les bars à jeux, les pauses café (et tarot évidemment), les soirées et les rires partagés. Merci d'avoir rendu les journées de travail plus agréables et pleines de sourires.

Je salue également Alberto et Lucas D pour toutes les soirées, Alejandro, Benjamin H, Benjamin L, Candice, Chifaa, Clement G, Clement C, Denis, Diego, Fanny, Fu-Hsuan, Louis, Lucas C, Mingmin, Mitja, Virgile et Viviana.

Je remercie aussi les docteurs : Joe d'avoir été toujours là quand j'en avais besoin ; Michèle pour ton énergie et bonne humeur, je salue aussi Clement B, Louis, Mahmoud et Mehdi.

Mes amis ont également été d'un grand soutien. À mes meilleures amies Cynthia, Karen et Mirella, avec qui j'ai partagé ma vie, mes secrets, mes douleurs et mes moments de bonheur, merci pour tout. Merci à Najm mon ami d'enfance, le plus cher, merci à Joelle pour tous les moments partagés, à Mariane pour ta gentillesse et ton aide, et à Dalal mon premier repère en France.

Et c'est avec un amour infini que je tiens à remercier Alain (*Habibi* pour ceux qui le connaissent comme ça :p) pour avoir été mon roc et mon confident. Merci du fond du cœur pour ta présence, ta patience et ton amour inconditionnel. J'adresse également un sincère merci à Sousou (spéciale dédicace à la droite :p), Barhoum et Micha pour leur soutien précieux.

Pour conclure mes remerciements j'aimerais partager mes dernières pensées avec ma famille qui fut d'une immense aide. Merci à toutes mes tantes et oncles et en particulier Elias et sa femme Amale, je vous aime et je vous serais toujours reconnaissante. Merci également à Sylvie (et Micho bien sûr), Marie et Salwa, d'être toujours là pour moi.

Le plus grand merci à ma mère, source d'amour et de soutien, sans toi je ne serais pas là aujourd'hui, à ma soeur Petra et mon frère Naim, merci pour votre soutien en tout moment de ma vie, vous êtes pour moi une vraie source de force et de motivation. Je vous aime inconditionnellement.

À mon père qui restera à jamais dans mon cœur et ma mémoire, j'espère t'avoir rendu fier.

Contents

Chapter 1

Introduction

1.1 Nonlinear Schrödinger equation

We consider the one dimensional nonlinear Schrödinger equation

$$i\partial_t u + \partial_x^2 u + f(u) = 0, \quad u(0,x) = u_0(x), \tag{1.1.1}$$

where $u : \mathbb{R}_t \times \mathbb{R}_x \to \mathbb{C}$, the nonlinearity $f : \mathbb{C} \to \mathbb{C}$ is defined for any $z \in \mathbb{C}$ by $f(z) = g(|z|^2)z$ with $g \in C^0([0,+\infty),\mathbb{R}) \cap C^1((0,+\infty),\mathbb{R})$, $g(0) = 0$ and $\lim_{s\to 0} sg'(s) = 0$. Moreover, we assume that there exist $C > 0$ and $1 < p < \infty$, such that $|s^2 g'(s^2)| \leqslant Cs^{p-1}$ for $s \geqslant 1$. A typical example for f is the sum of power type nonlinearities given by

$$f(u) = \sum_{j=1}^{m} a_j |u|^{p_j - 1} u, \quad a_j \in \mathbb{R}, \quad 1 < p_1 < ... < p_m < \infty.$$

There are two types of solutions that we will investigate: standing waves with a non-periodic spatial profile and standing waves with a spatially periodic profile. In the first case we can represent the spatial domain as $\mathbb{K} = \mathbb{R}$ and in the second case as $\mathbb{K} = [0,T]$, where T is the period of the profile function.

Equation (1.1.1) arises in various physical and biological contexts, for example in nonlinear optics, for Bose-Einstein condensates, in the modeling of the DNA structure, etc. For more details on the physical background see [24, 68].

The nonlinear Schrödinger equation (NLS) is invariant under the following transformations:

— Translation: $u(t,x) \mapsto u(t,x+x_0)$, $\forall x_0 \in \mathbb{R}$.

— Phase shift: $u(t,x) \mapsto e^{i\alpha} u(t,x)$, $\forall \alpha \in \mathbb{R}$.

— Galilean invariance: $u(t,x) \mapsto e^{-i\left(\frac{\beta}{2}x + \frac{\beta^2}{4}t\right)} u(t, x+\beta t)$, $\forall \beta \in \mathbb{R}$.

Moreover the one power type equation (i.e. $m = 1$) is invariant under

— Scaling: $u(t,x) \mapsto \lambda^{\frac{2}{p-1}} u(\lambda^2 t, \lambda x)$, $\forall \lambda > 0$.

In the case of one power nonlinearity the equation (1.1.1) is called focusing if $a_1 > 0$ and defocusing if $a_1 < 0$. In the case of double power nonlinearity when $a_1 < 0$, $a_2 > 0$, we say that the nonlinearity is defocusing-focusing, with analogous definitions for other possible signs combinations and powers.

1.1.1 The local Cauchy problem

For standing waves and periodic waves, we have the following result concerning the local well-posedness of the Cauchy problem for (1.1.1) (see, e.g. [24] and the references therein).

Proposition 1.1.1. For any initial condition $u_0 \in H^1(\mathbb{K})$, there exists $T_{\max} > 0$ such that the Cauchy problem of (1.1.1) admits a unique maximal solution $u \in C([0, T_{\max}), H^1(\mathbb{K}) \cap C([0, T_{\max}), H^{-1}(\mathbb{K}))$. Moreover we have the blow-up alternative: either $T_{\max} = +\infty$ or $\lim_{t \to T_{\max}} \|u(t)\|_{H^1} = +\infty$.

Note that the local well-posedness of the Cauchy Problem is independent of the nature (focusing or defocusing) of the nonlinearity .

For the physical properties of the model as well as for the mathematical study of the equation, it is interesting to look for quantities conserved along the time. Solutions u to (1.1.1) conserve the mass M, the momentum P and the energy $\mathcal{E}$:

$$M(u) = \frac{1}{2}\int_{\mathbb{K}} |u|^2 dx, \quad P(u) = \frac{1}{2}\mathcal{I}m \int_{\mathbb{K}} u\overline{u}_x dx,$$

$$\mathcal{E}(u) = \frac{1}{2}\int_{\mathbb{K}} |u_x|^2 dx - \int_{\mathbb{K}} F(u) dx, \quad \text{where } F(u) = \int_0^{|u|} f(s) ds.$$

Formally, the conservation of the mass is obtained from multiplying (1.1.1) with $\overline{u}$, integrating over $\mathbb{K}$ and taking the imaginary part. The second conserved quantity is the momentum obtained by multiplying (1.1.1) by $\partial_x \overline{u}$, integrating over $\mathbb{K}$ and taking the real part. Finally multiplying (1.1.1) by $\partial_t \overline{u}$, integrating over $\mathbb{K}$ and taking the real part we obtain the conservation of the energy.

1.1.2 The model case of the pure power nonlinearity

This section is focused on the investigation of the nonlinear Schrödinger equation with a single power nonlinearity. Within this context, we will present important results such as the global existence of solutions, the occurrence of blow-up, and the possibility of scattering. To simplify the notation, we will use $p = p_1$.

1.1.2.1 Global well-posedness

For the defocusing case, using the conservation of the mass and the energy we may prove that the H^1-norm of u is uniformly bounded in time. This implies that the solution exists globally in time. In the focusing case, the situation is more complex. The proof relies on the Gagliardo-Nirenberg's

inequality (see [2]). If $1 < p < 5$ or $p = 5$ and $\|u_0\|_{L^2}$ small enough then the solution is global. We only expect the existence of blow up solutions for $p \geqslant 5$. Thus in the focusing case, the case $p = 5$ is a threshold between global existence and blow up. This result is applicable to both standing waves and periodic solutions.

1.1.2.2 Blow-up of solution for the focusing case

Concerning the blow-up, we have the following result in the focusing case.

Proposition 1.1.2. Assume that $p \geqslant 5$ and let $u_0 \in H^1(\mathbb{R})$ be such that

$$|x|u_0 \in L^2(\mathbb{R}), \quad \mathcal{E}(u_0) < 0.$$

Then the solution u of (1.1.1) corresponding to u_0 blows up in finite time.

The proof of Proposition 1.1.2 relies on the Virial Theorem.

Proposition 1.1.3. (Virial Theorem) Let $u_0 \in H^1(\mathbb{R})$ be such that $|x|u_0 \in L^2(\mathbb{R})$ and let u be the solution of (1.1.1) corresponding to u_0. Then $|x|u(t) \in L^2(\mathbb{R})$ for all $t \in [0, T)$ and the function $t \to \|xu(t)\|^2_{L^2(\mathbb{R})}$ is of class C^2 and we have the following identities:

$$\frac{d}{dt}\int_{\mathbb{R}} |x|^2|u(t,x)|^2dx = 4\mathcal{I}m\int_{\mathbb{R}} \overline{u}(t)x.\nabla u(t)dx,$$

$$\frac{1}{2}\frac{d}{dt}\mathcal{I}m\int_{\mathbb{R}} \overline{u}(t)x.\nabla u(t)dx = \int_{\mathbb{R}} |\nabla u|^2dx - a_1\left(\frac{1}{2} - \frac{1}{p+1}\right)\int_{\mathbb{R}} |u|^{p+1}dx.$$

The Virial Theorem comes from the work of Glassey [42] in which the identities above were formally derived.

1.1.2.3 Scattering of solution for the defocusing case

In this section we present the cases where the scattering occurs. Let Σ be the weighted space defined by

$$\Sigma = \{u \in H^1(\mathbb{R}) : |.|u(.) \in L^2(\mathbb{R})\}.$$

(1.1.1) has the following equivalent integral equation

$$u(t) = S(t)u_0 + ia_p\int_0^t S(t-s)|u|^{p-1}u(s)ds,$$

where $S(t)$ is the Schrödinger group. We have the following result.

Proposition 1.1.4. Let $u_0 \in \Sigma$ and $u \in C([0, +\infty), \Sigma)$ the global solution of (1.1.1) for the defocusing case. Therefore there exists $u_{+\infty} \in \Sigma$ such that

$$\lim_{t \to +\infty} \|u(t) - S(t)u_{+\infty}\|_{H^1} = 0.$$

1.2 Standing waves

According to the theory of nonlinear Schrödinger equations, solutions can display either dispersion, caused by the linear aspect of the equation, or concentration at specific points due to nonlinear effects. However, in exceptional cases, these behaviors balance each other out, resulting in special solutions known as standing waves that do not disperse or focus. Standing waves belong to a broader category of solutions that arise in various nonlinear equations, such as the Korteweg-de Vries or Klein-Gordon equations. Solitary waves or solitons are another type of special solution that can be found in these equations, where their profile remains unchanged over time. (see [24, 30, 33, 68]).

A standing wave of (1.1.1) is a solution of the form $e^{i\omega t}\phi(x)$, in which the frequency $\omega \in \mathbb{R}$ and the profile $\phi \in H^1(\mathbb{R})$ satisfies

$$-\phi'' + \omega\phi - f(\phi) = 0. \tag{1.2.1}$$

Notice that $\phi = 0$ is always a trivial solution of (1.2.1), we are interested in nontrivial solutions, that is $\phi \neq 0$.

1.2.1 Existence of standing waves

We consider the following problem

$$u'' = g(u) = \omega u - f(u), \quad \omega > 0, \quad \lim_{u\to 0} \frac{f(u)}{u} = 0.$$

The following is a general result.

Proposition 1.2.1. Let $g \in C(\mathbb{R};\mathbb{R})$ be a locally Lipschitz continuous function with $g(0) = 0$ and let $G(t) = \int_0^T g(s)ds$. A necessary and sufficient condition for the existence of a solution ϕ of the problem

$$\phi \in C^2(\mathbb{R}), \quad \lim_{t\to\pm\infty} \phi(t) = 0, \quad \phi(0) > 0,$$

$$\phi'' = g(\phi),$$

is that

$$\phi_0 = \inf\{t > 0 : G(t) = 0\} \text{ exists}, \quad \phi(0) > 0, \quad g(\phi_0) < 0.$$

More precisely we have the following results for the single and double power case.

1.2.1.1 Existence for the single power case

For the single power nonlinearity case, no standing waves exist for (1.1.1) in the defocusing case. In the focusing case, standing waves only exist for $\omega > 0$. The statement that there are no standing wave solutions of (1.1.1) for $\omega \leqslant 0$ can be derived from the identity of Pohozhaev in [65], which is given by:

$$\|\nabla\phi\|^2_{L^2(\mathbb{R})} - a_1\frac{(p-1)}{2(p+1)}\|\phi\|^{p+1}_{L^{p+1}(\mathbb{R})} = 0.$$

Therefore we only consider the focusing case where we assume that $\omega > 0$. In this case we know the explicit formula for the standing wave solution of

$$-\phi'' + \omega\phi - \phi^p = 0,$$

it is given by

$$\phi(x) = \left(\frac{(p+1)\omega}{2}\operatorname{sech}^2\left(\frac{(p-1)\sqrt{\omega)}}{2}x\right)\right)^{\frac{1}{p-1}}.$$

1.2.1.2 Existence for the double power case

We define ω^* by

$$\omega^* = \sup\{\omega \geqslant 0 : \exists s > 0, \text{ such that } \frac{\omega}{2}s^2 - F(s) < 0\}.$$

It is well known (see [17]) that existence and uniqueness of non-trivial solutions of (1.2.1) with $\lim_{|x|\to\infty}\phi(x) = 0$ hold if and only if

$$\begin{cases} 0 \leqslant \omega < \omega^* & \text{when } a_1 < 0, a_2 > 0, \\ 0 < \omega < \omega^* & \text{otherwise .} \end{cases}$$

The case $\omega = 0$ corresponds to zero mass case in elliptic equations, and associated problems are more delicate in many cases compared with the case $\omega > 0$.

For the case $p_2 = 2p_1 - 1$, we know the explicit formula of the standing wave solution of

$$-\phi'' + \omega\phi - a_1\phi^{p_1} - a_2\phi^{p_2} = 0,$$

it is given by

$$\phi(x) = \left(\frac{\omega}{A + \sqrt{A^2 + B\omega}\cosh(\beta^{-1}\sqrt{\omega}x)}\right)^{\beta},$$

where

$$A = \frac{a_1}{2 + \frac{1}{\beta}}, \quad B = \frac{a_2}{2 + \frac{1}{\beta}}.$$

1.2.2 Orbital stability

To analyze the dynamics of (1.1.1), it is essential to have a comprehensive understanding of the dynamical properties of standing waves, particularly their stability. Several stability concepts are available for standing waves. The one most commonly used is *orbital stability*, which is defined as follows. The standing wave $e^{i\omega t}\phi(x)$ solution of (1.1.1) is said to be *orbitally stable* if the following holds. For any $\varepsilon > 0$ there exists $\delta > 0$ such that if $u_0 \in H^1(\mathbb{R})$ verifies

$$\|u_0 - \phi\|_{H^1} < \delta,$$

then the associated solution u of (1.1.1) exists globally and verifies

$$\sup_{t\in\mathbb{R}} \inf_{y\in\mathbb{R},\theta\in\mathbb{R}} \left\|u(t) - e^{i\theta}\phi(\cdot - y)\right\|_{H^1} < \varepsilon.$$

The groundwork for studying the orbital stability of standing wave solutions were established by Berestycki and Cazenave [15], Cazenave and Lions [25], and Weinstein [72, 71]. There are two approaches to obtaining stability or instability results: the variational approach of [15, 25] and the spectral approach of [72, 71]. Grillakis, Shatah and Strauss [43, 44] later developed an abstract theory that, under certain assumptions, reduces the stability analysis of a branch of standing waves $\omega \to \phi_\omega$ to the study of the sign of the quantity (usually called *slope*) $\frac{\partial}{\partial\omega}M(\phi_\omega)$.

Using the above techniques, the orbital stability of positive standing waves has been fully characterized for the single power case in any dimension $N \geqslant 1$ in [15, 25, 72, 71]. In dimension $N = 1$, we have the following results.

Theorem 1.2.2. Let ϕ be a ground state of (1.2.1). If $1 < p < 5$ then the standing wave $e^{i\omega t}\phi(x)$ is orbitally stable.

We give a precise definition of instability by blow-up. Suppose that ϕ is a solution of (1.2.1). We say that the standing wave $e^{i\omega t}\phi(x)$ is unstable by blow-up in finite time if for any given $\epsilon > 0$, there exists $u_{\epsilon,0} \in H^1(\mathbb{R})$ such that

$$\|u_{\epsilon,0} - \phi\|_{H^1(\mathbb{R})} < \epsilon,$$

but the corresponding maximal solution u_ϵ of (1.1.1) in the interval $[0, T_\epsilon)$ satisfies $T_\epsilon < +\infty$, which means that

$$\lim_{t\to T_\epsilon} \|u_\epsilon(t)\|_{H^1(\mathbb{R})} = +\infty.$$

We then have the following theorem.

Theorem 1.2.3. If $5 \leqslant p < \infty$ then the standing wave $e^{i\omega t}\phi(x)$ is unstable by blow-up in finite time.

Note that the scaling properties in the single power case play an important role in the proof of stability and instability results. These properties ensure in particular that stability and instability are independent of the value of the frequency parameter ω.

The absence of scaling invariance for double power nonlinearities makes the study of stability more challenging. Consequently, in higher dimensions, only limited results are currently available. However, in dimension 1, the ODE structure of the profile equation (1.2.1) can be exploited, which leads to some favorable outcomes in the analysis. In this regard, Iliev and Kirchev [49] conducted preliminary investigations for the stability of standing waves in dimension 1 for a generic nonlinearity, deriving a formula for the slope condition. Ohta [61] was the first to devote work to the stability of standing waves for the double power nonlinearity in dimension 1, using the integral expression for the slope condition from [49] to establish the stability/instability of standing waves in various cases. Maeda [59] later refined Ohta's approach, extending the stability/instability results to most of the situations not covered in [61]. Fukaya and Hayashi [36] improved Ohta's results on instability for small ω with a condition on the powers, but the stability picture is still not complete. We also mention the work of Colin and Ohta [27], on the stability of solitary waves for derivative nonlinear Schrödinger equation which is related to the double power nonlinearity.

Although stability and instability studies have been widely conducted, to the best of our knowledge, the contributions of Liu, Tsai, and Zwiers [58] and Tin [69] are the only known research works that specifically focuses on the stability and instability of the triple power nonlinearity.

1.3 Periodic waves

In this section we are interested in the standing waves $e^{-iat}\phi(x)$ where the profile function $\phi(x)$ is spatially periodic and satisfies the ordinary differential equation (1.2.1) with $a = -\omega$.

We define the spatially periodic setting

$$P_T = \{f \in L^2_{loc}(\mathbb{R}) : f(x+T) = f(x), \forall x \in \mathbb{R}\},$$

and the spatially anti-periodic setting

$$A_T = \{f \in L^2_{loc}(\mathbb{R}) : f(x+T) = -f(x), \forall x \in \mathbb{R}\}.$$

As previously mentioned, the Cauchy problem for (1.1.1) is locally well-posed in $H^1_{loc} \cap P_T$. Moreover in the cubic case the Cauchy problem is globally well posed in $H^1_{loc} \cap P_T$.

In this section, we will focus on presenting the results obtained from investigating the properties of periodic waves for the one dimensional nonlinear Schrödinger equation with cubic nonlinearity $f(u) = b|u|^2u$.

For this type of equation, non-constant, real-valued, periodic solutions of (1.2.1) are well known to be given by the Jacobi elliptic functions: dnoidal (dn), cnoidal (cn) (for $b > 0$), and snoidal (sn)(for $b < 0$). The Jacobi elliptic functions are standard forms of elliptic functions. The three basic functions are denoted $cn(x, k)$, $dn(x, k)$, and $sn(x, k)$, where $k \in (0, 1)$ is known as the elliptic modulus. The incomplete elliptic integral of the first kind is defined by

$$x = \mathbf{F}(\tau, k) := \int_0^\tau \frac{d\theta}{\sqrt{1 - k^2 \sin^2(\theta)}},$$

where τ is called the Jacobi amplitude, and the Jacobi elliptic functions are defined through the inverse of $F(., k)$:

$$sn(x, k) := \sin(\tau), \quad cn(x, k) := \cos(\tau), \quad dn(x, k) := \sqrt{1 - k^2 \sin^2(\tau)}.$$

The period of the elliptic functions can be expressed in terms of the complete elliptic integral of the first kind

$$\mathbf{K}(k) := F\left(\frac{\pi}{2}, k\right), \quad \mathbf{K}(k) \to \begin{cases} \frac{\pi}{2}, & k \to 0 \\ \infty, & k \to 1. \end{cases}$$

This will be further developed in the subsequent sections.

1.3.1 Variational characterization

A global variational characterization for each of the periodic waves described by Jacobi elliptic functions, constant solutions, and plane wave solutions has been provided by Gustafson, Le Coz and Tsai [46]. This approach offers alternative proofs of their stability. Specifically, the following results have been obtained.

Theorem 1.3.1. Let $b > 0$.

- For all $0 < m \leqslant \frac{\pi^2}{bT}$, the unique (up to translation and phase multiplication) minimizer of the energy, under the constraint of fixed mass alone (without momentum) or fixed mass with fixed momentum equal to 0, among periodic functions is the constant function $u_{\min} = \sqrt{\frac{2m}{T}}$.
- For all $\frac{\pi^2}{bT} < m < \infty$, the unique (up to translation and phase multiplication) minimizer of the energy, at fixed mass alone (without momentum) or fixed mass with fixed momentum equal to 0, among periodic functions is a (appropriately rescaled) dnoidal function.

— The unique (up to translation and phase multiplication) global minimizer of the energy, with fixed mass (without momentum) or fixed mass with fixed momentum equal to 0, among half-anti-periodic functions is a (appropriately rescaled) cnoidal function.

Theorem 1.3.2. Let $b < 0$.

— The unique (up to translation and phase multiplication) minimizer of the energy, with fixed mass, (and fixed momentum equal to 0) among periodic functions is the constant function $u_{\min} = \sqrt{\frac{2m}{T}}$.

— The unique (up to translation and phase multiplication) minimizer of the energy, with fixed mass, among half-anti-periodic functions is the plane wave $u_{\min} = \sqrt{\frac{2m}{T}} e^{\frac{i\pi x}{T}}$.

— The unique (up to phase shift) minimizer of the energy, with fixed mass, among odd half-anti-periodic functions is a (appropriately rescaled) snoidal function.

Moreover we have the following conjecture.

Conjecture 1.3.3. Assume $b < 0$. The unique (up to translation and phase multiplication) minimizer of the energy at fixed mass and fixed momentum equal to 0, among half-anti-periodic functions is a (appropriately rescaled) snoidal function.

1.3.2 Orbital stability

By Grillakis, Shatah and Strauss [43, 44] type methods, orbital stability against energy H^1_{loc}-norm perturbations for the same period is known for dnoidal waves [7], and for snoidal waves [38] under the additional constraint that perturbations are anti-symmetric with respect to the half-period.

In the work of Gallay and Haragus [38], they proved that periodic and quasi-periodic solutions are orbitally stable with respect to disturbances having the same period. They also showed that the cnoidal wave solution are stable with respect to perturbations of twice their period. We also mention the work of Antonelli and Shakarov [11], who proved the stability of cnoidal waves for the damped nonlinear Schrödinger equation.

The following results were obtained in the work of Gustafson, Le Coz and Tsai [46].

Theorem 1.3.4. The standing wave $e^{-iat}\phi(x)$ is a solution of (1.1.1), and is orbitally stable in X in the following cases. For Jacobi elliptic functions, for any $k \in (0, 1)$:

$$a = 1 + k^2, \quad b = -2k^2, \quad \phi = sn(., k), \quad X = H^1_{loc} \cap A^-_{2K};$$

$$a = 1 - 2k^2, \quad b = 2k^2, \quad \phi = cn(.,k), \quad X = H^1_{loc} \cap A_{2K};$$
$$a = -(2 - k^2), \quad b = 2, \quad \phi = dn(.,k), \quad X = H^1_{loc} \cap P_{2K}.$$

For constants and plane wave: $(b \neq 0)$

$$a = -\frac{2bm}{T}, \quad -\infty < b \leqslant \frac{\pi^2}{Tm}, \quad u = \sqrt{\frac{2m}{T}}, \quad X = H^1_{loc} \cap P_T;$$

$$a = \frac{4\pi^2}{T^2} - \frac{2bm}{T}, \quad b < 0, \quad u = e^{\pm\frac{i\pi x}{T}}\sqrt{\frac{2m}{T}}, \quad X = H^1_{loc} \cap A_{T/2}.$$

The proof follows the standard approach introduced by Cazenave and Lions [25].

Remark 1.3.5. In [38], the orbital stability of *cn* with respect to half-anti-periodic perturbations was obtained only for small amplitude *cn* and the orbital stability for *sn* in $H^1_{loc} \cap A_{T/2}$ was proved using the Grillakis-Shatah-Strauss approach.

Remark 1.3.6. Using the complete integrability of (1.1.1), Bottman and Deconinck and Nivala [21] and Gallay and Pelinovsky [40] thus showed that *sn* is in fact a minimizer of a higher-order functional in $H^2_{loc} \cap P_{nT}$ for any $n \in \mathbb{N}$ and thus showed it is orbitally stable in these spaces.

1.3.3 Spectral stability

Spectral stability with respect to long-wave disturbances has been examined first by Rowlands [66], who found that periodic waves with real-valued profile are unstable in the focusing case. More recently we mention the work of Gallay and Haragus [39], Gallay and Pelinovsky [40] and Ivey and Lafortune [50]. We also mention the work of Boussaïd and Comech [22] on the spectral stability of solitary waves. To examine the spectral stability of a standing wave $u(t,x) = e^{-iat}\phi(x)$ solution of (1.1.1), we consider the linearization of (1.1.1) around this solution: if $u(t,x) = e^{-iat}(\phi(x) + h)$, then h verifies

$$i\partial_t h - Lh + N(h) = 0,$$

where L denotes the linear part and N the nonlinear part. Assuming u is real-valued, we separate h into real and imaginary parts to get the equation

$$\begin{pmatrix} h_R \\ h_I \end{pmatrix}_t = JL \begin{pmatrix} h_R \\ h_I \end{pmatrix} + N(h),$$

where

$$L = \begin{pmatrix} L_+ & 0 \\ 0 & L_- \end{pmatrix}, \quad J = \begin{pmatrix} 0 & 1 \\ -1 & 0 \end{pmatrix},$$

$$L_+ = -\partial_{xx} - a - 3b\phi^2, \quad L_- = -\partial_{xx} - a - b\phi^2.$$

We call

$$JL = \begin{pmatrix} 0 & L_- \\ L_+ & 0 \end{pmatrix}$$

the linearized operator of (1.1.1) around the standing wave $e^{-iat}\phi(x)$. The spectral stability is concluded by examining whether the entire spectrum of JL is located on the imaginary axis. If this is the case, we consider the wave to be spectrally stable. We have the following results concerning the spectral stability (for more details see [46]).

Theorem 1.3.7. Spectral stability in P_T, $T = 4K(k)$, holds for:
- $\phi = sn, k \in (0,1)$,
- $\phi = cn$ and $k \in (0, k_c)$, where k_c is the unique $k \in (0,1)$ so that $K(k) = 2E(k)$, $k_c \approx 0.908$.

Moreover we have the following theorems.

Theorem 1.3.8. For $k \in (0,1)$, $K = K(k)$, dn is spectrally stable in P_{2K}, while cn and sn are spectrally stable in A_{2K}.

Theorem 1.3.9. Cnoidal waves are unstable against perturbations whose period is a sufficiently large multiple of its own, i.e the spectrum of JL^{cn} as an operator on P_{4nK} contains an eigenvalue with positive real part.

Remark 1.3.10. The orbital stability implies the spectral stability.

1.4 Main results

1.4.1 Double power nonlinearity

The results presented in this section have been published in "Comptes rendus mathématique" in collaboration with Stefan Le Coz and Tai-Peng Tsai [52].

As already mentioned the stability picture in the double power case was still not complete. Let $p_1 = p$, $p_2 = q$, $a_1 = a_p$ and $a_2 = a_q$. The following case was left partially open:

$$a_p < 0, \quad a_q > 0, \quad 1 < p < q < 5, \quad p + q \leqslant 6 \text{ or } p \leqslant \frac{7}{3}.$$

The above is the defocusing-focusing case where the stability of standing waves for large ω and their instability for small ω were established by Ohta [61]. The condition $p+q > 6$ was shown to be sufficient for instability by Ohta [61] and later improved by Fukaya and Hayashi [36] to $(p+3)(q+3) > 32$. However, the stability behavior in the intermediate range of ω where $(p+3)(q+3) > 32$ and

$p+q \leqslant 6$ or $p \leqslant \frac{7}{3}$, as well as the stability for small ω when $(p+3)(q+3) \leqslant 32$, were not fully understood in [36, 59, 61]. The only exception is the case of $p = 2$ and $q = 3$ where explicit calculations were possible, revealing the stability of the wave for any $\omega > 0$.

For the sake of simplicity, we will use the following convention. A standing wave is called type S if it is stable for any $\omega \in (0, \omega^*)$. If there exists $\omega_1 \in (0, \omega^*)$ such that the standing wave is unstable for $\omega \in (0, \omega_1)$ and stable for $\omega \in (\omega_1, \omega^*)$, we say it is type US. We define other types in a similar way. Note that the endpoint ω_1 may also fall within the range of instability, subject to regularity assumptions on the nonlinearity. This is possible due to the criterion established by Comech and Pelinovsky [29].

We aim to address the incomplete aspects of the earlier studies [36, 59, 61] and provide a complete stability picture for the standing waves of the Schrödinger equation with double power nonlinearity using the slope criterion of Grillakis, Shatah and Strauss.

Our main result is the following.

Theorem 1.4.1. Let $(\phi_\omega)_{\omega \in (0,\omega^*)}$ be the family of standing waves of (1.1.1). The following gives the stability type of the family of standing waves.

1. Assume that $a_p > 0$ and $a_q > 0$.
   (a) If $q \leqslant 5$, then it is of type S.
   (b) If $p \geqslant 5$, then it is of type U.
   (c) If $p < 5 < q$, then it is of type SU.
2. Assume that $a_p > 0$ and $a_q < 0$.
   (a) If $p \leqslant 5$, then it is of type S.
   (b) If $p > 5$, then it is of type US.
3. Assume that $a_p < 0$ and $a_q > 0$.
   (a) If $q \leqslant 7 - 2p$, then it is of type S.
   (b) If $7 - 2p < q < 5$, then it is of type US.
   (c) If $q \geqslant 5$, then it is of type U.

This theorem implies in particular that stability change occurs at most once, which is conjectured in [59, p. 265], and is in contrast to NLS with triple power nonlinearity considered in [58].

The cases (1), (2), and (3)(c) of Theorem 1.4.1 were previously addressed in [59, 61]. However, for the sake of completeness, we also include their proofs in our work. Cases (3)(a) and (b), they were only partially solved in previous works. We provide a definitive result for these cases.

Note that our results do not extend to the case of zero frequency, $\omega = 0$. However, it is conjectured that the stability or instability of the corresponding

algebraic standing waves, if they exist, should be the same as for small $\omega > 0$, which is consistent with the results of Fukaya and Hayashi [36].

Moreover, it should be noted that our statement does not include the critical frequency at which the stability change occurs. This frequency was shown by Comech and Pelinovsky to lead to instability under higher regularity assumptions on the nonlinearity. Alternative proofs with improved regularity assumptions are given in [60, 62], but they are still not sufficient to cover the entire range of double-power nonlinearities. Strategies have been developed to handle the critical frequency without relying on regularity assumptions for other types of equations, as seen in [45, 73]. However, in our work, we only verify the validity of the stability criterion and do not attempt to cover the critical frequency.

Finally, for the defocusing-focusing case where $a_p < 0$, $a_q > 0$, and $1 < p < q < 5$, we supplement our theoretical findings with numerical experiments. Initially, we first represent the critical surface, denoted by $\omega_c(p, q)$, at which the stability transition occurs and examine the various shapes of the surface based on the $\frac{a_p}{a_q}$ ratio. We then simulate the dynamics of (1.1.1) around a standing wave with the Crank-Nicolson scheme with relaxation of Besse [19]. We observe three distinct types of behaviors based on the initial data: stability, growth followed by oscillations, and scattering. This problem will be clearly detailed in Chapter 2.

1.4.2 Quasi-periodic case

In chapter 3 we focus on the one-dimensional cubic nonlinear Schrödinger equation, given by

$$i\psi_t + \psi_{xx} + b|\psi|^2\psi = 0,$$

where ψ is a complex-valued function defined on $\mathbb{R}_t \times \mathbb{R}_x$, and b is a nonzero real constant. We investigate the simplest non-trivial solutions of the equation, which are the standing waves of the form

$$\psi(t, x) = e^{-iat}u(x), \quad a \in \mathbb{R},$$

where the profile function u satisfies the ordinary differential equation

$$u_{xx} + au + b|u|^2u = 0. \tag{1.4.1}$$

We are particularly interested here in those standing waves whose profile u is quasi-periodic and defined on the space

$$H^\theta_T = \{f \in H^1_{\text{loc}}(\mathbb{R}) : f(x + T) = e^{i\theta}f(x), \quad \forall x \in \mathbb{R}\},$$

where θ is real and so-called Floquet multiplier.

In addition to the conserved quantities of the NLS, namely mass M, momentum P and energy $\mathcal{E}$, we also consider the conserved quantities of the ordinary differential equation, namely momentum J and energy E, given by

$$J = \mathrm{Im}(u_x\overline{u}), \quad E = \frac{1}{2}|u_x|^2 + \frac{a}{2}|u|^2 + \frac{b}{4}|u|^4.$$

The object of our interest is the minimization problem given by

$$\min\{\mathcal{E}(u) : u \in H_T^\theta, M(u) = m, P(u) = p\}, \tag{1.4.2}$$

where $m > 0$ and $p \in \mathbb{R}$.

The aim of this chapter is to establish a connection between the solutions of the minimization problem (1.4.2) and the solutions of the ordinary differential equation (1.4.1).

Starting from the ordinary differential equation, our objective is to establish a connection with the minimization problem. Specifically, we seek to find a correspondence between the solutions of the ordinary differential equation and the minimizers of the energy functional subject to fixed values of mass and momentum. Thus, we establish a diffeomorphic correspondence between them. We also study these conserved quantities and provide monotonicity results for some of them.

Next, we proceed in the opposite direction by starting from the minimization problem and establishing a link with the solutions of the ordinary differential equation. Our main result is the following.

Observation 1.4.2. For each defocusing and focusing case, for fixed (J, E), let u_{ode} be the associated solution of the ordinary differential equation. Then (up to phase shift and translation) the minimizer of the problem

$$\min\{\mathcal{E}(u) : u \in H_T^\theta,\ M(u) = M(u_{ode}), P(u) = P(u_{ode}), u \in H_T^\theta\},$$

is given by u_{ode}.

Our results were obtained through numerical computations. We first computed the ordinary differential equation (1.4.1) numerically and compared the resulting solution to the exact solution when available. We then utilized the gradient flow with discrete normalization method to find the minimizer of the energy $\mathcal{E}$ subject to fixed mass $m > 0$ and fixed momentum p. This method, also known as the "imaginary time method" in physics literature, has been applied to various equations, including nonlinear Schrödinger equations. We compared the minimizer obtained from the normalized gradient flow with the numerical solution of the ODE and made our conjecture based on the results.

1.4.3 General nonlinearity

In this section we present our work on the nonlinear Schrödinger equation with general nonlinearity:

$$i\psi_t + \psi_{xx} + bf(\psi) = 0, \tag{1.4.3}$$

where $\psi : \mathbb{R}_t \times \mathbb{R}_x \to \mathbb{C}$, the nonlinearity $f : \mathbb{C} \to \mathbb{C}$ is defined for any $z \in \mathbb{C}$ by $f(z) = g(|z|^2)z$ with $g \in C^0([0, +\infty), \mathbb{R}) \cap C^2((0, +\infty), \mathbb{R})$ and $b \in \mathbb{R} \setminus \{0\}$. Similarly to the other case, the simplest non-trivial solutions of (1.4.3) are the standing waves given by

$$\psi(t, x) = e^{-iat}u(x), \quad a \in \mathbb{R}.$$

The profile function u satisfies the ordinary differential equation

$$u_{xx} + au + bf(u) = 0. \tag{1.4.4}$$

We are particularly interested in the spatially periodic solutions $\psi(t, .) \in H^1_{loc} \cap P_T$, and anti-periodic solutions $\psi(t, .) \in H^1_{loc} \cap A_T$.

Our goal is to extend previous work on the cubic case to the case of a general nonlinearity. Specifically, we will consider the real and complex-valued solutions of the profile equation and represent their phase portraits for various parameter regimes. We will study the minimization problems for the energy functional with fixed mass and momentum constraints for the periodic and anti-periodic cases, extending the previous results to this more general setting. Consequently, we investigate the properties of minimizers in each case, including their existence and uniqueness. We have the following results for the periodic case.

Proposition 1.4.3. In the focusing case, for all $m > 0$, there exists a unique (up to phase shift) minimizer of the energy, under the constraint of fixed mass alone (without momentum) or fixed mass with fixed momentum equal to 0, among periodic functions. Moreover, the minimal energy is finite and negative. Furthermore, there exists $\tilde{m} > 0$ such that if $m > \tilde{m}$, then the minimizer is not a constant, the associated Lagrange multiplier $a < 0$, the minimizer is positive, and it is a solution of the ordinary differential equation (1.4.4).

Proposition 1.4.4. In the defocusing case, for all $m \in (0, \infty)$ the minimizer of the energy, under the constraint of fixed mass alone (without momentum) or fixed mass with fixed momentum equal to 0, among periodic functions is the same and unique (up to phase shift). It is the constant function $u_\infty \equiv \sqrt{\frac{2m}{T}}$.

For the anti-periodic case, we limit ourselves to the nonlinearity of the type $f(u) = |u|^{p-1}u + |u|^{q-1}u$, with $p, q > 1$. We prove that in this case there exists a unique (up to phase shift and complex conjugate) minimizer of the energy, under the constraint of fixed mass among anti-periodic functions. It is the plane wave $u_\infty \equiv \sqrt{\frac{2m}{T}} e^{\frac{i\pi x}{T}}$.

Finally, we investigate the minimization problem on the Nehari manifold. We restrict ourselves to the nonlinearity of the form $f(u) = |u|^{p-1}u$, with $p > 1$. We define a functional $S : H^1(\mathbb{R}) \to \mathbb{R}$ by setting for $v \in H^1(\mathbb{R})$

$$S(v) := \frac{1}{2}\|\nabla v\|^2_{L^2(\mathbb{R})} + \frac{\omega}{2}\|v\|^2_{L^2(\mathbb{R})} - \frac{a_1}{p+1}\|v\|^{p+1}_{L^{p+1}(\mathbb{R})}.$$

The functional S is often called action. We are interested in the following minimization problems on the Nehari manifold:

$$\min\{S(u) : u \in H^1_{loc} \cap P_T, u \neq 0, I(u) = 0\}, \tag{1.4.5}$$

and

$$\min\{S(u) : u \in H^1_{loc} \cap A_{\frac{T}{2}}, u \neq 0, I(u) = 0\}, \tag{1.4.6}$$

where I is defined by

$$I(u) = \|\partial_x u\|^2_{L^2} - a\|u\|^2_{L^2} - b\|u\|^{p+1}_{L^{p+1}}.$$

We also consider the following minimization problem

$$\min\left\{\left(\frac{1}{2} - \frac{1}{p+1}\right)\|v\|^2_{H^1} : v \neq 0, I(v) \leqslant 0, v \in H^1_{loc} \cap A_{\frac{T}{2}}\right\}. \tag{1.4.7}$$

We prove that in the periodic case, with $b > 0$ and $a < 0$, the minimum of (1.4.5) is finite and there exists a unique minimizer which is solution of (1.4.4). In the anti-periodic case, with $b > 0$ and $a < \frac{4\pi^2}{T^2}$, the minimization problems (1.4.6) and (1.4.7) share the same minimizer. Moreover when p is an odd integer the minimizer is real and it is the solution of the ordinary differential equation (1.4.4).

1.5 Outline of the thesis

The thesis is organized as follows. In Chapter 2, we focus on the double power nonlinear Schrödinger equation, where we provide a complete stability analysis of the standing waves. In Chapter 3, we investigate the one-dimensional cubic nonlinear Schrödinger equation and establish a variational characterization of the minimizer of the energy with fixed mass and momentum. We also establish a connection between these minimizers and the solutions of the ordinary differential equation. Chapter 4 extends the work on the cubic case to the more general case of a nonlinearity, where we consider various minimization problems.

Chapter 2

Analysis of stability and instability for standing waves of the double power one dimensional nonlinear Schrödinger equation

Abstract

For the double power one dimensional nonlinear Schrödinger equation, we establish a complete classification of the stability or instability of standing waves with positive frequencies. In particular, we fill out the gaps left open by previous studies. Stability or instability follows from the analysis of the slope criterion of Grillakis, Shatah and Strauss. The main new ingredients in our approach are a reformulation of the slope and the explicit calculation of the slope value in the zero-frequency case. Our theoretical results are complemented with numerical experiments.

2.1 Introduction

Consider the one dimensional nonlinear Schrödinger equation with double power nonlinearity

$$i\partial_t u + \partial_x^2 u + a_p|u|^{p-1}u + a_q|u|^{q-1}u = 0, \tag{2.1.1}$$

where $u : \mathbb{R}_t \times \mathbb{R}_x \to \mathbb{C}$, $a_p, a_q \in \mathbb{R} \setminus \{0\}$ and $1 < p < q < \infty$. When $a_p < 0$, $a_q > 0$, we say that the nonlinearity is *defocusing-focusing*, with analogous definitions for other possible signs combinations.

Nonlinear Schrödinger equations appear in many areas of physics such as nonlinear optics (see e.g. [3]) or Bose-Einstein condensation. The double power nonlinearity is an important example of the possible nonlinearities appearing in soliton theory (see e.g. [4]). Via gauge transformations, the double power nonlinearity is also connected with the derivative nonlinear Schrödinger equation (see e.g. [48, 56, 70]). The double power nonlinearity is also a typical example of a nonlinearity breaking the scaling invariance of the pure power

case, while still being relatively tractable, and it may be used to study phenomena in the absence of scaling symmetry (see e.g. [55] for the construction of blowing-up solutions).

The Cauchy problem for (2.1.1) is well known (see [24] and the references therein) to be well-posed in the energy space $H^1(\mathbb{R})$: for any $u_0 \in H^1(\mathbb{R})$, there exists a unique maximal solution $u \in C((-T_*, T^*), H^1(\mathbb{R})) \cap C^1((-T_*, T^*), H^{-1}(\mathbb{R}))$ of (2.1.1) such that $u(t=0) = u_0$. Moreover, the energy E and the mass M, defined by

$$E(u) = \frac{1}{2}\|u_x\|_{L^2}^2 - \frac{a_p}{p+1}\|u\|_{L^{p+1}}^{p+1} - \frac{a_q}{q+1}\|u\|_{L^{q+1}}^{q+1}, \quad M(u) = \frac{1}{2}\|u\|_{L^2}^2,$$

are conserved along the flow and the blow-up alternative holds (i.e. if $T^* < \infty$ (resp. $T_* < \infty$), then $\lim_{t \to T^* \text{ (resp } -T_*)} \|u(t)\|_{H^1} = \infty$).

A *standing wave* is a solution of (2.1.1) of the form $u(t,x) = e^{i\omega t}\phi(x)$ for some $\omega \in \mathbb{R}$ and a *profile* $\phi \in C^2(\mathbb{R})$, which then satisfies

$$-\phi'' + \omega\phi - a_p|\phi|^{p-1}\phi - a_q|\phi|^{q-1}\phi = 0. \tag{2.1.2}$$

We only consider real-valued ϕ in this paper. Define ω^* by

$$\omega^* = \sup\left\{\omega \geqslant 0 : \exists s > 0 \text{ such that } \frac{\omega}{2}s^2 - \frac{a_p}{p+1}s^{p+1} - \frac{a_q}{q+1}s^{q+1} < 0\right\}.$$

It is well known (see [17]) that existence of non-trivial solutions of (2.1.2) with $\lim_{|x|\to\infty}\phi(x) = 0$ holds if and only if

$$\begin{cases} 0 \leqslant \omega < \omega^* & \text{when } a_p < 0, a_q > 0, \\ 0 < \omega < \omega^* & \text{otherwise.} \end{cases}$$

In that case, the solution is positive (up to phase shift), even (up to translation) and unique. We denote it by ϕ_ω, or simply ϕ when there is no ambiguity.

Solitary waves are the building blocks for the nonlinear dynamics of (2.1.1), as it is expected that, generically, a solution of (2.1.1) will decompose into a dispersive linear part and a combination of nonlinear structures as solitary waves. This vague statement is usually referred to as the *Soliton Resolution Conjecture*.

Therefore, understanding the dynamical properties of standing waves, in particular their stability, is a key step in the analysis of the dynamics of (2.1.1). Several stability concepts are available for standing waves. The most commonly used is *orbital stability*, which is defined as follows. The standing wave $e^{i\omega t}\phi(x)$ solution of (2.1.1) is said to be *orbitally stable* if the following holds. For any $\varepsilon > 0$ there exists $\delta > 0$ such that if $u_0 \in H^1(\mathbb{R})$ verifies

$$\|u_0 - \phi\|_{H^1} < \delta,$$

then the associated solution u of (2.1.1) exists globally and verifies

$$\sup_{t\in\mathbb{R}} \inf_{y\in\mathbb{R},\theta\in\mathbb{R}} \left\| u(t) - e^{i\theta}\phi(\cdot - y)\right\|_{H^1} < \varepsilon.$$

In the rest of this paper, when we talk about stability/instability, we always mean *orbital* stability/instability.

The groundwork for orbital stability studies was laid down by Berestycki and Cazenave [15], Cazenave and Lions [25] and Weinstein [72, 71]. Two approaches lead to stability or instability results: the variational approach of [15, 25], which exploits global variational characterizations combined with conservation laws or the virial identity, and the spectral approach of [72, 71], which exploits spectral and coercivity properties of linearized operators to construct a suitable Lyapunov functional. Later on, Grillakis, Shatah and Strauss [43, 44] developed an abstract theory which, under certain assumptions, boils down the stability study of a branch of standing waves $\omega \to \phi_\omega$ to the study of the sign of the quantity (usually called *slope*) $\frac{\partial}{\partial\omega} M(\phi_\omega)$. Note that the theory of Grillakis, Shatah and Strauss has known recently a considerable revamping in the works of De Bièvre, Genoud and Rota-Nodari [31, 32].

With the above mentioned techniques, the orbital stability of positive standing waves has been completely determined in the single power case (i.e. $a_q = 0$) in any dimension $d \geqslant 1$ in [15, 25, 72, 71]. If $a_q = 0$, positive standing waves exist if and only if $a_p > 0$ and $\omega > 0$. In this case, they are stable if $1 < p < 1 + \frac{4}{d}$ (i.e. $1 < p < 5$ in dimension $d = 1$), and they are unstable if $1 + \frac{4}{d} \leqslant p < 1 + \frac{4}{(d-2)_+}$ (i.e. $5 \leqslant p < \infty$ in dimension $d = 1$). Scaling properties of the single power nonlinearity play an important role in the proof and ensure in particular that stability and instability are independent of the value of the frequency ω. It turns out that there is no scaling invariance for double power nonlinearities, which makes the stability study more delicate. As a matter of fact, only very partial results are available so far in higher dimensions. In dimension 1, the situation is a bit more favorable, as one might exploit the ODE structure of the profile equation (2.1.2) in the analysis.

Preliminary investigations for the stability of standing waves in dimension 1 were conducted by Iliev and Kirchev [49] in the case of a generic nonlinearity. In particular, a formula for the slope condition was obtained in [49]. The earliest work devoted to the stability of standing waves for nonlinear Schrödinger equations with double power nonlinearity in dimension 1 is the work of Ohta [61]. In this work, using the integral expression for the slope condition derived by Iliev and Kirchev [49], Ohta established the stability/instability of standing waves in a number of cases. Later on, Maeda [59] further refined the approach of Ohta and established the stability/instability in most of the situations not covered in [61]. However, the stability picture was still not complete, as the

following case was left partially open:

$$a_p < 0, \quad a_q > 0, \quad 1 < p < q < 5, \quad p + q \leqslant 6 \text{ or } p \leqslant \frac{7}{3}.$$

In the above case, Ohta [61] established the stability of standing waves for ω large enough. The instability for small ω was obtained by Ohta [61] for $p + q > 6$, a condition which was later improved to $(p + 3)(q + 3) > 32$ by Fukaya and Hayashi [36]. What happens in the intermediate range of ω when

$$(p + 3)(q + 3) > 32 \quad \text{and} \quad \left(p + q \leqslant 6 \text{ or } p \leqslant \frac{7}{3}\right),$$

was not elucidated in [36, 59, 61], nor what happens for small ω when $(p + 3)(q + 3) \leqslant 32$, (except for the notable case $p = 2$, $q = 3$, where explicit calculations are possible and show that the wave is stable for any $\omega > 0$).

For convenience, we adopt the following convention. When a standing wave is stable for any $\omega \in (0, \omega^*)$, we say that it is of type S. When there exists $\omega_1 \in (0, \omega^*)$ such that the standing wave is unstable for $\omega \in (0, \omega_1)$ and stable for $\omega \in (\omega_1, \omega^*)$, we say that it is of type US. Other types are defined in a similar manner.

Note that when instability holds the endpoint ω_1 could be included in the instability range under regularity assumptions on the nonlinearity (thanks to the criterion of Comech and Pelinovsky [29], see (2.2.4) and Remark 2.1.2).

Our goal in this paper is to fill out the gaps left open by the previous works [36, 59, 61] and to provide a complete stability picture for the standing waves of the Schrödinger equations with double power nonlinearity. Our main result is the following.

Theorem 2.1.1. Let $(\phi_\omega)_{\omega \in (0,\omega^*)}$ be the family of standing waves of (2.1.1). The following gives the stability type of the family of standing waves.

1. Assume that $a_p > 0$ and $a_q > 0$.
   (a) If $q \leqslant 5$, then it is of type S.
   (b) If $p \geqslant 5$, then it is of type U.
   (c) If $p < 5 < q$, then it is of type SU.
2. Assume that $a_p > 0$ and $a_q < 0$.
   (a) If $p \leqslant 5$, then it is of type S.
   (b) If $p > 5$, then it is of type US.
3. Assume that $a_p < 0$ and $a_q > 0$.
   (a) If $q \leqslant 7 - 2p$, then it is of type S.
   (b) If $7 - 2p < q < 5$, then it is of type US.

(c) If $q \geqslant 5$, then it is of type U.

This theorem implies in particular that stability change occurs at most once, which is conjectured in [59, p. 265], and is in contrast to NLS with triple power nonlinearity considered in [58].

Remark 2.1.2. The critical frequency at which the stability change occurs is not included in our statement. Indeed, it was established by Comech and Pelinovsky under a higher regularity assumption on the nonlinearity that the standing wave at the critical frequency is unstable if (2.2.4) holds. Alternative proofs with improved assumptions on the regularity are provided in [60, 62]. However, the regularity required is still too high to cover the whole range of double-power nonlinearities. Strategies to treat the critical frequency without regularity assumptions have been developed for other types of equations, see e.g. [45, 73]. In this paper, we will not try to cover the critical frequency and we simply verify that the criterion (2.2.4) holds.

In Theorem 2.1.1, cases (1), (2) and (3)(c) were already covered in [59, 61]. For the sake of completeness, and as the proofs are not very long, we will also cover them in our work. Cases (3)(a) and (b) were only partially solved. We provide a definitive result for these cases. Our approach relies on several ingredients. First of all, we express the slope condition in a concise, while easily tractable integral, factoring out terms which are in any case positive. Instead of working with the parameter ω, we manipulate the slope condition with the parameter $\phi_0 = \phi_\omega(0)$ (which is in a bijective relation with ω). We are left with an integral expression $F(\phi_0)$ (see (2.3.2)), of which we need to determine the sign. A refactorisation allows us to introduce an auxiliary parameter γ, and differentiation with respect to ϕ_0 gives us an expression which we can prove to have sign, provided we have suitably chosen the parameter γ. This gives the information that $F(\phi_0)$ changes sign at most once. The sign for large ω (or equivalently large ϕ_0) had already been established in [61]. On the other hand, the sign for ω close to 0 had not been computed before. Here, an astute rewriting of the slope in terms of Beta functions allows us to determine the sign for ω close to 0.

Observe that our results are not covering the zero-frequency case $\omega = 0$. Stability or instability of the corresponding (algebraic) standing waves (when existing) can be conjectured to be the same as the one for small $\omega > 0$ (which is consistent with the results obtained by Fukaya and Hayashi [36]).

In the case $a_p < 0$, $a_q > 0$ and $1 < p < q < 5$, we complement our theoretical results with numerical experiments. We first represent the critical surface $\{\omega_c(p, q)\}$ at which the stability change occurs and discuss the different possible shapes of the surface depending on the ratio a_p/a_q. We then simulate the dynamics of (2.1.1) around a standing wave with the Crank-Nicolson scheme

with relaxation of Besse [19]. Three types of behaviors are observed depending on the type of initial data : stability, growth followed by oscillations, and scattering.

To end this introduction, we point out that many works are devoted to standing waves of the double power nonlinear Schrödinger in higher dimension (for which our approach does not apply), and just give a small sample of the existing literature. The cubic quintic case in higher dimension was investigated in [23]. Stability of standing waves in higher dimension for generic nonlinearities was considered in [37]. Strong instability was studied in [63]. Stability results for algebraic standing waves were obtained in [36]. Uniqueness and non-degeneracy was considered in [57]. Existence or non-existence of minimizers of the energy at fixed mass was obtained in [14]. Let us also mention in dimension 1 the work [41], which is devoted to the stability of standing waves for cubic-quintic nonlinearities in the presence of a δ potential (see [8, 9] for further developments).

This paper is organized as follows. We start by some preliminaries in Section 2.2, recalling in particular the properties of the standing wave profiles and the stability criterion. In Section 2.3, we reformulate the slope condition for stability, using the profile equation. In Section 2.4, we analyze the limit of the slope at the endpoints of the interval of admissible frequencies ω and in particular determine the sign of the slope at the endpoints. The sign of the slope on the full interval of admissible frequencies is recovered in Section 2.5, which shows Theorem 2.1.1. Finally, numerical experiments are presented in Section 2.6.

After the first version of this paper was posted to arXiv, Professor Hayashi kindly informed us he had an independent similar result and posted it as [47]. His Theorem 1.3 is similar to our Theorem 1.1 although it does not include the case $1 < p < 9/5$.

We would like to thank the anonymous referee for his valuable comments which helped in the improvement of our paper.

2.2 Preliminaries

2.2.1 The profile equation

We start by some analysis around the ordinary differential equation (2.1.2) and its solutions (ϕ_ω). Apart in a few specific cases (e.g. when $q = 2p-1$, see e.g. [58]), there does not exist an explicit formula for the full standing waves profile. Note that $\omega^* = \infty$ when $a_q > 0$, $0 < \omega^* < \infty$ when $a_p > 0$ and $a_q < 0$, and $\omega^* = -\infty$ (i.e. there is no solution of (2.1.2) in $H^1(\mathbb{R})$) when $a_p, a_q < 0$.

All along this paper, we assume that $0 < \omega < \omega^*$ (excluding in particular the possibility that $a_p, a_q < 0$). Under this assumption, there exists $\phi_0 > 0$ (depending implicitly on ω) such that

$$\phi_0 = \inf\{\phi > 0 : \frac{\omega}{2}\phi^2 - \frac{a_p}{p+1}|\phi|^{p+1} - \frac{a_q}{q+1}|\phi|^{q+1} = 0\},$$

and we have

$$\phi_\omega(0) = \phi_0.$$

Observe that ω may be expressed in terms of ϕ_0 as follows

$$\omega = \frac{2a_p}{p+1}\phi_0^{p-1} + \frac{2a_q}{q+1}\phi_0^{q-1}. \tag{2.2.1}$$

Moreover, as $\omega < \omega^*$, we have

$$\omega - a_p\phi_0^{p-1} - a_q\phi_0^{q-1} < 0.$$

This implies in particular ϕ_0 is a C^1-function of ω. Moreover, we always have

$$\frac{\partial\phi_0}{\partial\omega} = \left(\frac{2a_p(p-1)}{p+1}\phi_0^{p-2} + \frac{2a_q(q-1)}{q+1}\phi_0^{q-2}\right)^{-1} > 0. \tag{2.2.2}$$

As a consequence, the following result holds.

Lemma 2.2.1. The function $\omega \to \phi_0$ is a strictly increasing bijection from $(0, \omega^*)$ to (ϕ_*, ϕ^*) where

$$\phi_* = \begin{cases} \left(-\frac{a_p}{a_q}\frac{q+1}{p+1}\right)^{\frac{1}{q-p}} & \text{if } a_p < 0, \\ 0 & \text{if } a_p > 0, \end{cases} \quad \phi^* = \begin{cases} \infty & \text{if } a_q > 0, \\ \left(-\frac{a_p}{a_q}\frac{p-1}{q-1}\frac{q+1}{p+1}\right)^{\frac{1}{q-p}} & \text{if } a_q < 0. \end{cases} \tag{2.2.3}$$

2.2.2 The stability criterion

As we already mentioned, stability criteria have been derived in the general case in [43, 49]. For the double power nonlinearity, the stability of the standing wave is determined by a slope condition (the spectral condition of [43] being always verified in this case when $\omega > 0$). The standing wave $e^{i\omega t}\phi_\omega(x)$ will be stable if

$$\frac{\partial}{\partial\omega}M(\phi_\omega) > 0,$$

and it will be unstable if

$$\frac{\partial}{\partial\omega}M(\phi_\omega) < 0.$$

When $\partial_\omega M(\phi_\omega) = 0$, under regularity assumption on the nonlinearity, the stability can be decided by looking at the second derivative, as was established by Comech and Pelinovsky [29]: If $\partial_\omega M(\phi_\omega) = 0$ and

$$\frac{\partial^2}{\partial\omega^2} M(\phi_\omega) \neq 0, \tag{2.2.4}$$

then the standing wave $e^{i\omega t}\phi_\omega(x)$ is unstable.

2.3 Reformulation of the slope

For notational convenience, we introduce the function J defined by

$$J(\omega, p, q) = \frac{\partial}{\partial\omega} M(\phi_\omega).$$

Hence the sign of J determines the stability of the corresponding standing wave.

The main idea in this section is to express J in terms of ϕ_0 instead of ω. Before doing that, we introduce some convenient notation. Let Φ_p and Φ_q be defined by

$$\Phi_p = \frac{2a_p}{p+1}\phi_0^{p+1}(1 - s^{p-1}), \quad \Phi_q = \frac{2a_q}{q+1}\phi_0^{q+1}(1 - s^{q-1}), \tag{2.3.1}$$

where $a_p, a_q \neq 0$, $1 < p < q < \infty$ and $0 < s < 1$.

Lemma 2.3.1. The function J may be expressed in terms of ϕ_0 as follows

$$J(\omega, p, q) = C(\phi_0)F(\phi_0),$$

where

$$F(\phi_0) = \int_0^1 \frac{(5-p)\Phi_p + (5-q)\Phi_q}{(\Phi_p + \Phi_q)^{\frac{3}{2}}} s ds, \tag{2.3.2}$$

and $C(\phi_0)$ is positive and explicitly known (see (2.3.4)).

Proof. We multiply the equation (2.1.2) of the profile by ϕ_x and we integrate to obtain

$$-\frac{1}{2}|\phi_x|^2 + \frac{\omega}{2}|\phi|^2 - \frac{a_p}{p+1}|\phi|^{p+1} - \frac{a_q}{q+1}|\phi|^{q+1} = c.$$

When $x \to \infty$, we know that $\phi(x) \to 0$ and $\phi'(x) \to 0$. Therefore $c = 0$, and

$$-\frac{1}{2}|\phi_x|^2 + \frac{\omega}{2}|\phi|^2 - \frac{a_p}{p+1}|\phi|^{p+1} - \frac{a_q}{q+1}|\phi|^{q+1} = 0. \tag{2.3.3}$$

For $x > 0$, as ϕ is decreasing, from (2.3.3) we have

$$\phi_x = -\sqrt{\omega\phi^2 - \frac{2a_p}{p+1}\phi^{p+1} - \frac{2a_q}{q+1}\phi^{q+1}}.$$

Still for $x > 0$, let $t = \phi(x)$, then

$$dx = \frac{dt}{\phi_x} = -\frac{dt}{\sqrt{\omega\phi^2 - \frac{2a_p}{p+1}\phi^{p+1} - \frac{2a_q}{q+1}\phi^{q+1}}}.$$

Therefore we may perform the following change of variable:

$$M(\phi) = \frac{1}{2}\int_{\mathbb{R}} |\phi(x)|^2 dx = \int_0^\infty |\phi(x)|^2 dx = \int_0^{\phi_0} \frac{t^2}{\sqrt{\omega t^2 - \frac{2a_p}{p+1}t^{p+1} - \frac{2a_q}{q+1}t^{q+1}}} dt.$$

Changing again variable by setting $t = \phi_0 s$, we have

$$M(\phi) = \int_0^1 \frac{\phi_0^3 s^2}{s\sqrt{\omega\phi_0^2 - \frac{2a_p}{p+1}\phi_0^{p+1}s^{p-1} - \frac{2a_q}{q+1}\phi_0^{q+1}s^{q-1}}} ds.$$

Replacing ω by its value (2.2.1) in terms of ϕ_0, we have

$$M(\phi) = \int_0^1 \frac{\phi_0^3 s}{\sqrt{\frac{2a_p}{p+1}\phi_0^{p+1} + \frac{2a_q}{q+1}\phi_0^{q+1} - \frac{2a_p}{p+1}\phi_0^{p+1}s^{p-1} - \frac{2a_q}{q+1}\phi_0^{q+1}s^{q-1}}} ds,$$

which, using the notation (2.3.1) for Φ_p and Φ_q, gives

$$M(\phi) = \int_0^1 \frac{\phi_0^3 s}{\sqrt{\Phi_p + \Phi_q}} ds.$$

Differentiating with respect to ω, we have

$$\partial_\omega \Phi_p = (p+1)\Phi_p \phi_0^{-1}\partial_\omega\phi_0, \quad \partial_\omega \Phi_q = (q+1)\Phi_q\phi_0^{-1}\partial_\omega\phi_0.$$

Therefore we obtain

$$\begin{aligned}
J(\omega, p, q) &= \partial_\omega M(\phi) \\
&= \int_0^1 \frac{3\phi_0^2\partial_\omega\phi_0 s(\Phi_p + \Phi_q) - \frac{1}{2}\phi_0^3 s\left((p+1)\Phi_p\phi_0^{-1} + (q+1)\Phi_q\phi_0^{-1})\right)\partial_\omega\phi_0}{(\Phi_p + \Phi_q)^{\frac{3}{2}}} ds, \\
&= \frac{\partial_\omega\phi_0}{2}\phi_0^2 \int_0^1 \frac{6(\Phi_p + \Phi_q) - ((p+1)\Phi_p + (q+1)\Phi_q))}{(\Phi_p + \Phi_q)^{\frac{3}{2}}} s ds, \\
&= \frac{\partial_\omega\phi_0}{2}\phi_0^2 \int_0^1 \frac{(5-p)\Phi_p + (5-q)\Phi_q}{(\Phi_p + \Phi_q)^{\frac{3}{2}}} s ds, = C(\phi_0)F(\phi_0),
\end{aligned}$$

where $F(\phi_0)$ is defined in (2.3.2) and

$$C(\phi_0) = \frac{\partial_\omega \phi_0}{2} \phi_0^2. \tag{2.3.4}$$

This concludes the proof. □

We will now analyze the variations of $J(\omega, p, q)$ in terms of ϕ_0. For future convenience (the reason for such a choice will appear clearly later), we introduce an auxiliary parameter γ in the following way

$$J(\omega, p, q) = C(\phi_0)\phi_0^{-\gamma} F_\gamma(\phi_0),$$

where

$$F_\gamma(\phi_0) = \int_0^1 \phi_0^\gamma \left(\frac{(5-p)\Phi_p + (5-q)\Phi_q}{(\Phi_p + \Phi_q)^{\frac{3}{2}}} \right) sds.$$

Denote the integrand of F_γ by

$$I_\gamma(\phi_0) = \phi_0^\gamma \left(\frac{(5-p)\Phi_p + (5-q)\Phi_q}{(\Phi_p + \Phi_q)^{\frac{3}{2}}} \right). \tag{2.3.5}$$

Observe that there is a implicit dependency in s. In the following lemma we differentiate $I_\gamma(\phi_0)$ with respect to ϕ_0.

Lemma 2.3.2. For any $0 < s < 1$, the following holds:

$$\frac{\partial I_\gamma}{\partial_{\phi_0}} = \phi_0^{\gamma-1} \left(\frac{((5-p)(2\gamma-(p+1))\Phi_p + (5-q)(2\gamma-(q+1))\Phi_q)\,(\Phi_p+\Phi_q)}{2\,(\Phi_p+\Phi_q)^{\frac{5}{2}}} \right) - \phi_0^{\gamma-1} \left(\frac{3(q-p)^2\Phi_p\Phi_q}{2\,(\Phi_p+\Phi_q)^{\frac{5}{2}}} \right).$$

Proof. We start by differentiating the term in parenthesis in $I_\gamma(\phi_0)$. We have

$$\partial_{\phi_0}\Phi_p = (p+1)\Phi_p\phi_0^{-1}, \quad \partial_{\phi_0}\Phi_q = (q+1)\Phi_q\phi_0^{-1}.$$

Therefore, we have

$$\begin{aligned}
&\partial_{\phi_0}\left(\frac{(5-p)\Phi_p+(5-q)\Phi_q}{(\Phi_p+\Phi_q)^{\frac{3}{2}}}\right)\\
&\quad=\phi_0^{-1}\left(\frac{((5-p)(p+1)\Phi_p+(5-q)(q+1)\Phi_q)\,(\Phi_p+\Phi_q)}{(\Phi_p+\Phi_q)^{\frac{5}{2}}}\right)\\
&\quad-\phi_0^{-1}\left(\frac{\frac{3}{2}\,((5-p)\Phi_p+(5-q)\Phi_q)\,((p+1)\Phi_p+(q+1)\Phi_q)}{(\Phi_p+\Phi_q)^{\frac{5}{2}}}\right)\\
&\quad=\phi_0^{-1}\left(\frac{-(5-p)(p+1)\Phi_p^2-(5-q)(q+1)\Phi_q^2}{2\,(\Phi_p+\Phi_q)^{\frac{5}{2}}}\right)\\
&\quad+\phi_0^{-1}\left(\frac{((5-p)(2p-3q-1)+(5-q)(2q-3p-1))\Phi_p\Phi_q}{2\,(\Phi_p+\Phi_q)^{\frac{5}{2}}}\right)\\
&=\phi_0^{-1}\left(\frac{-((5-p)(p+1)\Phi_p+(5-q)(q+1)\Phi_q)\,(\Phi_p+\Phi_q)-3(q-p)^2\Phi_p\Phi_q}{2\,(\Phi_p+\Phi_q)^{\frac{5}{2}}}\right).
\end{aligned}$$

Before going on, observe that we may rewrite the term in parentheses in $I_\gamma(\phi_0)$ as

$$\frac{(5-p)\Phi_p+(5-q)\Phi_q}{(\Phi_p+\Phi_q)^{\frac{3}{2}}}=\frac{2\,((5-p)\Phi_p+(5-q)\Phi_q)\,(\Phi_p+\Phi_q)}{2\,(\Phi_p+\Phi_q)^{\frac{5}{2}}}.$$

Finally, the full derivative of $I_\gamma(\phi_0)$ is given by

$$\begin{aligned}
\frac{\partial I_\gamma}{\partial\phi_0}&=\partial_{\phi_0}\left(\phi_0^\gamma\left(\frac{(5-p)\Phi_p+(5-q)\Phi_q}{(\Phi_p+\Phi_q)^{\frac{3}{2}}}\right)\right),\\
&=\phi_0^{\gamma-1}\left(\frac{((5-p)(2\gamma-(p+1))\Phi_p+(5-q)(2\gamma-(q+1))\Phi_q)\,(\Phi_p+\Phi_q)}{2\,(\Phi_p+\Phi_q)^{\frac{5}{2}}}\right)\\
&\qquad-\phi_0^{\gamma-1}\left(\frac{3(q-p)^2\Phi_p\Phi_q}{2\,(\Phi_p+\Phi_q)^{\frac{5}{2}}}\right).
\end{aligned}$$

This concludes the proof. □

For future reference, we establish here the following technical lemma which we will use at several occasions.

Lemma 2.3.3. The function $s\to\frac{1-s^{q-1}}{1-s^{p-1}}$ is an increasing bijection from $(0,1)$ to $(1,\frac{q-1}{p-1})$.

Proof. Let $h(s)=\frac{1-s^{q-1}}{1-s^{p-1}}$. We have

$$h'(s)=\frac{s^{p-2}}{(1-s^{p-1})^2}l(s),$$

where

$$l(s) = (q-p)s^{q-1} + p - 1 - (q-1)s^{q-p}.$$

Note that $l(1) = 0$ and for $0 < s < 1$,

$$l'(s) = (q-p)(q-1)(s^{q-2} - s^{q-p-1}) < 0.$$

Hence $l'(s) < 0$ and $l(s) > 0$ for $0 < s < 1$. We conclude that $h'(s) > 0$ for $0 < s < 1$. As a consequence, h is increasing on the interval $(0, 1)$. Moreover, we have $h(0) = 1$ and, by L'Hospital's rule,

$$\lim_{s \to 1} h(s) = \frac{q-1}{p-1}.$$

This concludes the proof. □

2.4 The slope at the endpoints

Our goal in this section is to investigate what happens for $J(\omega, p, q)$ when ω is close to 0 and ω^*.

2.4.1 The zero frequency case

In this section, we determine the limit of $J(\omega, p, q)$ when ω tends to zero. Let J_0 be defined by

$$J_0(p, q) = \lim_{\omega \to 0} J(\omega, p, q).$$

We first consider the case where $a_p > 0$.

Proposition 2.4.1. Let $a_p > 0$. The following holds.

1. If $1 < p < \frac{7}{3}$, then $J_0(p, q) = 0^+$.
2. If $p = \frac{7}{3}$, then $0 < J_0(p, q) < \infty$.
3. If $\frac{7}{3} < p < 5$, then $J_0(p, q) = \infty$.
4. If $p = 5$, then three cases have to be distinguished.
   (a) If $q < 9$, then $J_0(p, q) = -\operatorname{sign}(a_q)\infty$.
   (b) If $q = 9$, then $0 < -\operatorname{sign}(a_q) J_0(p, q) < \infty$.
   (c) If $q > 9$, then $J_0(p, q) = 0^{-\operatorname{sign}(a_q)}$.
5. If $5 < p$, then $J_0(p, q) = -\infty$.

Proof. When $a_p > 0$, we have

$$\lim_{\omega \to 0} \phi_0 = \phi_* = 0.$$

Recall that we have shown in Lemma 2.3.1 that J may be written as $J(\omega,p,q) = C(\phi_0)F(\phi_0)$. We have (recalling the definition (2.3.4) of C and the expression (2.2.2) of $\partial_\omega\phi_0$)

$$C(\phi_0) = \frac{1}{2}\partial_\omega\phi_0\phi_0^2 = \frac{1}{4}\left(\frac{a_p(p-1)}{p+1}\phi_0^{p-4} + \frac{a_q(q-1)}{q+1}\phi_0^{q-4}\right)^{-1}$$
$$= \phi_0^{4-p}\frac{1}{4}\left(\frac{a_p(p-1)}{p+1} + \frac{a_q(q-1)}{q+1}\phi_0^{q-p}\right)^{-1} = \phi_0^{4-p}\left(\frac{p+1}{4a_p(p-1)} + o(1)\right).$$

The function F (defined in (2.3.2)) can be written, substituting Φ_p and Φ_q by their expressions (2.3.1), as

$$F(\phi_0) = \int_0^1 \frac{\frac{2a_p(5-p)}{p+1}(1-s^{p-1})\phi_0^{p+1} + \frac{2a_q(5-q)}{q+1}(1-s^{q-1})\phi_0^{q+1}}{\left(\frac{2a_p}{p+1}(1-s^{p-1})\phi_0^{p+1} + \frac{2a_q}{q+1}(1-s^{q-1})\phi_0^{q+1}\right)^{\frac{3}{2}}}sds.$$

As we are interested in the limit $\phi_0 \to 0$, we factor out the terms in ϕ_0^{p+1} to get

$$F(\phi_0) = \phi_0^{-\frac{p+1}{2}}\int_0^1 \frac{\frac{2a_p(5-p)}{p+1}(1-s^{p-1}) + \frac{2a_q(5-q)}{q+1}(1-s^{q-1})\phi_0^{q-p}}{\left(\frac{2a_p}{p+1}(1-s^{p-1}) + \frac{2a_q}{q+1}(1-s^{q-1})\phi_0^{q-p}\right)^{\frac{3}{2}}}sds$$
$$= (5-p)\phi_0^{-\frac{p+1}{2}}\left(\int_0^1\left(\frac{2a_p}{p+1}(1-s^{p-1})\right)^{-\frac{1}{2}}sds + o(1)\right).$$

In the particular case $p=5$, we instead write

$$F(\phi_0) = a_q(5-q)\phi_0^{q-8}\left(\int_0^1 \frac{\frac{2}{q+1}(1-s^{q-1})}{\left(\frac{a_p}{3}(1-s^4)\right)^{\frac{3}{2}}}sds + o(1)\right).$$

In summary, when $\phi_0 \to 0$ (i.e. $\omega \to 0$), we have established that there exists $C = C(p,q) > 0$ such that when $p \neq 5$ we have

$$J(\omega,p,q) = (5-p)\phi_0^{\frac{7-3p}{2}}C(1+o(1)),$$

and when $p=5$ we have

$$J(\omega,p,q) = (5-q)a_q\phi_0^{q-9}C(1+o(1)).$$

This gives the desired result. □

We now discuss the case $a_p < 0$ and $a_q > 0$.

Proposition 2.4.2. Let $a_p < 0$ and $a_q > 0$.

1. Assume that $p < \frac{7}{3}$. Then $J_0(p,q) \in \mathbb{R}$ and the following holds.
   (a) If $2p + q < 7$, then $J_0(p,q) > 0$.
   (b) If $2p + q = 7$, then $J_0(p,q) = 0$.
   (c) If $2p + q > 7$, then $J_0(p,q) < 0$.
2. Assume that $p \geqslant \frac{7}{3}$. Then $J_0(p,q) = -\infty$.

We start with some preliminaries. To establish the first part of Proposition 2.4.2, we will calculate J_0 in terms of the Beta function. Recall that the Beta function, also called Euler integral of the first kind, is a special function closely related to the Gamma function. It is defined for $x > 0$ and $y > 0$ by the integral

$$B(x,y) = \int_0^1 t^{x-1}(1-t)^{y-1}dt. \tag{2.4.1}$$

The relation between the Beta function and the Gamma function is given by (see e.g [1])

$$B(x,y) = \frac{\Gamma(x)\Gamma(y)}{\Gamma(x+y)}.$$

We introduce the function H defined for $x > 0$ and $y > 0$ by

$$H(x,y) = \int_0^1 \frac{t^{x-1}(1-t^y)}{(1-t)^{\frac{3}{2}}}dt. \tag{2.4.2}$$

The relation between H and B is given in the following lemma.

Lemma 2.4.3. For $x > 0$ and $y > 0$, we have

$$H(x,y) = -(2x-1)B\left(x, \frac{1}{2}\right) + (2x+2y-1)B\left(x+y, \frac{1}{2}\right). \tag{2.4.3}$$

Proof. Let

$$u(t) = t^{x-1}(1-t^y).$$

Rewrite

$$\frac{1}{(1-t)^{\frac{3}{2}}} = v'(t) - \frac{1}{(1-t)^{\frac{1}{2}}},$$

where

$$v(t) = \frac{2}{(1-t)^{\frac{1}{2}}} - 2(1-t)^{\frac{1}{2}} = \frac{2t}{(1-t)^{\frac{1}{2}}}.$$

We have

$$\begin{aligned} H(x,y) =& \int_0^1 u(t)\left(v'(t) - \frac{1}{(1-t)^{\frac{1}{2}}}\right)dt, \\ =& u(1_-)v(1_-) - u(0_+)v(0_+) - \int_0^1 u'(t)v(t)dt - \int_0^1 \frac{u(t)}{(1-t)^{\frac{1}{2}}}dt, \\ =& 0 - \int_0^1 \frac{2tu'(t)+u(t)}{(1-t)^{\frac{1}{2}}}dt. \end{aligned}$$

Above we have used $u(1) = 0$ of order 1 to cancel the singularity of $v(1_-)$ of order $\frac{1}{2}$, and $v(0) = 0$ with order 1 to cancel the singularity of $u(0_+)$ of order $x - 1$. Note that

$$2tu'(t) + u(t) = (2x-1)t^{x-1} - (2x+2y-1)t^{x+y-1}.$$

Therefore, using the definition of B given in (2.4.1) with $y = \frac{1}{2}$, we have

$$H(x,y) = -(2x-1)B\left(x, \frac{1}{2}\right) + (2x+2y-1)B\left(x+y, \frac{1}{2}\right).$$

This concludes the proof. □

The value $J_0(p,q)$ may be expressed using B as follows.

Lemma 2.4.4. Let $a_p < 0$ and $a_q > 0$. Assume that $1 < p < 7/3$. Then

$$J_0(p,q) = (7-2p-q)C_0 B\left(\frac{7-3p}{2(q-p)}, \frac{1}{2}\right),$$

where C_0 is a positive constant explicitly known (given by (2.4.5)).

The first part of Proposition 2.4.2 is a direct consequence of Lemma 2.4.4.

Proof of Lemma 2.4.4. Let $1 < p < 7/3$. Recall that $J(\omega,p,q) = C(\phi_0)F(\phi_0)$, with $C(\phi_0) > 0$ and F given by (2.3.2). Observe that, using the value of ϕ_* given in (2.2.3), we may introduce the constant

$$C_* = \frac{2a_q}{q+1}\phi_*^{q+1} = -\frac{2a_p}{(p+1)}\phi_*^{p+1}.$$

Using the definition (2.3.4) of $C(\phi_0)$ and the expression (2.2.2) of $\partial_\omega\phi_0$, we have

$$\begin{aligned} \lim_{\phi_0\to\phi_*} C(\phi_0) = C(\phi_*) &= \frac{\phi_*^5}{2C_*(q-p)} > 0, \\ \lim_{\phi_0\to\phi_*} \Phi_p &= \frac{2a_p}{(p+1)}\phi_*^{p+1}(1-s^{p-1}) = -C_*(1-s^{p-1}), \\ \lim_{\phi_0\to\phi_*} \Phi_q &= \frac{2a_q}{(q+1)}\phi_*^{q+1}(1-s^{q-1}) = C_*(1-s^{q-1}). \end{aligned}$$

As a consequence, we get

$$\lim_{\phi_0\to\phi_*}(\Phi_p+\Phi_q)=C_*(s^{p-1}-s^{q-1}),$$
$$\lim_{\phi_0\to\phi_*}((5-p)\Phi_p+(5-q)\Phi_q)=C_*\left(-(5-p)(1-s^{p-1})+(5-q)(1-s^{q-1})\right).$$

As a consequence,

$$\begin{aligned}F(\phi_*)&=C_*^{-\frac12}\int_0^1\frac{-(5-p)(1-s^{p-1})+(5-q)(1-s^{q-1})}{(s^{p-1}-s^{q-1})^{\frac32}}sds\\&=C_*^{-\frac12}\int_0^1\frac{-(q-p)(1-s^{p-1})+(5-q)(s^{p-1}-s^{q-1})}{(1-s^{q-p})^{\frac32}}s^{\frac{5-3p}{2}}ds\\&=C_*^{-\frac12}\left(-(q-p)\int_0^1\frac{(1-s^{p-1})s^{\frac{5-3p}{2}}}{(1-s^{q-p})^{\frac32}}ds+(5-q)\int_0^1 s^{\frac{3-p}{2}}\left(1-s^{q-p}\right)^{-\frac12}ds\right).\end{aligned}\tag{2.4.4}$$

Changing variable $t=s^{q-p}$, we obtain

$$F(\phi_*)=C_*^{-\frac12}\left(-\int_0^1\frac{(1-t^{\frac{p-1}{q-p}})t^{\frac{7-p-2q}{2(q-p)}}}{(1-t)^{\frac32}}ds+\frac{5-q}{q-p}\int_0^1 t^{\frac{5+p-2q}{2(q-p)}}(1-t)^{-\frac12}ds\right).$$

We now use B and H to express the above quantity. Setting

$$\begin{aligned}(x_1,y_1)&=\left(\frac{7-p-2q}{2(q-p)}+1,\frac{p-1}{q-p}\right)=\left(\frac{7-3p}{2(q-p)},\frac{p-1}{q-p}\right),\\(x_2,y_2)&=\left(\frac{5+p-2q}{2(q-p)}+1,\frac12\right)=\left(\frac{5-p}{2(q-p)},\frac12\right),\end{aligned}$$

we get

$$F(\phi_*)=C_*^{-\frac12}\left(-H(x_1,y_1)+\frac{5-q}{q-p}B(x_2,y_2)\right).$$

Observe that we have assumed $p<\frac73$, $p<q$, which ensures that x_1,x_2,y_1,y_2 are positive. This a posteriori justifies the fact that $J_0(p,q)$ is finite. The formula (2.4.3) allows us to express $H(x_1,y_1)$ in the following way (using $y_2=1/2$):

$$H(x_1,y_1)=-(2x_1-1)B(x_1,y_2)+(2x_1+2y_1-1)B(x_1+y_1,y_2).$$

It turns out that

$$-(2x_1-1)=-\frac{7-2p-q}{q-p},\quad(2x_1+2y_1-1)=\frac{5-q}{q-p},\quad x_1+y_1=\frac{5-p}{2(q-p)}=x_2.$$

As a consequence, there is a simplification in the expression of $F(\phi_*)$, which becomes

$$F(\phi_*)=C_*^{-\frac12}\frac{7-2p-q}{q-p}B(x_1,y_2).$$

Setting

$$C_0 = \frac{C_*^{-\frac{1}{2}}}{q-p} C(\phi_*) > 0 \tag{2.4.5}$$

gives the desired result. □

Lemma 2.4.5. Assume that $a_p < 0$ and $a_q > 0$. For $p \geqslant 7/3$ and $1 < p < q$, we have

$$\lim_{\omega \to 0} J(\omega, p, q) = -\infty.$$

The second part of Proposition 2.4.2 is a direct consequence of Lemma 2.4.5.

Proof. Coming back to the expression (2.4.4) of $F(\phi_*)$ in the proof of Lemma 2.4.4, we observe that if $\frac{5-3p}{2} \leqslant -1$, i.e. $p \geqslant \frac{7}{3}$, then $F(\phi_*) = -\infty$, and, since $\lim_{\phi_0 \to \phi_*} C(\phi_0) = C(\phi_*) > 0$, we also have $J_0(p, q) = -\infty$ when $p \geqslant \frac{7}{3}$. □

2.4.2 The large frequency case

In this section, we determine the limit of $J(\omega, p, q)$ when ω tends to ω^*. Let J^* be defined by

$$J^*(p, q) = \lim_{\omega \to \omega^*} J(\omega, p, q).$$

We first consider the case where $a_q > 0$.

Proposition 2.4.6. Let $a_q > 0$. The following holds.

1. If $1 < q < \frac{7}{3}$, then $J^*(p, q) = 0^+$.
2. If $q = \frac{7}{3}$, then $0 < J^*(p, q) < \infty$.
3. If $\frac{7}{3} < q < 5$, then $J^*(p, q) = \infty$.
4. If $q = 5$, then $J^*(p, q) = 0^{\operatorname{sign}(a_p)}$.
5. If $5 < q$, then $J^*(p, q) = -\infty$.

Proof. Since $a_q > 0$, we have $\omega^* = \infty$ and therefore $\phi^* = \infty$. Following similar arguments as in the proof of Proposition 2.4.1, as $\phi_0 \to \infty$, for $q \neq 5$, we have

$$C(\phi_0) = \phi_0^{4-q} \left(\frac{q+1}{4a_q(q-1)} + o(1) \right),$$
$$F(\phi_0) = (5-q)\phi_0^{-\frac{q+1}{2}} \left(\int_0^1 \left(\frac{2a_q}{q+1}(1 - s^{q-1}) \right)^{-\frac{1}{2}} s ds + o(1) \right).$$

As a consequence, for $q \neq 5$, when $\phi_0 \to \infty$ (i.e. $\omega \to \infty$), there exists $C = C(a_q, q) > 0$ such that

$$J(\omega, p, q) = (5-q)\phi_0^{\frac{7-3q}{2}} C(1 + o(1)).$$

In the particular case $q = 5$, we instead write

$$F(\phi_0) = a_p(5-p)\phi_0^{p-8}\left(\int_0^1 \frac{\frac{2}{p+1}(1-s^{p-1})}{\left(\frac{a_q}{3}(1-s^4)\right)^{\frac{3}{2}}} sds + o(1)\right).$$

and therefore we get

$$J(\omega, p, q) = a_p(5-p)\phi_0^{p-9}C(1+o(1)).$$

The two estimates on J lead to the desired result. □

Then we consider the case where $a_q < 0$ (and thus $a_p > 0$ to ensure existence of standing waves).

Proposition 2.4.7. Let $a_p > 0$, $a_q < 0$ and $5 \leqslant p$. Then

$$J^*(p, q) = \infty.$$

Proposition 2.4.7 does not cover the whole possible range of p and q. As it was not necessary in our analysis, we did not try to cover the remaining cases.

Proof of Proposition 2.4.7. By construction, $\omega_* = \omega(\phi_*)$ is the value of ω at which $\partial_{\phi_0}\omega(\phi^*) = 0$. As a consequence, we have

$$\lim_{\phi_0 \to \phi^*} \frac{\partial \phi_0}{\partial \omega} = \infty,$$

which, given the value (2.3.4) of $C(\phi_0)$, readily implies

$$\lim_{\phi_0 \to \phi^*} C(\phi_0) = \infty.$$

Using the expressions of (2.3.1) of Φ_p and Φ_q and the expression (2.3.2) of F we have

$$F(\phi^*) = \int_0^s \frac{2a_p\frac{(5-p)(\phi^*)^{p+1}(1-s^{p-1})}{p+1} + 2a_q\frac{(5-q)(\phi^*)^{q+1}(1-s^{q-1})}{q+1}}{\left(2a_p\frac{(\phi^*)^{p+1}(1-s^{p-1})}{p+1} + 2a_q\frac{(\phi^*)^{q+1}(1-s^{q-1})}{q+1}\right)^{\frac{3}{2}}} sds.$$

If $p = 5$, then we have $F(\phi_*) > 0$ and the conclusion follows. From now on, assume that $p > 5$. Recalling the value of ϕ^* given in (2.2.3), we infer that

$$\begin{aligned}
&2a_p\frac{(5-p)(\phi^*)^{p+1}(1-s^{p-1})}{p+1} + 2a_q\frac{(5-q)(\phi^*)^{q+1}(1-s^{q-1})}{q+1} \\
&= 2a_q(\phi^*)^{p+1}(1-s^{q-1})\frac{(5-q)}{q+1}\left(\frac{a_p(5-p)(q+1)}{a_q(5-q)(p+1)}\frac{(1-s^{p-1})}{(1-s^{q-1})} + (\phi^*)^{q-p}\right) \\
&= 2a_p(\phi^*)^{p+1}(1-s^{q-1})\frac{(5-q)}{q+1}\left(\frac{(5-p)(q+1)}{(5-q)(p+1)}\frac{(1-s^{p-1})}{(1-s^{q-1})} - \frac{p-1}{q-1}\frac{q+1}{p+1}\right) \\
&= 2a_p(\phi^*)^{p+1}(1-s^{q-1})\frac{(5-q)}{p+1}\left(\frac{(5-p)}{(5-q)}\frac{(1-s^{p-1})}{(1-s^{q-1})} - \frac{p-1}{q-1}\right) > 0,
\end{aligned}$$

where we have used in particular Lemma 2.3.3 for the last inequality. This implies that $F(\phi^*) > 0$ which, since $J(\omega, p, q) = C(\phi_0)F(\phi_0)$, finishes the proof. □

2.5 Determination of the sign of the slope

In this section, we determine for each possible values of a_p, a_q, p and q the sign of $J(\omega, p, q)$. Combined with the stability criteria of Section 2.2.2, this will prove Theorem 2.1.1. The general strategy of our proofs is the following. Recall from Lemma 2.3.1 that $J(\omega, p, q) = C(\phi_0)F(\phi_0)$, where

$$F(\phi_0) = \int_0^1 \frac{(5-p)\Phi_p + (5-q)\Phi_q}{(\Phi_p + \Phi_q)^{\frac{3}{2}}} s ds,$$

and $C(\phi_0) > 0$. Moreover, ω and ϕ_0 are in an increasing one to one correspondence. Hence, to determine the sign of J, it is sufficient to determine the sign of $F(\phi_0)$. To do this, we have two ingredients at our disposal. First, it is usually not difficult to establish that F has a constant sign on intervals of the type $(\phi_*, \phi_{0,1})$ or $(\phi_{0,1}, \phi^*)$. On the other hand, the expression for $\partial_{\phi_0} F(\phi_0)$ given in Lemma 2.3.2 allows us to show that $\partial_{\phi_0} F(\phi_0)$ has a constant sign on intervals of the type $(\phi_*, \phi_{0,2})$ or $(\phi_{0,2}, \phi^*)$. If the intervals of the two ingredients overlap and if the signs are matching, the conclusion will follow. For example, if $F(\phi_0) > 0$ on $(\phi_*, \phi_{0,1})$, and $\partial_{\phi_0} F(\phi_0) > 0$ on $(\phi_{0,2}, \phi^*)$ and $\phi_{0,1} > \phi_{0,2}$, then $F(\phi_0) > 0$ on (ϕ_*, ϕ^*). The detail of each case is given in the following sections.

2.5.1 The focusing-focusing case

In this section, we consider the case $a_p > 0$, $a_q > 0$. In this case we have $\Phi_p > 0$ and $\Phi_q > 0$.

Lemma 2.5.1. Let $a_p > 0$, $a_q > 0$ and $q \leqslant 5$. Then for all $\omega \in (0, \infty)$ we have

$$J(\omega, p, q) > 0,$$

and the family of standing waves is of type S.

Proof. If $q \leqslant 5$, then $5 - p > 0$ and $5 - q \geqslant 0$. Therefore for any $\phi_0 \in (0, \infty)$ we have

$$F(\phi_0) > 0,$$

which gives the desired conclusion. □

Lemma 2.5.2. Let $a_p > 0$, $a_q > 0$ and $p \geqslant 5$. Then for all $\omega \in (0, \infty)$ we have

$$J(\omega, p, q) < 0,$$

and the family of standing waves is of type U.

Proof. If $p \geqslant 5$, then $5 - p \leqslant 0$ and $5 - q < 0$. Therefore for any $\phi_0 \in (0, \infty)$ we have

$$F(\phi_0) < 0,$$

which gives the desired conclusion. □

The remaining case $p < 5 < q$ is a bit more involved to consider.

Lemma 2.5.3. Let $a_p > 0$, $a_q > 0$ and $p < 5 < q$. There exists $\phi_{0,1}$ (explicitly given in (2.5.1)) such that if $\phi_0^{q-p} > \phi_{0,1}^{q-p}$ then

$$F(\phi_0) < 0.$$

Proof. Using the formula (2.3.2) of $F(\phi_0)$ and replacing in the numerator of the integrand Φ_p and Φ_q by their expressions (2.3.1), we obtain

$$F(\phi_0) = \int_0^1 \frac{(5-p)\frac{2a_p}{p+1}\phi_0^{p+1}(s - s^p) + (5-q)\frac{2a_q}{q+1}\phi_0^{q+1}(s - s^q)}{(\Phi_p + \Phi_q)^{\frac{3}{2}}} ds.$$

Let

$$l(s) = (5-p)\frac{2a_p}{p+1}\phi_0^{p+1}(s - s^p) + (5-q)\frac{2a_q}{q+1}\phi_0^{q+1}(s - s^q),$$

and

$$k(s) = (\Phi_p + \Phi_q)^{\frac{3}{2}}.$$

We may reformulate $l(s)$ in the following way:

$$l(s) = \left((5-p)\frac{2a_p}{p+1}\phi_0^{p+1} + (5-q)\frac{2a_q}{q+1}\phi_0^{q+1}\frac{1 - s^{q-1}}{1 - s^{p-1}}\right)(s - s^p).$$

From Lemma 2.3.3, we know that the function $s \to \frac{1-s^{q-1}}{1-s^{p-1}}$ is increasing from 1 to $\frac{q-1}{p-1}$ when s goes from 0 to 1. Let $\phi_{0,0}$ be given by

$$\phi_{0,0}^{q-p} = -\frac{a_p(5-p)(q+1)(p-1)}{a_q(5-q)(p+1)(q-1)},$$

and assume from now on that $\phi_0 > \phi_{0,0}$. Then

$$\lim_{s \to 1} \frac{l(s)}{s - s^p} < 0,$$

and there exists $s^* \in [0,1)$ such that $l(s) > 0$ for $s \in (0, s^*)$ and $l(s) < 0$ for $s \in (s^*, 1)$.

Define $\tilde{k}$ by $\tilde{k}(s) = \frac{k(s)}{k(s^*)}$. Then $\tilde{k}(s^*) = 1$. As k and therefore $\tilde{k}$ is a positive decreasing function of s, for all $s \in (0,1)$ we have

$$\frac{l(s)}{\tilde{k}(s)} < l(s).$$

Integrating over $(0,1)$, we obtain

$$F(\phi_0) < \frac{1}{k(s^*)} \int_0^1 l(s) ds,$$

and $F(\phi_0)$ will be negative if the integral in the right member is. Define $\phi_{0,1} > \phi_{0,0}$ by

$$\phi_{0,1}^{q-p} = -\frac{a_p(5-p)(p-1)(q+1)^2}{a_q(5-q)(q-1)(p+1)^2}. \tag{2.5.1}$$

If $\phi_0 > \phi_{0,1}$, then

$$\int_0^1 l(s) ds = (5-p)\frac{a_p}{p+1}\phi_0^{p+1}\left(\frac{p-1}{p+1}\right) + (5-q)\frac{a_q}{q+1}\phi_0^{q+1}\left(\frac{q-1}{q+1}\right) < 0.$$

Hence for any $\phi_0 > \phi_{0,1}$ we have $F(\phi_0) < 0$. This concludes the proof. □

Lemma 2.5.4. Let $a_p > 0$, $a_q > 0$ and $p < 5 < q$. Let $\gamma = \frac{p+1}{2}$. There exists $\phi_{0,2}$ (explicitly given in (2.5.4)) such that the integrand I_γ of F_γ defined in (2.3.5) verifies

$$\frac{\partial I_\gamma}{\partial \phi_0} < 0$$

for all $\phi_0 \in (0, \phi_{0,2})$.

Proof. As $\gamma = \frac{p+1}{2}$, from Lemma 2.3.2 we have

$$\begin{aligned}\frac{\partial I_\gamma}{\partial \phi_0} &= \frac{1}{2}\phi_0^{\gamma-1}\left(\frac{((5-q)(p-q)\Phi_q)\,(\Phi_p+\Phi_q) - 3(p-q)^2\Phi_p\Phi_q}{(\Phi_p+\Phi_q)^{\frac{5}{2}}}\right), \\ &= \frac{1}{2}\phi_0^{\gamma-1}\Phi_q(p-q)\left(\frac{(5+2q-3p)\Phi_p + (5-q)\Phi_q}{(\Phi_p+\Phi_q)^{\frac{5}{2}}}\right).\end{aligned}$$

As a consequence $\partial_{\phi_0} I_\gamma < 0$ if

$$(5+2q-3p)\Phi_p + (5-q)\Phi_q > 0.$$

Replacing Φ_p and Φ_q by their expressions (2.3.1), this is equivalent to

$$(5+2q-3p)\frac{a_p}{p+1}\phi_0^{p+1}(1-s^{p-1})+(5-q)\frac{a_q}{q+1}\phi_0^{q+1}(1-s^{q-1})>0. \quad (2.5.2)$$

Since $p<5<q$, we have $5+2q-3p>0$, and therefore (2.5.2) becomes

$$\phi_0^{q-p}<-\frac{a_p}{a_q}\frac{(5+2q-3p)}{(5-q)}\frac{(q+1)}{(p+1)}\frac{(1-s^{p-1})}{(1-s^{q-1})}. \quad (2.5.3)$$

We know from Lemma 2.3.3 that

$$\frac{p-1}{q-1}<\frac{1-s^{p-1}}{1-s^{q-1}}.$$

Define

$$\phi_{0,2}^{q-p}=-\frac{a_p}{a_q}\frac{(5+2q-3p)}{(5-q)}\frac{(q+1)}{(p+1)}\frac{(p-1)}{(q-1)}. \quad (2.5.4)$$

If $\phi_0<\phi_{0,2}$ then (2.5.3) is verified, which concludes the proof. □

Lemma 2.5.5. Let $a_p>0$, $a_q>0$ and $p<5<q$. The function $F_\gamma(\phi_0)$ has at most one zero in $(0,\infty)$.

Proof. As $p<q$, we have

$$3(p-1)(p-q)<0,$$

hence

$$(5-p)(q+1)<(p+1)(5+2q-3p).$$

It implies

$$-\frac{a_p}{a_q}\frac{(5-p)}{(5-q)}\frac{(q+1)^2}{(p+1)^2}\frac{(p-1)}{(q-1)}<-\frac{a_p}{a_q}\frac{(5+2q-3p)}{(5-q)}\frac{(q+1)}{(p+1)}\frac{(p-1)}{(q-1)}.$$

Therefore, we have

$$\phi_{0,1}^{q-p}<\phi_{0,2}^{q-p}.$$

We know from Lemma 2.5.3 that $F_\gamma(\phi_0)<0$ if $\phi_0\in(\phi_{0,1},\infty)$, and from Lemma 2.5.4 that $F_\gamma(\phi_0)$ is decreasing for all $\phi_0\in(0,\phi_{0,2})$. As $\phi_{0,1}<\phi_{0,2}$, this implies that $F_\gamma(\phi_0)$ has at most one zero. □

Lemma 2.5.6. Let $a_p>0$, $a_q>0$ and $p<5<q$. There exists $\omega_1\in(0,\infty)$ such that

$$J(\omega,p,q)>0 \text{ for } \omega<\omega_1,\quad J(\omega_1,p,q)=0,\quad J(\omega,p,q)<0 \text{ for } \omega>\omega_1,$$

and the family of standing waves is of type SU.

Proof. From Proposition 2.4.1, we know that $J(\omega,p,q)>0$ for ω close to 0. Combined with Lemmas 2.5.3 and 2.5.5, this implies the desired result. □

2.5.2 The focusing-defocusing case

In this section, we consider the case $a_p > 0$, $a_q < 0$. In this case $\Phi_p > 0$ and $\Phi_q < 0$.

Lemma 2.5.7. Let $a_p > 0$, $a_q < 0$ and $p \leqslant 5 < q$. For any $\omega \in (0, \omega^*)$, we have

$$J(\omega, p, q) > 0,$$

and the family of standing waves is of type S.

Proof. We have $5 - p \geqslant 0$, and $5 - q < 0$. Therefore $F(\phi_0) > 0$ for any $\phi_0 \in (0, \phi^*)$, which gives the desired result. □

Lemma 2.5.8. Let $a_p > 0$, $a_q < 0$ and $p < q \leqslant 5$. Let $\gamma = \frac{p+1}{2}$. Then the integrand I_γ of F_γ defined in (2.3.5) verifies

$$\frac{\partial I_\gamma}{\partial \phi_0} > 0$$

for all $\phi_0 \in (0, \phi^*)$.

Proof. From Lemma 2.3.2 with $\gamma = \frac{p+1}{2}$, we have

$$\frac{\partial I_\gamma}{\partial \phi_0} = \frac{1}{2}\phi_0^{\gamma-1}\left(\frac{((5-q)(p-q)\Phi_q)\,(\Phi_p + \Phi_q) - 3(p-q)^2\Phi_p\Phi_q}{(\Phi_p + \Phi_q)^{\frac{5}{2}}}\right).$$

Since $5-q \geqslant 0$, $p-q < 0$ and $\Phi_q < 0$, we have $\frac{\partial I_\gamma}{\partial \phi_0} > 0$ for any $\phi_0 \in (0, \phi^*)$. □

Lemma 2.5.9. Let $a_p > 0$, $a_q < 0$ and $5 < p < q$. Let $\gamma = p - q + 3$. Then the integrand I_γ of F_γ defined in (2.3.5) verifies

$$\frac{\partial I_\gamma}{\partial \phi_0} > 0$$

for all $\phi_0 \in (0, \phi^*)$.

Proof. Let $\gamma = p - q + 3$.

$$\frac{\partial I_\gamma}{\partial \phi_0} = \phi_0^{\gamma-1}\left(\frac{((5-p)(p-2q+5)\Phi_p + (5-q)(2p-3q+5)\Phi_q)\,(\Phi_p + \Phi_q)}{2\,(\Phi_p + \Phi_q)^{\frac{5}{2}}}\right) - \phi_0^{\gamma-1}\left(\frac{3(p-q)^2\Phi_p\Phi_q}{2\,(\Phi_p + \Phi_q)^{\frac{5}{2}}}\right).$$

The sign of $\frac{\partial I_\gamma}{\partial \phi_0}$ is the same as the sign of the numerator of the fraction. Factoring out Φ_p^2, the sign is the same as the one of the second order polynomial in $\frac{\Phi_q}{\Phi_p}$ given by

$$(5-q)(2p-3q+5)\left(\frac{\Phi_q}{\Phi_p}\right)^2+2(5-p)(2p-3q+5)\left(\frac{\Phi_q}{\Phi_p}\right)+(5-p)(p-2q+5).$$

As $2p-3q+5<0$ and $5-q<0$, the coefficient of the term of order 2 is positive. Therefore to show that the polynomial is positive, it is sufficient to show that the discriminant Δ, given by

$$\begin{aligned}\Delta &= 4(5-p)(2p-3q+5)((5-p)(2p-3q+5)-(5-q)(p-2q+5)),\\ &= -8(5-p)(2p-3q+5)(p-q)^2,\end{aligned}$$

is negative. We have $2p-3q+5<0$ and $5-p<0$, therefore $\Delta<0$. This concludes the proof. □

Lemma 2.5.10. Let $a_p>0$, $a_q<0$.

— Let $p<q\leqslant 5$. Then for any $\omega\in(0,\omega^*)$, we have

$$J(\omega,p,q)>0,$$

and the family of standing waves is of type S.

— Let $5<p<q$. Then there exist $\omega_1\in(0,\infty)$ such that

$$J(\omega,p,q)<0 \text{ for } \omega<\omega_1,\quad J(\omega_1,p,q)=0,\quad J(\omega,p,q)>0 \text{ for } \omega>\omega_1,$$

and the family of standing waves is of type US.

Proof. In both cases, we infer from Lemmas 2.5.8 and 2.5.9 that for any $\omega\in(0,\omega^*)$, the function $\omega\to J(\omega,p,q)$ changes sign (from negative to positive) at most once on $\omega\in(0,\omega^*)$.

To establish the desired conclusion, we consider the values of J close to the endpoints. As $\omega\to 0$, we have established in Proposition 2.4.1 that for ω close to 0, we have

$$J(\omega,p,q)>0 \text{ for } p\leqslant 5,\quad J(\omega,p,q)<0 \text{ for } p>5.$$

As J is increasing, this gives the conclusion for the first part of the Lemma.

For the second part of the Lemma, we look at the limit $\omega\to\omega^*$ (i.e. $\phi_0\to\phi^*$). From Proposition 2.4.7, for $5<p<q$ and for ω close to ω^* we have

$$J(\omega,p,q)>0,$$

which gives the second part of the Lemma. □

2.5.3 The defocusing-focusing case

In this section, we consider the case $a_p < 0$, $a_q > 0$. In this case $\Phi_p < 0$ and $\Phi_q > 0$.

Lemma 2.5.11. Let $a_p < 0$, $a_q > 0$ and $p < q < 5$. Let $\gamma = \frac{q+1}{2}$. If $3q \geqslant 2p+5$, then the integrand I_γ of F_γ defined in (2.3.5) verifies

$$\frac{\partial I_\gamma}{\partial \phi_0} > 0$$

for all $\phi_0 \in (\phi_*, \infty)$.

Proof. As $\gamma = \frac{q+1}{2}$, from Lemma 2.3.2 we have

$$\begin{aligned}
\frac{\partial I_\gamma}{\partial \phi_0} &= \frac{1}{2}\phi_0^{\gamma-1}\left(\frac{((5-p)(q-p)\Phi_p)\,(\Phi_p+\Phi_q) - 3(p-q)^2\Phi_p\Phi_q}{(\Phi_p+\Phi_q)^{\frac{5}{2}}}\right), \\
&= \frac{1}{2}\phi_0^{\gamma-1}\Phi_p(q-p)\left(\frac{(5-p)\Phi_p + (5-p)\Phi_q + 3(p-q)\Phi_q}{(\Phi_p+\Phi_q)^{\frac{5}{2}}}\right), \\
&= \frac{1}{2}\phi_0^{\gamma-1}\Phi_p(q-p)\left(\frac{(5-p)\Phi_p + (5+2p-3q)\Phi_q}{(\Phi_p+\Phi_q)^{\frac{5}{2}}}\right).
\end{aligned}$$

As $0 < 5-p$ and $2p+5-3q \leqslant 0$ we have

$$(5-p)\Phi_p + (5+2p-3q)\Phi_q < 0.$$

As a consequence $\frac{\partial I_\gamma}{\phi_0} > 0$ for all $\phi_0 \in (\phi_*, \infty)$ when $5+2p-3q \leqslant 0$, which is the desired conclusion. □

Lemma 2.5.12. Let $a_p < 0$, $a_q > 0$ and $p < q < 5$. Let $\gamma = p - q + 3$. If $3q < 2p+5$ then the integrand I_γ of F_γ defined in (2.3.5) verifies

$$\frac{\partial I_\gamma}{\partial \phi_0} > 0$$

for all $\phi_0 \in (\phi_*, \infty)$.

Proof. As $\gamma = p - q + 3$, from Lemma 2.3.2 we have

$$\begin{aligned}
\frac{\partial I_\gamma}{\partial \phi_0} = \phi_0^{\gamma-1}\left(\frac{((5-p)(p-2q+5)\Phi_p + (5-q)(2p-3q+5)\Phi_q)\,(\Phi_p+\Phi_q)}{2\,(\Phi_p+\Phi_q)^{\frac{5}{2}}}\right) \\
+ \phi_0^{\gamma-1}\left(\frac{-3(p-q)^2\Phi_p\Phi_q}{2\,(\Phi_p+\Phi_q)^{\frac{5}{2}}}\right).
\end{aligned}$$

If the numerator of the fraction is positive then the derivative is positive. Factorizing out Φ_p^2, the sign of the numerator is the same as the one of the quadratic polynomial in $\frac{\Phi_q}{\Phi_p}$ given by

$$(5-q)(2p-3q+5)\left(\frac{\Phi_q}{\Phi_p}\right)^2+2(5-p)(2p-3q+5)\left(\frac{\Phi_q}{\Phi_p}\right)+(5-p)(p-2q+5).$$

As $2p-3q+5>0$ and $5-q>0$, the coefficient of the term of order 2 is positive. Therefore to show that the polynomial is positive, it is sufficient to show that the discriminant Δ, given by

$$\begin{aligned}\Delta &= 4(5-p)(2p-3q+5)((5-p)(2p-3q+5)-(5-q)(p-2q+5)),\\ &= -8(5-p)(2p-3q+5)(p-q)^2,\end{aligned}$$

is negative. We have $2p-3q+5>0$ and $5-p>0$, therefore $\Delta<0$. This concludes the proof. □

Lemma 2.5.13. Let $a_p<0$, $a_q>0$ and $p<q<5$.

— If $q\leqslant 7-2p$, then for any $\omega\in(0,\infty)$, we have

$$J(\omega,p,q)>0,$$

and the family of standing waves is of type S.

— If $q>7-2p$, then there exist $\omega_1\in(0,\infty)$ such that

$$J(\omega,p,q)<0 \text{ for } \omega<\omega_1,\quad J(\omega_1,p,q)=0,\quad J(\omega,p,q)>0 \text{ for } \omega>\omega_1,$$

and the family of standing waves is of type US.

Proof. Lemmas 2.5.11 and 2.5.12 implies F_γ changes sign only once on $(0,\omega^*)$. From Proposition 2.4.2, we know that as $\omega\to 0$, we have $J(\omega,p,q)>0$ when $q\leqslant 7-2p$, which gives the conclusion for the first part of the Lemma. When $q>7-2p$, from Proposition 2.4.2, we know that as $\omega\to 0$, we have $J(\omega,p,q)<0$. Since, from Proposition 2.4.6, we know that $J(\omega,p,q)>0$ for large ω, the conclusion follows for the second part of the Lemma. □

Lemma 2.5.14. Let $a_p<0$, $a_q>0$ and $p<5\leqslant q$. For any $\omega\in(0,\infty)$, we have

$$J(\omega,p,q)<0,$$

and the family of standing waves is of type U.

Proof. We have $5-p>0$, $5-q\leqslant 0$, $\Phi_p<0$ and $\Phi_q>0$. Therefore we directly see on the expression (2.3.2) of $F(\phi_0)$ that $F(\phi_0)<0$, which gives the desired result. □

Lemma 2.5.15. Let $a_p < 0$, $a_q > 0$ and $5 \leqslant p < q$. For any $\omega \in (0, \infty)$, we have

$$J(\omega, p, q) < 0,$$

and the family of standing waves is of type U.

Proof. We know that $\phi_* < \phi_0$, therefore $-\frac{a_p}{a_q}\frac{q+1}{p+1} < \phi_0^{q-p}$. As $\frac{5-p}{5-q} < 1$, we have $-\frac{a_p}{a_q}\frac{q+1}{p+1}\frac{5-p}{5-q} < \phi_0^{q-p}$. From Lemma 2.3.3 we know that $\frac{1-s^{p-1}}{1-s^{q-1}} < 1$, hence

$$-\frac{a_p}{a_q}\frac{(q+1)}{(p+1)}\frac{(5-p)}{(5-q)}\frac{1-s^{p-1}}{1-s^{q-1}} < \phi_0^{q-p},$$

which is equivalent to

$$\frac{(5-p)}{(5-q)} < -\frac{\Phi_q}{\Phi_p},$$

which implies

$$(5-p)\Phi_p + (5-q)\Phi_q < 0.$$

This implies that $F(\phi_0) < 0$ which gives the desired result. □

2.5.4 The critical frequency

Observe that, as a by-product of the analysis of the previous sections, we should have instability at the critical frequency (under regularity assumptions on the nonlinearity) when there is a stability change. Indeed, we have

$$\begin{aligned}\partial_\omega^2 M(\phi_\omega) &= \partial_\omega \left(C(\phi_0)\phi_0^{-\gamma} F_\gamma(\phi_0)\right) \\ &= \partial_\omega\phi_0 \left(\partial_{\phi_0}\left(C(\phi_0)\phi_0^{-\gamma}\right) F_\gamma(\phi_0) + C(\phi_0)\phi_0^{-\gamma}\partial_{\phi_0} F_\gamma(\phi_0)\right).\end{aligned}$$

At the stability change, we have $F(\phi_0) = 0$. Therefore, at the stability change,

$$\partial_\omega^2 M(\phi_\omega) = (\partial_\omega\phi_0) C(\phi_0)\phi_0^{-\gamma}\partial_{\phi_0} F_\gamma(\phi_0).$$

As we have shown that in this case $\partial_{\phi_0} F_\gamma(\phi_0) \neq 0$, the criterion (2.2.4) holds.

2.6 Numerical experiments

To explore further the stability/instability of standing waves, we have performed a series of numerical experiments in the case $a_p < 0$, $a_q > 0$, $1 < p < q < 5$.

The Python language and the specific libraries Numpy, Scipy and Matplotlib have been used to perform the experiments. The code is made available in [53].

2.6.1 The critical surface for stability/instability

We first analyzed the critical surface in (ω, p, q) separating instability from stability. To this aim, we first have implemented the calculation of $J(\omega, p, q)$. The function `integrate.quad` has been used to perform the integration. While the results are overall satisfactory, in some cases the function returned incorrect results, with problems increasing as ω was taken closer to 0.

To estimate the critical ω at given (p, q), we have used the classical bisection method, which has the advantage of being very robust. The algorithm is divided into two parts.

First, we find an initial interval $[\omega_0, \omega_1]$ in which we are sure that $\omega \to J(\omega, p, q)$ changes sign. A natural choice for ω_0 is 0. To find a suitable ω_1, we simply start with $\omega_1 = 1$ and test if $J(\omega_1, p, q) > 0$. If not, we replace ω_1 by $2\omega_1$ and repeat until $J(\omega_1, p, q) > 0$. To avoid running an infinite loop, we break it when $\omega_1 > 10^{10}$ and do not search for ω_c in these cases. Second, we apply the bisection method to search for a root of $J(\omega, p, q)$ inside $[\omega_0, \omega_1]$. As this approach, while being efficient, is also relatively slow, we took advantage of the computer power of our department to run computations in parallel on the $(p, q) \in [1, 5] \times [1, 5]$ grid with $dp = dq = 0.01$.

We have represented the critical surface

$$\{(p, q, \omega_c(p, q))\}$$

for $a_p = -1$ and three different values of $a_q = 1/2, 1, 2$ in Figure 2.1.

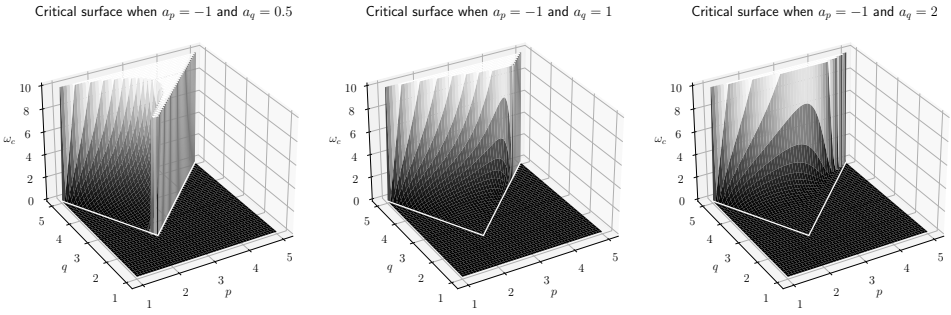

Figure 2.1 – Critical surface $\{(p, q, \omega_c(p, q))\}$ for $a_p = -1$ and $a_q = 1/2, 1, 2$. The white lines represent $q = 7 - 2p$ and $q = p$, where the transition from $\omega_c = 0$ to $\omega_c > 0$ occurs.

Several observations can be made on the critical surface. As (p, q) approaches the line $q = 5$, we have $\omega_c(p, q) \to \infty$, which is consistent with the fact that standing waves are all unstable on this line.

It can be observed that on the line $q = 7 - 2p$ the transition is continuous, no matter the value of a_q. To the contrary, the transition is continuous on the line $p = q$ when $a_q \geqslant 1$, whereas it becomes discontinuous when $a_q < 1$, in which case $\omega_c(p, q) \to \infty$ as $q \to p$.

To investigate more the transition close to the lines $q = 7 - 2p$ and $q = p$, we plot slices of the critical surface for a fixed value of q in Figure 2.2. We chose to present the results when $q = 4$, but similar results are obtained with other values of q. On Figure 2.2, we observe that when $a_q = |a_p| = 1$, the transition between $\omega_c(p, q) = 0$ and $\omega_c(p, q) > 0$ at $q = p$ and $q = 7 - 2p$ is Lipschitz. When $a_q = 2 > |a_p| = 1$, the transition seems smoother (but closer observations will reveal otherwise) when $q = p$, whereas it remains Lipchitz when $q = 7 - 2p$. To the contrary, when $a_q = 1/2 < |a_p| = 1$, the transition is discontinuous when $q = p$, whereas it seems smoother at $q = 7 - 2p$.

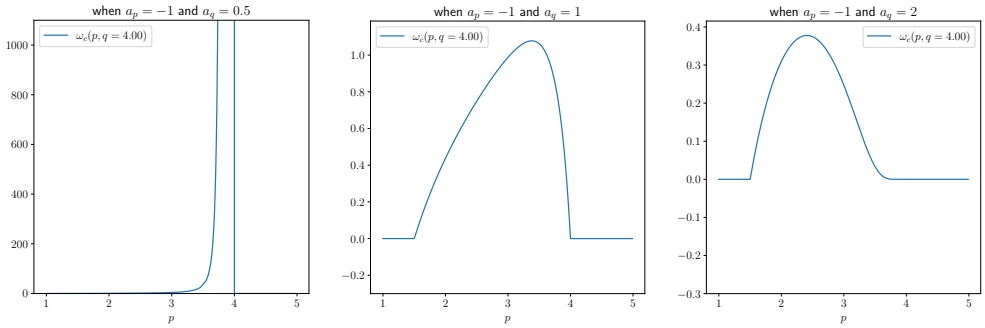

Figure 2.2 – Slices of the critical surface for fixed value of $q = 4$

To confirm our previous observations, we zoomed on the slices of Figure 2.2 and obtained the results presented in Figure 2.3. Observing closer the

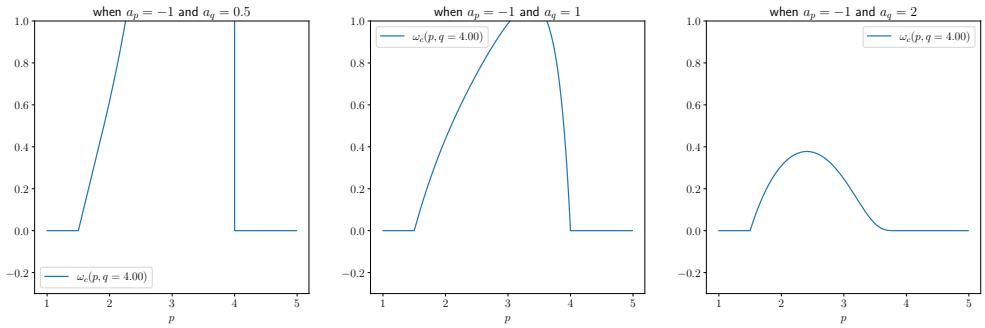

Figure 2.3 – Zoom on slices of the critical surface for fixed value of $q = 4$

transition from $\omega_c > 0$ to $\omega_c = 0$ on fixed q slices of Figure 2.3, we realize that the transition on the left ($q = 7 - 2p$) seems to be always only Lipschitz, contrary to what could be inferred from the previous observation. On the

other hand, the previous observation when $p = q$ is confirmed: the transition seems smooth when $a_q = 2$, Lipschitz when $a_q = 1$, and discontinuous when $a_q = 1/2$. This is reflecting the fact that when $p \to q$, the family of soliton profiles has a different behavior for different values of a_q. When $a_q > |a_p|$, soliton profiles for $p = q$ exist and are stable (hence $\omega_c(p, q = p) = 0$), whereas for $a_q = |a_p|$ the two nonlinearities exactly compensate and for $|a_p| > a_q$ the defocusing nonlinearity becomes the dominant one (and solitary waves do not even exist).

From the previous observations, we know that at fixed q the map $p \to \omega_c(p, q)$ has a unique maximum if $a_q = 1$ or $a_q = 2$ (if $a_q = 1/2$, we have seen that the map increases towards infinity as p approaches q). Denote by $p_{\max}(q)$ the value realizing this maximum, i.e.

$$\omega_c(p_{\max}(q), q) = \max_{1<p<5} \omega_c(p, q).$$

The line $\{(p_{\max}(q), q), q > 7/3\}$ is represented in Picture 2.4. When $a_q = 1$,

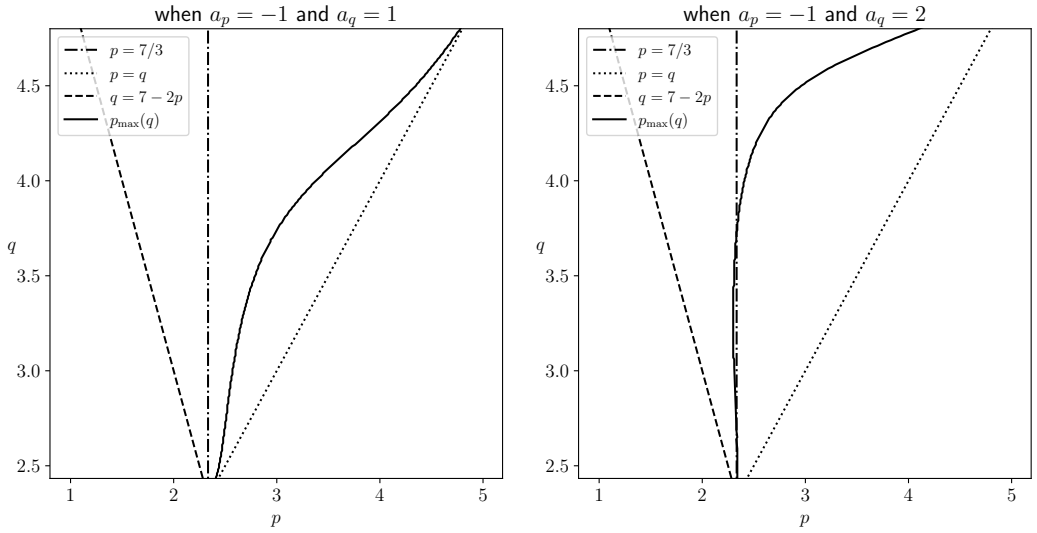

Figure 2.4 – Curve of the argument of $\max_p \omega_c(p, q)$ in terms of q

we observe that the line is tangent to the line $p = q$ when q is close to $7/3$ or close to 5. On the other hand, when $a_q = 2$, the line seems to be tangent to the line $p = 7/3$ when q is close to $7/3$. It approaches the point $(5, 5)$ as q goes to 5, but does not seem to be tangent to the line $p = q$ (it was however not possible to obtain numerically a relevant picture closer to $q = 5$, which leaves open the question of the behavior when q is close to 5).

2.6.2 Evolution for initial data close to standing waves

We now turn to numerical experiments for the stability/instability of solitary waves for the flow of (2.1.1). For the experiments, we have used the Crank-Nicolson scheme with relaxation presented in [19] which has been proved to be efficient for the numerical simulation of the Schrödinger flow (see e.g. [10] for the comparison of various schemes used for the dynamical simulations of the nonlinear Schrödinger flow).

For a time discretization step δ_t (typically $\delta_t = 10^{-3}$), denote by u^n the approximation of u at time $t_n = n\delta_t$. The semi-discrete (in time) relaxation scheme is then given by

$$\begin{cases} \frac{\phi^{n+\frac{1}{2}}+\phi^{n-\frac{1}{2}}}{2} = a_p|u^n|^p + a_q|u^n|^q, \\ i\frac{u^{n+1}-u^n}{\delta_t} + \partial_{xx}\left(\frac{u^{n+1}+u^n}{2}\right) = -\left(\frac{u^{n+1}+u^n}{2}\right)\phi^{n+\frac{1}{2}}, \end{cases}$$

with the understanding that $u^0 = u_0$ and $\phi^{-\frac{1}{2}} = a_p|u^0|^p + a_q|u^0|^q$. For the implementation, the scheme is further discretized in space with second order finite differences for the second derivative operator, with Dirichlet boundary conditions.

We have performed simulations for (p, q) on the line $q = 2p-1$, as for this range of exponents explicit formulas are available for solitary wave profiles (see e.g. [58]) and can be used easily to construct initial data. Considering other ranges of (p, q) would have been possible, to the extend of additional computations to first obtain numerically solitary waves. As we do not expect different behavior to occur for other values of (p, q), the restriction to the line $q = 2p - 1$ is harmless.

The initial data that we construct are all based on a solitary wave profile ϕ_ω. They are of the form

$$u_0 = \phi_\omega + \varepsilon\psi,$$

where $0 < \varepsilon \ll 1$ is used to adjust the size of the perturbation and ψ is the direction of perturbation, which can be for example

$$\psi = \phi_\omega, \quad \psi = \phi_\omega \cos, \quad \psi = \phi_\omega \tanh, \quad \psi = \phi_\omega(\cdot - 3).$$

As our numerical scheme uses Dirichlet conditions at the bounds of the space interval, we have chosen to work with well-localized perturbation in order to avoid possible numerical reflections due to the boundary conditions. Our experiments consisted in taking one of the previous possibility as initial data, running the simulation of the nonlinear Schrödinger flow, and observe the pattern of the outcome. It turns out that after running numerous simulations, we have observed only three possible types of behavior:

— Stability;
— Growth followed by slightly decreasing oscillations;
— Dispersion.

Observe that our numerical results are in part similar to the ones obtained and discussed in further details in [23, Section 4] in the case of the $2d$ cubic-quintic (focusing-defocusing) nonlinear Schrödinger equation.

Stability means that the solution does not leave the neighborhood of ϕ_ω (up to phase shift and translations). We obviously expect to see this behavior in the cases where the values of the parameters p, q, and ω ensure that the solitary wave will be stable. However, one thing which is not easily decided by the theory is the size of the basin of stability of the solitary wave. In other words, finding a perturbation of the solitary wave sufficiently large to be visible, but small enough so that the corresponding solution remains in the vicinity of the solitary wave requires delicate adjustments.

An example of a stable behavior is provided in Figure 2.5. Observe that while on the global scale the solution seems to be behave exactly as a solitary wave (left picture), when getting a closer look at the maximum value (right picture) we observe small oscillations (with an amplitude of order 0.03).

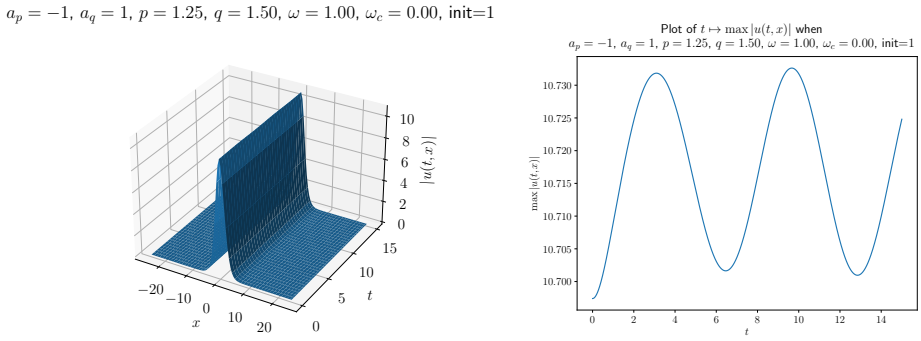

Figure 2.5 – Example of a stable numerical solution. The initial data is $u^0 = (1+\varepsilon)\phi_\omega$, $\varepsilon = 10^{-2}$.

The second behavior consists in a first phase of focusing growth of the profile, which is similar to what can be observed when instability of solitons is by blow-up (e.g. for power-type supercritical nonlinearities. However, after a certain time, the focusing phase stops and is followed by a phase in which the solution seems to oscillate around another profile. The size of the oscillation is decaying, but at a slow pace, and we have not run the simulation long enough to observe convergence toward a final state. An example of such a behavior is presented in Figure 2.6.

Finally, the third behavior that we have observed could be characterized as scattering, as the profile of the solution is simultaneously decreasing in height

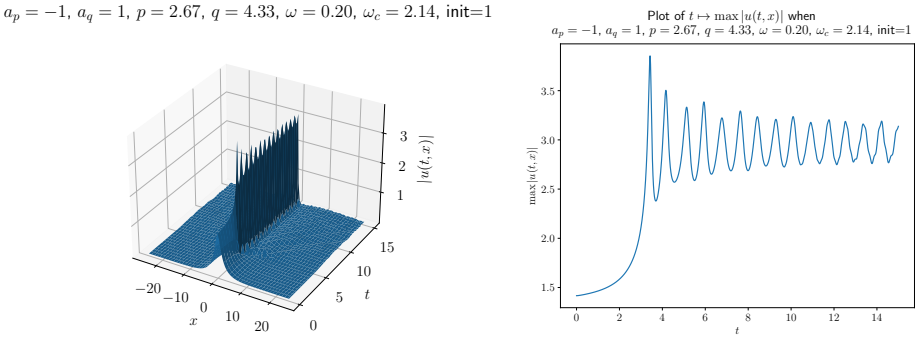

Figure 2.6 – Example of a growing/oscillating numerical solution. The initial data is $u^0 = (1+\varepsilon)\phi_\omega$, $\varepsilon = 10^{-2}$.

while spreading over the whole line. As before, the decay is rather slow and we have not run the simulation long enough for the solution to converge to 0. An example of such a behavior is presented in Figure 2.7. Observe that the domain of calculation is $[-50, 50]$, but the solution is represented only on $[-20, 20]$, which explains the non-zero values observed at the boundaries on the left figure.

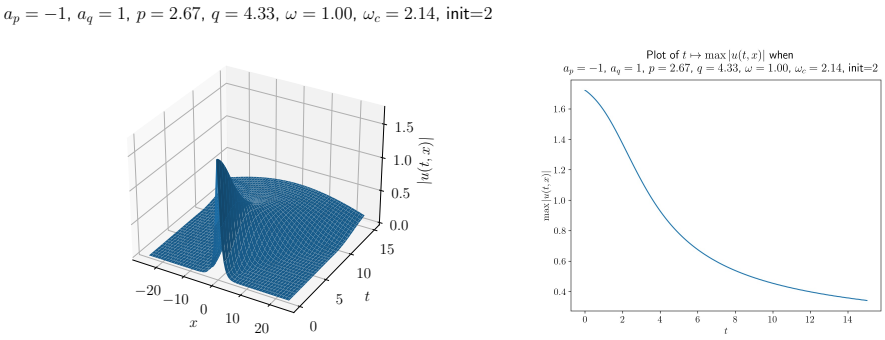

Figure 2.7 – Example of a scattering numerical solution. The initial data is $u^0 = (1-\varepsilon)\phi_\omega$, $\varepsilon = 10^{-2}$.

2.7 Notebooks

This section contains the Python code that we have developed in order to illustrate our results. The first notebook provided is dedicated to the identification of the critical ω value, at which stability changes occur. The critical surface has been represented in (ω, p, q) to provide a clear visual representation of the transition between instability and stability. In addition, we have also included a second notebook in this section. This notebook centers on numerical experiments and specifically explores the evolution of initial data close to standing waves.

Notebook 1

[1]:
```
%%file script_critical_omega.py

"""
Script for the surface w_critical(p1,p2).
Here with small values of p1 p2.
True script is runned on a dedicated server where multiprocessing will␣
 ↪allow rapid calculations.
Outcomes of the script are saved under w_critical_{date}.out
Exploitation of datas obtained with the script is given at the end of␣
 ↪the notebook.
"""

import numpy as np
import scipy as sp
import scipy.optimize as sco
from scipy import integrate
import time
from datetime import datetime
from concurrent.futures import ProcessPoolExecutor
from functools import partial
import shelve
```

```
Overwriting script_critical_omega.py
```

[2]:
```
%%file --append script_critical_omega.py


def f1(z,p1,p2,a1=-1,a2=1):
    s=np.abs(z)
    return -a1*s**((p1-1)/2)-a2*s**((p2-1)/2)

def F1(z,p1,p2,a1=-1,a2=1):
    s=np.abs(z)
    return -(a1*s**((p1+1)/2))*2/(p1+1)-(a2*s**((p2+1)/2))*(2/(p2+1))

def U(s,w,p1,p2,a1=-1,a2=1):
    s=np.abs(s)
    return w*s+F1(s,p1,p2,a1,a2)

def U_der(s,w,p1,p2,a1=-1,a2=1):
    s=np.abs(s)
    return w+f1(s,p1,p2,a1,a2)

def U_div_s(s,w,p1,p2,a1=-1,a2=1):
    s=np.abs(s)
    return (w-(a1*s**((p1-1)/2))*2/(p1+1)-(a2*s**((p2-1)/2))*(2/(p2+1)))
```

```
def U_div_s_prime(s,w,p1,p2,a1=-1,a2=1):
    s=np.abs(s)
    return -(a1*s**((p1-3)/2))*2/(p1+1)*(p1-1)/2-(a2*s**((p2-3)/2))*(2/
 ↪(p2+1))*(p2-1)/2

def a(w,p1,p2,a1=-1,a2=1):
    a=sco.fsolve(U_div_s,␣
 ↪10,args=(w,p1,p2,a1,a2),fprime=U_div_s_prime,xtol=10**(-12))
    a=np.abs(a)
    if a==0:
        print("error in a , a is 0")
    return a

def J(w,p1,p2,a1=-1,a2=1):
    A=a(w,p1,p2,a1,a2)
    def integrand(s):
        C=-A**(1.5)/(2*U_der(A,w,p1,p2,a1,a2))
        I=(3+A*s*(U_der(A,w,p1,p2,a1,a2)-U_der(A*s,w,p1,p2,a1,a2))/
 ↪U(A*s,w,p1,p2,a1,a2))*np.sqrt(s)/np.sqrt(np.
 ↪abs(U(A*s,w,p1,p2,a1,a2)))
        return C*I
    I=integrate.quad(integrand, 0, 1,epsabs=10**(-100),limit=100)
    return I[0]

# construction of a function returning the critical omega

def w_critical(p1,p2,a1=-1,a2=1):
    dp1=0.0001
    dp2=0.0001
    if ((p2<=p1+dp1/2) or (p2-dp2/2<(-2*p1+7))):
        return 0
    else:
        try:
            precision=1
            tol=0.00001
            w1,w2=0,1
            while J(w2,p1,p2,a1,a2)<0:
                w2=2*w2
                if w2>10**(10):
                    w1=10**(10)
                    break
            while precision>tol:
                w_tmp=w1+(w2-w1)/2
                if J(w_tmp,p1,p2,a1,a2)>0:
                    w2=w_tmp
                else:
```

```
                    w1=w_tmp
                precision=(w2-w1)/w2
                if w2<10**(-12):
                    break
        except:
            pass
    return w1
```

```
Appending to script_critical_omega.py
```

[13]:
```
%%file --append script_critical_omega.py

# computation of the critical omega map with multi-processing


p1 = np.linspace(2, 5, 5, endpoint=False)
p2 = np.linspace(2, 5, 5, endpoint=False)
P1,P2 = np.meshgrid(p1,p2)
#P1P2=np.array([P1.flatten(),P2.flatten()])

# construct a new w_critical function for fixed values of a1 and a2
a1=-1
a2=0.5
partial_w_critical = partial(w_critical,a1=a1,a2=a2)


w_critical_P1P2=[]
if __name__ == "__main__":
    PPE = ProcessPoolExecutor()
    w_critical_P1P2 = list(PPE.map(partial_w_critical,P1.flatten(),P2.
 ↪flatten()))
```

```
Appending to script_critical_omega.py
```

[14]:
```
%%file --append script_critical_omega.py

# Save all variables (with in particular w_critical) to file with date␣
 ↪in file name
date = datetime.now().strftime("%Y_%m_%d-%I_%M_%S_%p")

filename=f'w_critical_{date}.out'
my_shelf = shelve.open(filename,'n') # 'n' for new

for key in dir():
    try:
        my_shelf[key] = globals()[key]
    except:
        #
```

```
        # __builtins__, my_shelf, and imported modules can not be␣
 ↪shelved.
        #
        pass
my_shelf.close()
```

```
Appending to script_critical_omega.py
```

[15]:
```
# To restore all needed variables (with in particular p1,p2, and␣
 ↪w_critical)
import shelve

#filename='w_critical_2021_07_10-07_59_17_PM.out' # a2=2
filename='w_critical_2021_07_10-08_00_51_PM.out' # a2=1
#filename='w_critical_a1_is_-1_a2_is_0.5_2021_07_20-01_03_33_PM.out'#␣
 ↪a2=1/2

my_shelf = shelve.open(filename)
list_of_variables = ['a1','a2','p1','p2','P1','P2','w_critical_P1P2']
for key in list_of_variables:#my_shelf:
    try:
        globals()[key]=my_shelf[key]
    except:
        print(f'Houston, we have a problem with {key}')
        pass
my_shelf.close()
```

[16]:
```
print(f"a1={a1}")
print(f"a2={a2}")
print(f"p1={p1[1]} {p1[2]} ... {p1[-2]} {p1[-1]}")
print(f"p2={p2[1]} {p2[2]} ... {p2[-2]} {p2[-1]}")
```

```
a1=-1
a2=1
p1=1.01 1.02 ... 4.98 4.99
p2=1.01 1.02 ... 4.98 4.99
```

[7]:
```
#%matplotlib notebook
%matplotlib inline
%config InlineBackend.figure_format = 'retina'
import numpy as np
import matplotlib
import matplotlib.pyplot as plt
```

[8]:
```
TeXFont = True
#plt.rcParams['figure.figsize']=[6,(3/4)*6]
if TeXFont:
    plt.rcParams['font.size'] = 14.0          # font size
    plt.rcParams['mathtext.fontset'] = 'cm'   # computer moder math font
```

```
    plt.rcParams['text.usetex'] = True       # use tex engine for␣
 ↪everything (useful for the axes labels)
else:
    plt.rcParams['text.usetex'] = False
FontSize = 14
```

[9]:
```
w_critical_P1P2=np.reshape(w_critical_P1P2,(-1,np.shape(P2)[1]))
w_critical_P1P2_clip=np.copy(w_critical_P1P2)
w_critical_P1P2_clip[w_critical_P1P2_clip>10]=10# clipping the larger␣
 ↪values of w_critical
fig1 = plt.figure(figsize=[6,6])
ax1 = plt.axes(projection='3d')
ax1.plot_surface(P1,P2,w_critical_P1P2_clip,cmap='gist_gray',␣
 ↪edgecolor='none')
ax1.plot(p1[p1>7/3],p1[p1>7/3],zorder=3,color='w')
ax1.plot(p1[p1<7/3],7-2*p1[p1<7/3],zorder=3,color='w')
ax1.azim = -120
ax1.set_title(rf"Critical surface when $a_p={a1}$ and $a_q={a2}$")
# choose colormap from https://matplotlib.org/stable/tutorials/colors/
 ↪colormaps.html
# e.g. gist_gray or binary or inferno or viridis
ax1.set_xlabel(r"$p$",fontsize=FontSize)
ax1.set_ylabel(r"$q$",fontsize=FontSize)
ax1.set_zlabel(r"$\omega_c$",fontsize=FontSize)
ax1.xaxis.set_rotate_label(False)  # disable automatic rotation
ax1.yaxis.set_rotate_label(False)  # disable automatic rotation
ax1.zaxis.set_rotate_label(False)  # disable automatic rotation
fig1.savefig(f'surface_w_c_a1_is_{a1}_a2_is_{a2}.
 ↪pdf',transparent=True,orientation='landscape',format='pdf',
bbox_inches='tight')
```

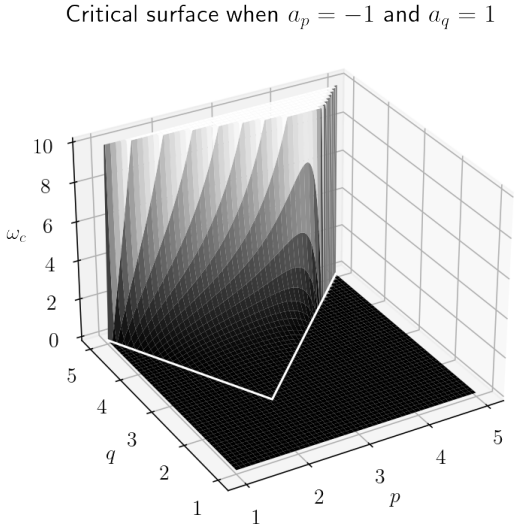

Legend: Critical surface $\{(p,q,\omega_c(p,q))\}$ for $a_p = -1$ and $a_q = 1/2, 1, 2$. The white lines represent $q = 7 - 2p$ and $q = p$, where the transition from $\omega_c = 0$ to $\omega_c = 0$ occurs.

Several observations can be made on the critical surface. As (p,q) approaches the line $q = 5$, we have $\omega_c(p,q) \to \infty$, which is consistent with the fact that standing waves are all unstable on this line, or in other word $\omega_2(p, q = 5) = \infty$.

Different behaviors appear close to the line $p = q$ depending on the value of a_p and a_q. When $a_q > a_p$, the transition is smooth, when $a_q = a_p$, the transition is sharp, whereas when $a_q < a_p$ we have $\omega_c(p,q) \to \infty$ as $q \to p$.

To investigate more the transition close the lines $q = 7 - 2p$ and $q = p$, we plot slices of the critical surface for fixed values of q.

[10]:
```
value_p2=4
index=np.argmax(p2>=value_p2)

fig2 = plt.figure(figsize=[6,6])
ax2 = plt.axes()
# Slice of the critical surface for $q={value_p2}$\n
ax2.set_title(f"when $a_p={a1}$ and $a_q={a2}$")
if np.isclose(a2,0.5) and np.isclose(value_p2,4):
    to_pop=np.where((p1 > 3.465) & (p1 < 3.525))
    newp1=p1
    neww_critical=w_critical_P1P2[index,:]
    for ind in to_pop[0][::-1]:
        newp1=np.concatenate((newp1[:ind],newp1[ind+1:]), axis=0)
        neww_critical=np.concatenate((neww_critical[:
 ↪ind],neww_critical[ind+1:]),axis=0)
    ax2.plot(newp1,neww_critical,label=f'$\omega_c(p,q={p2[index]:.
 ↪2f})$')
else:
    ax2.plot(p1,w_critical_P1P2[index,:
 ↪],label=f'$\omega_c(p,q={p2[index]:.2f})$')
ax2.set_xlabel(r"$p$", rotation=0, fontsize=FontSize)
y_max=np.min([np.max(w_critical_P1P2[index,:]),1000])*1.1
ax2.set_ylim(-0.3,y_max)

legend = ax2.legend()
fig2.savefig(f'slice_w_c_a1_is_{a1}_a2_is_{a2}_p2_is_{value_p2}.
 ↪pdf',transparent=True,orientation='landscape',format='pdf',
bbox_inches='tight')
```

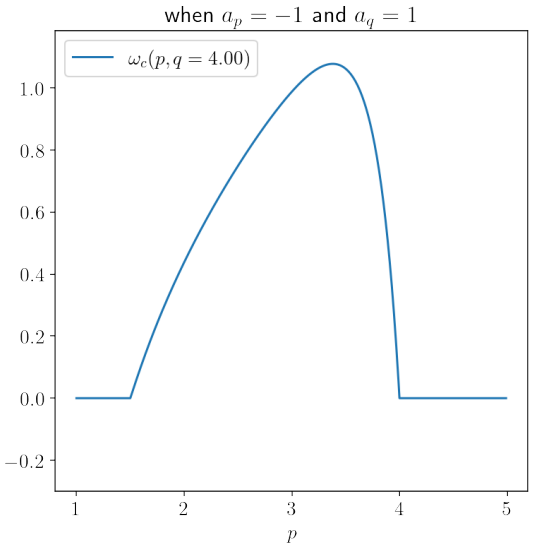

Observing closer the transition from $\omega_c > 0$ to $\omega_c = 0$ on fixed q slices, we realize that the transition on the left ($q = 7 - 2p$) is never smooth, whereas it is smooth when $a_q = 2$ not smooth but continuous when $a_q = 1$, and discontinuous when $a_q = 1/2$. This is reflecting the fact that when $p \to q$, the family of soliton profiles has a different behavior for different values of a_q. When $a_q > a_p$, soliton profiles for $p = q$ exist and are stable (hence $\omega_c(p, q = p) = 0$), whereas for $a_p = a_q$ the two nonlinearities exactly compensate and for $a_p > a_q$ the defocusing nonlinearity becomes the dominant one.

[11]:
```
# close up view to check the regularity on the left and on the right
fig3 = plt.figure(figsize=[6,6])
ax3 = plt.axes()
# Slice of the critical surface for $q={value_p2}$\n
ax3.set_title(f"when $a_p={a1}$ and $a_q={a2}$")
ax3.plot(p1,w_critical_P1P2[index,:],label=f'$\omega_c(p,q={p2[index]:.
 ↪2f})$')
ax3.set_xlabel(r"$p$", rotation=0, fontsize=FontSize)
y_max=1
ax3.set_ylim(-0.3,y_max)

legend = ax3.legend()
fig3.
 ↪savefig(f'slice_close_up_w_c_a1_is_{a1}_a2_is_{a2}_p2_is_{value_p2}.
 ↪pdf',transparent=True,orientation='landscape',format='pdf',
bbox_inches='tight')
```

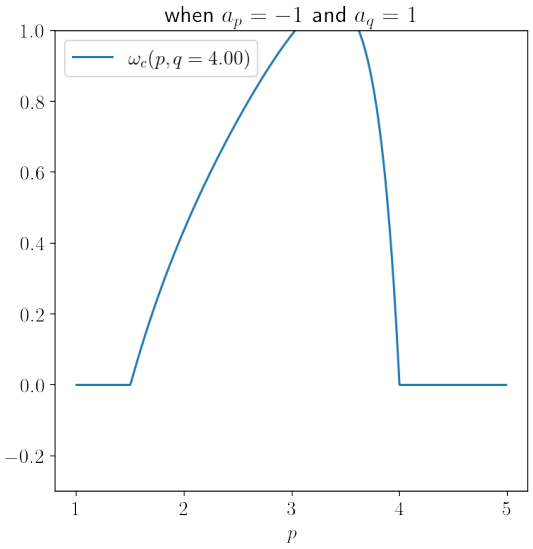

From the previous observations, we know that at fixed q the map $p \to \omega_c(p,q)$ has a unique maximum if $a_q = 1$ or $a_q = 2$ (if $a_q = 1/2$, we have seen that the map increases towards infinity as p approaches q. Denote by $p_{\max}(q)$ the value realizing this maximum, i.e.

$$\omega_c(p_{\max}(q), q) = \max_{1<p<5} \omega_c(p,q).$$

The line $\{(p_{\max}(q), p2), q > 7/3\}$ is represented in Picture **??**. When $a_q = 1$, we observe that the line is tangent to the line $p = q$ when q is close to $7/3$ or close to 5. On the other hand, when $a_q = 2$, the line seems to be tangent to the line $p = 7/3$ when q is close to $7/3$. It approaches the point $(5,5)$ as q goes to 5, but does not seem to be tangent to the line $p = q$ (it was however not possible to obtain numerically a relevant picture closer to $q = 5$, which leaves open the question of the behavior when q is close to 5).

[12]:
```
fig4 = plt.figure(figsize=[6,6])
ax4 = plt.axes()
ax4.plot(np.ones_like(p2)*7/3,p2,'k-.',label='$p=7/
↪3$')#,linestyle='dashdot')
ax4.plot(p1,p2,'k:',label='$p=q$')
ax4.plot(p1,7-2*p1,'k--',label='$q=7-2p$')#,linestyle='dashed')
ax4.set_title(f"when $a_p={a1}$ and $a_q={a2}$")
ax4.set_xlabel(r"$p$", rotation=0, fontsize=FontSize)
ax4.set_ylabel(r"$q$", rotation=0, fontsize=FontSize)
ax4.set_ylim(7/3+0.1,4.8)

w_critical_P1P2=np.reshape(w_critical_P1P2,(-1,np.shape(P2)[1]))
p1_of_p2=p1[np.argmax(w_critical_P1P2,axis=1)]

if a2==2:
```

```
    # remove obviously wrong values
    to_delete=[]
    for index,pp1 in enumerate(p1_of_p2):
        if p2[index]<3 and np.abs(pp1-7/3)>0.01:
            to_delete.append(index)
    new_p1_of_p2=np.delete(p1_of_p2,to_delete)
    new_p2=np.delete(p2,to_delete)
    ax4.plot(new_p1_of_p2,new_p2,'k',label='$p_{\max}(q)$')
    legend=ax4.legend(loc="upper left",prop={'size': 12})
    fig4.savefig(f'p1_line_of_max_w_c_a1_is_{a1}_a2_is_{a2}.
 ↪pdf',transparent=True,orientation='landscape',format='pdf',
    bbox_inches='tight')
elif a2==1:
    ax4.plot(p1_of_p2,p2,'k',label='$p_{\max}(q)$')
    legend=ax4.legend(loc="upper left",prop={'size': 12})
    fig4.savefig(f'p1_line_of_max_w_c_a1_is_{a1}_a2_is_{a2}.
 ↪pdf',transparent=True,orientation='landscape',format='pdf',
    bbox_inches='tight')
#p$ which realizes $\max_{p}\omega_c(p,q)
```

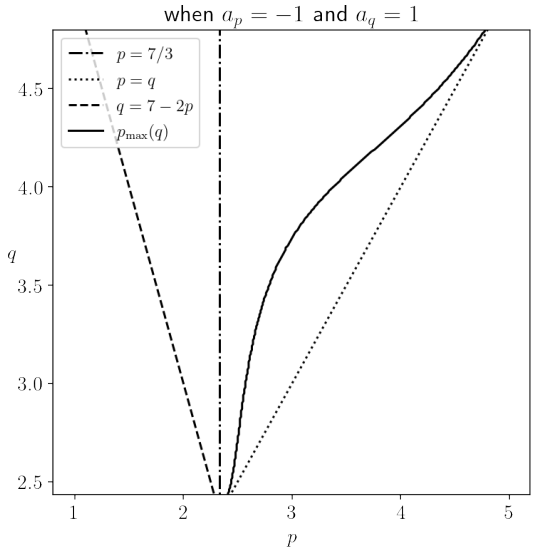

Notebook 2

[15]:
```
# This can be used also as a script (created by uncommenting the␣
 ↪following line in each cell)
#%%file 2021_07_23_script_nls_evolution.py
#%matplotlib notebook
import numpy as np
from numpy.linalg import norm
import scipy as sp
import scipy.special
import scipy.sparse as scs
import scipy.sparse.linalg as scl
import scipy.integrate as integrate
from scipy.integrate import solve_bvp
import scipy.optimize as sco
from scipy import integrate
import time
from datetime import datetime
import sys
import shelve
import matplotlib
import matplotlib.pyplot as plt
import matplotlib.animation as animation
from mpl_toolkits.mplot3d import Axes3D # <--- This is important for 3d␣
 ↪plotting
import plotly.express as px
import plotly.graph_objects as go
import pandas as pd
from concurrent.futures import ProcessPoolExecutor
from functools import partial
```

[16]:
```
#%%file --append 2021_07_23_script_nls_evolution.py
TeXFont = True
#plt.rcParams['figure.figsize']=[6,(3/4)*6]
if TeXFont:
    plt.rcParams['font.size'] = 14.0          # font size
    plt.rcParams['mathtext.fontset'] = 'cm'   # computer moder math font
    plt.rcParams['text.usetex'] = True        # use tex engine for␣
 ↪everything (useful for the axes labels)
else:
    plt.rcParams['text.usetex'] = False

FontSize = 14
```

In the following cell, we introduce the discretization of the real line $\mathbb{R}$ as a finite number N of points equally distributed between $-L$ and L and we construct the discretized Laplacian matrix with Dirichlet boundary conditions.

[3]:
```
#%%file --append 2021_07_23_script_nls_evolution.py

L=50 # half length of the interval on which we discretize
N=10000+1 # number of discretization points
#x,dx=np.linspace(-L, L, num=N, endpoint=False,retstep=True) # without␣
 ↪right end point for periodic
x,dx=np.linspace(-L, L, num=N,retstep=True) # with right end point for␣
 ↪Dirichlet

# construction of the Laplacian matrix with Dirichlet conditions
def Laplace(N,dx):
    main_diag = [-2 for i in range(N)]
    upper_diag= [1 for i in range(N-1)]
    lower_diag= upper_diag
    diagonals=[lower_diag,main_diag,upper_diag]
    Lap=scs.diags(diagonals,[-1,0,1])/dx**2
    return Lap
Lap=Laplace(N,dx)
```

Before simulating the evolution flow, we compute the critical omega associated with our parameters.

[4]:
```
#%%file --append 2021_07_23_script_nls_evolution.py

def f1(z,p1,p2,a1=-1,a2=1):
    s=np.abs(z)
    return -a1*s**((p1-1)/2)-a2*s**((p2-1)/2)

def F1(z,p1,p2,a1=-1,a2=1):
    s=np.abs(z)
    return -(a1*s**((p1+1)/2))*2/(p1+1)-(a2*s**((p2+1)/2))*(2/(p2+1))

def U(s,w,p1,p2,a1=-1,a2=1):
    s=np.abs(s)
    return w*s+F1(s,p1,p2,a1,a2)

def U_der(s,w,p1,p2,a1=-1,a2=1):
    s=np.abs(s)
    return w+f1(s,p1,p2,a1,a2)

def U_div_s(s,w,p1,p2,a1=-1,a2=1):
    s=np.abs(s)
    return (w-(a1*s**((p1-1)/2))*2/(p1+1)-(a2*s**((p2-1)/2))*(2/(p2+1)))

def U_div_s_prime(s,w,p1,p2,a1=-1,a2=1):
    s=np.abs(s)
    return -(a1*s**((p1-3)/2))*2/(p1+1)*(p1-1)/2-(a2*s**((p2-3)/2))*(2/
 ↪(p2+1))*(p2-1)/2
```

```
def a(w,p1,p2,a1=-1,a2=1):
    a=sco.fsolve(U_div_s,␣
 ↪10,args=(w,p1,p2,a1,a2),fprime=U_div_s_prime,xtol=10**(-12))
    a=np.abs(a)
    if a==0:
        print("error in a , a is 0")
    return a

def J(w,p1,p2,a1=-1,a2=1):
    A=a(w,p1,p2,a1,a2)
    def integrand(s):
        C=-A**(1.5)/(2*U_der(A,w,p1,p2,a1,a2))
        I=(3+A*s*(U_der(A,w,p1,p2,a1,a2)-U_der(A*s,w,p1,p2,a1,a2))/
 ↪U(A*s,w,p1,p2,a1,a2))*np.sqrt(s)/np.sqrt(np.
 ↪abs(U(A*s,w,p1,p2,a1,a2)))
        return C*I
    I=integrate.quad(integrand, 0, 1,epsabs=10**(-100),limit=100)
    return I[0]

# construction of a function returning the critical omega

def w_critical(p1,p2,a1=-1,a2=1):
    dp1=0.0001
    dp2=0.0001
    if ((p2<=p1+dp1/2) or (p2-dp2/2<(-2*p1+7))):
        return 0
    else:
        try:
            precision=1
            tol=0.00001
            w1,w2=0,1
            while J(w2,p1,p2,a1,a2)<0:
                w2=2*w2
                if w2>10**(10):
                    w1=10**(10)
                    break
            while precision>tol:
                w_tmp=w1+(w2-w1)/2
                if J(w_tmp,p1,p2,a1,a2)>0:
                    w2=w_tmp
                else:
                    w1=w_tmp
                precision=(w2-w1)/w2
                if w2<10**(-12):
                    break
        except:
```

```
            pass
    return w1
```

To perform the numerical simulations, it might be helpful to restrict ourselves to the case $q = 2p - 1$, for which we have explicit formulas for the standing waves (as given in the next cell).

[5]:
```
#%%file --append 2021_07_23_script_nls_evolution.py

def profile_explicit(x,beta,w=1,a1=-1,a2=1):
    # Explicit standing wave profile
    # for double power nonlinearities of the form p1=1+1/beta,p2=1+2/
 ↪beta
    # in such a way that p2=2p1-1
    # See 234nls-v218.pdf page 36
    A=a1/(2+1/beta)
    B=a2/(1+1/beta)
    return (w/(A+np.sqrt(A**2+B*w)*np.cosh(beta**(-1)*np.
 ↪sqrt(w)*x)))**beta
```

"scipy.integrate.solve_bvp" Solve a boundary value problem for a system of ODEs.

This function numerically solves a first order system of ODEs subject to two-point boundary conditions.

Our system is

$$y_1' = y_2$$
$$y_2' = \omega y_1 - a_p |y_1|^{p-1} y_1 - a_q |y_1|^{q-1} y_1$$

with the boundary conditions $\phi(0) = initialvalue(\phi), \quad \phi(L) = 0.$

[6]:
```
#%%file --append 2021_07_23_script_nls_evolution.py

def initialvalue(phi,p1,p2,w=1,a1=-1,a2=1):
    return (a1/(p1+1)*phi**(p1-1)+a2/(p2+1)*phi**(p2-1)-w/2)

def fun(x, y,p1,p2,w=1,a1=-1,a2=1):
    return np.vstack((y[1], w*y[0]-a1*np.abs(y[0])**(p1-1)*y[0]-a2*np.
 ↪abs(y[0])**(p2-1)*y[0]))

def bc(ya, yb,p1,p2,w=1,a1=-1,a2=1):
    partial_initialvalue = partial(initialvalue,␣
 ↪p1=p1,p2=p2,w=w,a1=a1,a2=a2)
    return [ya[0]-sco.fsolve(partial_initialvalue,1), yb[0]]

def profile(x,p1,p2,w=1,a1=-1,a2=1):
    # if p2=2p1-1, we use the explicit formula
```

```
    if np.abs(p2-2*p1+1)<1e-14:
        beta=1/(p1-1)
        return profile_explicit(x,beta,w,a1,a2)
    # else, we compute with the solve_bvp method
    # not working well for larger w (above 2 or 3 ?)
    else:
        N=len(x)
        partial_initialvalue = partial(initialvalue,␣
↪p1=p1,p2=p2,w=w,a1=a1,a2=a2)
        partial_fun = partial(fun, p1=p1,p2=p2,w=w,a1=a1,a2=a2)
        partial_bc = partial(bc, p1=p1,p2=p2,w=w,a1=a1,a2=a2)
        y_init =[1/(np.cosh(x)),np.tanh(x)/(np.cosh(x))]*sco.
↪fsolve(partial_initialvalue,1)
        sol = solve_bvp(partial_fun, partial_bc, x, y_init,tol=0.
↪00001,max_nodes=N)
        # to get the right solution, we even it
        even_sol_left=sol.y[0][int((N-1)/2):]
        even_sol_right=sol.y[0][int((N+1)/2):]
        even_sol=np.concatenate([even_sol_right[::-1],even_sol_left])
        return even_sol
```

[7]:
```
#%%file --append 2021_07_23_script_nls_evolution.py

def initial_data(x,p1,p2,w=1,c=0,a1=-1,a2=1,init=0):
    # return a soliton profile with frequency w and speed c,
    # modified according to the following rule:
    # init=0 -> no modification
    # init=1 -> profile multiplied by 1.01
    # init=2 -> profile multiplied by 0.99
    # init=3 -> profile multiplied by randn(x)*0.01
    # init=4 -> profile multiplied by 1+cos(x)*0.01
    # init=5 -> profile multiplied by 1+sin(x)*0.01
    # init=6 -> profile multiplied by 1+sech(x)*0.01
    # init=7 -> profile multiplied by 1+tanh(x)*0.01
    # init=8 -> profile multiplied by 1+sech(x-1)*0.01
    if init==0:
        return profile(x,p1,p2,w,a1,a2)
    elif init==1:
        return profile(x,p1,p2,w,a1,a2)*1.01
    elif init==2:
        return profile(x,p1,p2,w,a1,a2)*0.99
    elif init==3:
        return profile(x,p1,p2,w,a1,a2)*(np.ones_like(x)+np.random.
↪randn(np.shape(x)[0])*0.01)
    elif init==4:
        return profile(x,p1,p2,w,a1,a2)*(np.ones_like(x)+np.cos(x)*0.01)
    elif init==5:
```

```
        return profile(x,p1,p2,w,a1,a2)*(np.ones_like(x)+np.sin(x)*0.01)
    elif init==6:
        return profile(x,p1,p2,w,a1,a2)*(np.ones_like(x)+1/np.cosh(x)*0.
↪01)
    elif init==7:
        return profile(x,p1,p2,w,a1,a2)*(np.ones_like(x)+np.tanh(x)*0.
↪01)
    elif init==8:
        shift=np.argmax(x>1)-len(x)//2
        x_shifted=np.roll(x, shift)
    return profile(x,p1,p2,w,a1,a2)*(np.ones_like(x)+1/np.
↪cosh(x_shifted)*0.01)
```

In the next cell, we implement a Crank-Nicolson scheme with relaxation.

[8]:
```
#%%file --append 2021_07_23_script_nls_evolution.py

# Numerical simulation of NLS with Crank-Nicolson scheme with␣
↪relaxation (see Besse 2004)
# SIAM Journal on Numerical Analysis, 2004, Vol. 42, No. 3 : pp.␣
↪934-952
# A Relaxation Scheme for the Nonlinear Schrödinger Equation
# Christophe Besse
# https://doi.org/10.1137/S0036142901396521

def nls(x,p1,p2,T=1,delta_t = 1e-3,w=1,c=0,a1=-1,a2=1,init=0):
    # Warning: output is trimmed so that only approximately 100 values␣
↪in x and in t are kept.
    # Use next cell for full output
    Id=scs.identity(N)
    M_1 = Id - 1j*delta_t/2*Lap
    psi=initial_data(x,p1,p2,w,c,a1,a2,init)
    # u_t_x stores the values of psi troncated in such a way that a bit␣
↪more than 100 values of x and t are taken into account
    N_x=len(x)
    psi_tmp=psi[N_x//4:3*N_x//4]
    u_t_x=psi_tmp[::len(psi_tmp)//100]
    #initialisation step
    phi = -(a1*np.abs(psi)**(p1-1)+a2*np.abs(psi)**(p2-1))
    nb_iter=int(T//delta_t)
    iter_save_step=nb_iter//100
    y_size_u_t_x=1
    max_u_t_x=np.max(np.abs(psi))
    for n in range(nb_iter):
        phi = -2*(a1*np.abs(psi)**(p1-1)+a2*np.abs(psi)**(p2-1)) - phi
        M = M_1 + 1j*delta_t/2*scs.diags(phi)
        varphi = scl.spsolve(M,psi)
        psi = 2*varphi - psi
```

```
        max_u_t_x = np.append(max_u_t_x,np.max(np.abs(psi)))
        if n%iter_save_step==0:
            print(f'iteration {n+1} over {nb_iter}',end='\r')
            psi_tmp=psi[N_x//4:3*N_x//4]
            u_t_x=np.append(u_t_x,psi_tmp[::len(psi_tmp)//100])
            y_size_u_t_x=y_size_u_t_x+1
    u_t_x=np.reshape(u_t_x,(y_size_u_t_x,-1))
    u_t_x=u_t_x.T
    return u_t_x,max_u_t_x
```

[9]:
```
#%%file --append 2021_07_23_script_nls_evolution.py

def make_pdf_figure(u_t_x,x,p1,p2,T=1,delta_t =␣
↪1e-3,w=1,w_c=float("nan"),c=0,a1=-1,a2=1,init=0):
    N_x=len(x)
    x_clip=x[N_x//4:3*N_x//4]
    x_clip=x_clip[::len(x_clip)//100]
    nb_x_clip,nb_iter_clip=np.shape(u_t_x)
    Tt_clip=np.linspace(0,T,nb_iter_clip)
    u_t_x_clip=np.abs(u_t_x)
    fig = plt.figure()
    fig.suptitle(rf"$a_p={a1}$, $a_q={a2}$, $p={p1:.2f}$, $q={p2:.2f}$,␣
↪$\omega={w:.2f}$, $\omega_c={w_c:.2f}$, init=${init}$")
    ax = fig.add_subplot(111, projection='3d')
    X, TT = np.meshgrid(x_clip,Tt_clip)
    ax.plot_surface(X,TT,u_t_x_clip.T)
    ax.set_xlabel(r"$x$",fontsize=FontSize)
    ax.set_ylabel(r"$t$",fontsize=FontSize)
    ax.set_zlabel(r"$|u(t,x)|$",fontsize=FontSize)
    ax.xaxis.set_rotate_label(False)  # disable automatic rotation
    ax.yaxis.set_rotate_label(False)  # disable automatic rotation
    #ax.zaxis.set_rotate_label(False)  # disable automatic rotation
    fig.savefig(f"nls_evol_a1_is_{a1}_a2_is_{a2}_p1_is_{p1:.
↪2f}_p2_is_{p2:.2f}_w_is_{w:.2f}_w_c_is_{w_c:.2f}_init_is_{init}.
↪pdf",transparent=True,orientation='landscape',format='pdf',
    bbox_inches='tight')
```

[10]:
```
#%%file --append 2021_07_23_script_nls_evolution.py

def make_html_figure(u_t_x,x,p1,p2,T=1,delta_t =␣
↪1e-3,w=1,w_c="nc",c=0,a1=-1,a2=1,init=0):
    N_x=len(x)
    x_clip=x[N_x//4:3*N_x//4]
    x_clip=x_clip[::len(x_clip)//100]
    nb_x_clip,nb_iter_clip=np.shape(u_t_x)
    Tt_clip=np.linspace(0,T,nb_iter_clip)
```

```
    u_t_x_clip=np.abs(u_t_x.T)
    fig = go.Figure(data=[go.Surface(z=u_t_x_clip, x=x_clip,␣
↪y=Tt_clip)])
    fig.update_layout(  title=f'a1={a1}, a2={a2}, p1={p1:.2f}, p2={p2:.
↪2f}, w={w:.2f}, w_c={w_c:.2f}, init={init}',
                      scene = dict(
                      xaxis_title=r"space x",
                      yaxis_title='time t',
                      zaxis_title='|u(t,x)|'))
    # known limitation : latex cannot be displayed in axis title
    fig.show()
    fig.write_html(f"nls_evol_a1_is_{a1}_a2_is_{a2}_p1_is_{p1:.
↪2f}_p2_is_{p2:.2f}_w_is_{w:.2f}_w_c_is_{w_c:.2f}_init_is_{init}.
↪html")
    #https://plotly.com/python/3d-surface-plots/
```

[11]:
```
#%%file --append 2021_07_23_script_nls_evolution.py

def make_max_figure(max_u_t_x,p1,p2,T=1,delta_t =␣
↪1e-3,w=1,w_c=float("nan"),c=0,a1=-1,a2=1,init=0):
    N_t=len(max_u_t_x)
    Tt=np.linspace(0,T,N_t)
    fig = plt.figure(figsize=(8,6))
    fig.suptitle(f"Plot of $t\mapsto\max|u(t,x)|$ when\n$a_p={a1}$,␣
↪$a_q={a2}$, $p={p1:.2f}$, $q={p2:.2f}$, $\omega={w:.2f}$,␣
↪$\omega_c={w_c:.2f}$, init=${init}$")
    ax = fig.add_subplot(111)
    ax.plot(Tt,max_u_t_x)
    ax.set_xlabel(r"$t$",fontsize=FontSize)
    ax.set_ylabel(r"$\max|u(t,x)|$",fontsize=FontSize)
    fig.savefig(f"nls_max_a1_is_{a1}_a2_is_{a2}_p1_is_{p1:.
↪2f}_p2_is_{p2:.2f}_w_is_{w:.2f}_w_c_is_{w_c:.2f}_init_is_{init}.
↪pdf",transparent=True,orientation='landscape',format='pdf',
    bbox_inches='tight')
```

[12]:
```
#%%file --append 2021_07_23_script_nls_evolution.py

def variables_backup(u_t_x,max_u_t_x,x,p1,p2,T=1,delta_t =␣
↪1e-3,w=1,w_c="nc",c=0,a1=-1,a2=1,init=0):
    # Save all variables (with in particular w_critical) to file with␣
↪date in file name
    filename=f"nls_var_bckup_a1_is_{a1}_a2_is_{a2}_p1_is_{p1:.
↪2f}_p2_is_{p2:.2f}_w_is_{w:.2f}_w_c_is_{w_c:.2f}_init_is_{init}.npy"
    with open(filename, 'wb') as f:
        np.save(f, T)
        np.save(f, a1)
        np.save(f, a2)
```

```
        np.save(f, p1)
        np.save(f, p2)
        np.save(f, c)
        np.save(f, delta_t)
        np.save(f, init)
        np.save(f, w)
        np.save(f, w_c)
        np.save(f, x)
        np.save(f, u_t_x)
        np.save(f, max_u_t_x)

# to reload the variables :
#with open(filename, 'rb') as f:
#    T = np.load(f)
#    a1 = np.load(f)
#    a2 = np.load(f)
#    p1 = np.load(f)
#    p2 = np.load(f)
#    c = np.load(f)
#    delta_t = np.load(f)
#    init = np.load(f)
#    w = np.load(f)
#    w_c = np.load(f)
#    x = np.load(f)
#    u_t_x = np.load(f)
```

[13]:
```
#%%file --append 2021_07_23_script_nls_evolution.py

def nls_evolution_process(p1,p2,w,init):
    T=40
    delta_t=1e-3
    c=0
    a1=0
    a2=1
    try:
        u_t_x,max_u_t_x=nls(x,p1,p2,T,delta_t,w,c,a1,a2,init)
        w_c=w_critical(p1,p2,a1,a2)
        make_html_figure(u_t_x,x,p1,p2,T,delta_t,w,w_c,c,a1,a2,init)
        make_pdf_figure(u_t_x,x,p1,p2,T,delta_t,w,w_c,c,a1,a2,init)
        make_max_figure(max_u_t_x,p1,p2,T,delta_t,w,w_c,c,a1,a2,init)
        ␣
 ↪variables_backup(u_t_x,max_u_t_x,x,p1,p2,T,delta_t,w,w_c,c,a1,a2,init)
    except Exception as e:
        print(f"we have a problem with p1={p1}, p2={p2}, w={w},␣
 ↪init={init}")
```

```
        print(e)
```

#Run the cell to complete and run script #%%file –append 2021_07_23_script_nls_evolution.py

p1=np.arange(1.1,3,0.1)

w=np.arange(0.1,3.01,0.1)

init=np.arange(0,9,1)

P1,W,INIT=np.meshgrid(p1,w,init)

#list(map(nls_evolution_process,P1.flatten(),2*P1.flatten()-1,W.flatten(),INIT.flatten()))

if **name** == "**main**": PPE = ProcessPoolExecutor() list(PPE.map(nls_evolution_process,P1.flatten(),2*P1.flatten()-1,W.flatten(),INIT.flatten()))

!python 2021_07_23_script_nls_evolution.py

[14]:
```
# Cell for simulations one by one
plt.close()
#beta=5/8
#beta=0.6
#p1=1+1/beta
#p2=1+2/beta
p1=1.25
p2=1.5
w=1
#w=0.2
#init=2
init=1
T=15
delta_t=1e-3
c=0,
a1=-1
a2=1
u_t_x,max_u_t_x=nls(x,p1,p2,T,delta_t,w,c,a1,a2,init)
w_c=w_critical(p1,p2)
#make_html_figure(u_t_x,x,p1,p2,T,delta_t,w,w_c,c,a1,a2,init)
make_pdf_figure(u_t_x,x,p1,p2,T,delta_t,w,w_c,c,a1,a2,init)
make_max_figure(max_u_t_x,p1,p2,T,delta_t,w,w_c,c,a1,a2,init)
```

```
iteration 14901 over 14999
```

$a_p = -1,\ a_q = 1,\ p = 1.25,\ q = 1.50,\ \omega = 1.00,\ \omega_c = 0.00,$ init=1

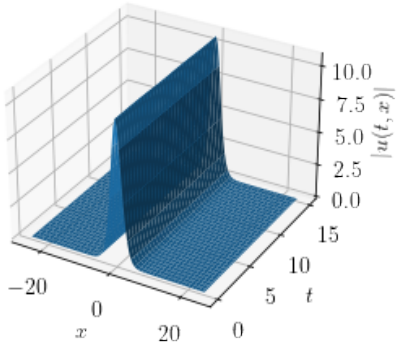

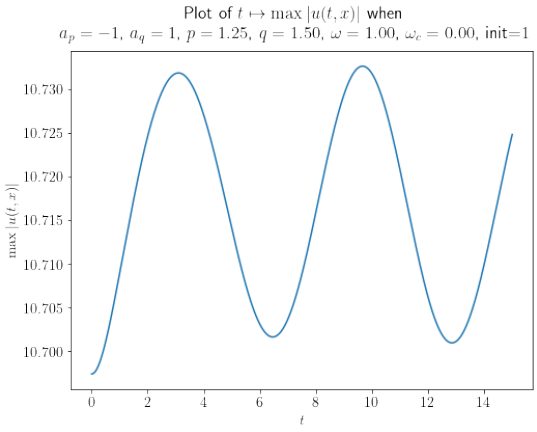

Chapter 3

Analysis of the quasi-periodic waves for the cubic nonlinear Schrödinger equation

3.1 Introduction

In this chapter, we consider the one dimensional cubic nonlinear Schrödinger equation

$$i\psi_t + \psi_{xx} + b|\psi|^2\psi = 0, \tag{3.1.1}$$

where $\psi : \mathbb{R}_t \times \mathbb{R}_x \to \mathbb{C}$ and $b \in \mathbb{R} \setminus \{0\}$. Equation (3.1.1) appears in many areas of physics such as quantum mechanics, optics, water waves and serves as a model for nonlinear dispersive wave phenomena, more generally see [35, 68]. It is said to be focusing if $b > 0$, where the nonlinearity is attractive and defocusing if $b < 0$, where the nonlinearity is repulsive. Note that (3.1.1) is invariant under the following transformations:

— spatial translation: $\psi(t, x) \to \psi(t, x + \xi)$, for $\xi \in \mathbb{R}$,

— phase multiplication: $\psi(t, x) \to e^{i\alpha}\psi(t, x)$, for $\alpha \in \mathbb{R}$.

We are particularly interested in the spatially quasi-periodic solutions to (3.1.1). At least formally, they conserve the mass M, the momentum P, and the energy $\mathcal{E}$, which are defined by

$$M(\psi) = \frac{1}{2}\int_0^T |\psi|^2 dx, \quad P(\psi) = \frac{1}{2}\mathcal{I}m\int_0^T \psi\overline{\psi}_x dx,$$

$$\mathcal{E}(\psi) = \frac{1}{2}\int_0^T |\psi_x|^2 dx - \frac{b}{4}\int_0^T |\psi|^4 dx.$$

The simplest non-trivial solutions of (3.1.1) are the standing waves, which have the form

$$\psi(t, x) = e^{-iat}u(x), \quad a \in \mathbb{R}.$$

The profile function $u(x)$ satisfies the ordinary differential equation

$$u_{xx} + au + b|u|^2u = 0. \tag{3.1.2}$$

The conserved quantities of (3.1.2) on $\mathbb{C}$ are the angular momentum J and the ordinary differential equation energy E, defined by

$$J = \mathcal{I}m(u_x\overline{u}), \quad E = \frac{1}{2}|u_x|^2 + \frac{a}{2}|u|^2 + \frac{b}{4}|u|^4.$$

To find the angular momentum J, we start by multiplying (3.1.2) by $\overline{u}$, then we take the imaginary part to obtain $\mathcal{I}m(u_{xx}\overline{u}) = 0$. On the other side $\partial_x(u_x\overline{u}) = u_{xx}\overline{u} + |u_x|^2$, then $\partial_x(\mathcal{I}m(u_x\overline{u})) = 0$, therefore there exists $J \in \mathbb{R}$ such that $\mathcal{I}m(u_x\overline{u}) \equiv J$. To find the energy E we multiply (3.1.2) by $\overline{u}_x$ and then we take the real part.

Define the space

$$H_T^\theta = \{f \in H^1_{loc}(\mathbb{R}) : f(x+T) = e^{i\theta}f(x), \forall x \in \mathbb{R}\},$$

where θ the Floquet multiplier, i.e. the increment of the phase over a period. When the Floquet multiplier is 0 we are talking about periodic waves and when it is π we are in the case of anti-periodic solutions. Non-constant, real-valued, periodic solutions of (3.1.2) are well known to be given by the Jacobi elliptic functions: dnoidal (dn), cnoidal (cn) and snoidal (sn), see Section 3.2.1 for details.

We are interested in the following minimization problem:

$$\min\{\mathcal{E}(u) : u \in H_T^\theta,\ M(u) = m, P(u) = p\}. \tag{3.1.3}$$

It is known that there exists u_∞ minimizer of (3.1.3), and there exist Lagrange-multipliers ω and σ such that

$$-\mathcal{E}'(u_\infty) + \omega M'(u_\infty) + \sigma P'(u_\infty) = 0,$$

that is

$$-\partial_{xx}u_\infty + \omega u_\infty - b|u_\infty|^2 u_\infty \pm i\sigma\partial_x u_\infty = 0.$$

Our main goal is to characterize variationally the solutions of the ordinary differential equation (3.1.2) by identifying them as the minimizers of the minimization problem (3.1.3). This will be achieved using a mixture of analytical and numerical methods.

In Section 3.2 we start from the ordinary differential equation (3.1.2) and we consider the links between the solution of this equation and the solution of the minimization problem (3.1.3). We establish a diffeomorphic correspondence between the conserved quantities of the ordinary differential equation (3.1.2) and the conserved quantities of the nonlinear Schrödinger equation (3.1.1). To do so we start in Section 3.2.1, by reviewing the well-known properties of Jacobi elliptic functions. Next, in Section 3.2.2 we study the analysis

of the profile of the ordinary differential equation (3.1.2) for the two different cases depending whether or not $J = 0$. For each case we describe the solutions whether we know them explicitly or not. Then we give some monotonicity results on the period T. Moreover, in Section 3.2.3 we find the expressions of the mass M and the momentum P inside the domain and on its boundaries. Afterwards, in Section 3.2.4 we prove the diffeomorphism between (J, E) and $(\tilde{M}(J, E), \tilde{P}(J, E))$ where we used a part of the results and methods of Gallay and Haragus [38].

In Section 3.3 we start from the solution of the minimization problem (3.1.3) and consider the links between the minimizer of this problem and the solution of the ordinary differential equation (3.1.2). By that means, we start in Section 3.3.1 by recalling the results concerning global variational characterizations of elliptic function periodic waves as constrained-mass energy minimizers among periodic functions and subspaces of periodic functions. After, in Section 3.3.2 we explain how to proceed to compute numerically the solution of the ordinary differential equation (3.1.2). When we know the exact solution we compare it to the numerical solution. In Section 3.3.3, we present the method of the gradient flow with discrete normalization in order to find the minimizer of the energy $\mathcal{E}$ with fixed mass $m > 0$ and fixed momentum p: at each step of time, we evolve in the direction of the gradient of the energy and renormalize the mass and the momentum of the outcome. Such scheme is popular in the physics literature under the name "imaginary time method". When there is no momentum, and only real-valued functions are considered, such approach to compute the minimizers was developed by Bao and Du [13]. In the case of the nonlinear Schrödinger equation on the line $\mathbb{R}$ with focusing cubic non linearity, Faou and Jezequel [34] performed a theoretical analysis of the various level of the discretization of the method, from the continuous one to the fully discrete scheme. To characterize variationally the Jacobi elliptic functions, Gustafson, Le Coz and Tsai [46] developed a numerical method to obtain the minimizer of the energy with fixed mass $m > 0$ and fixed momentum $p = 0$. Another study is presented in the work of Besse, Duboscq and Le Coz [20] for the gradient flow on nonlinear quantum graphs. They implemented a method based on normalized gradient flow of the energy to compute ground states of nonlinear Schrödinger equations on metric graphs. Accordingly, in Section 3.3.5 we performed different tests using the scheme described above. In every test we were comparing the minimizer that we obtained from the normalized gradient flow with the numerical solution of the ordinary differential equation. Finally, in Section 3.3.6, we evaluate the order of the scheme by making various simulations, using the numerical solution of the ODE and the solution of minimization problem.

3.2 From the ordinary differential equation to the minimization problem

3.2.1 Jacobi elliptic functions

The Jacobi elliptic functions are standard forms of elliptic functions. The three basic functions are denoted $cn(x,k)$, $dn(x,k)$, and $sn(x,k)$, where $k \in (0,1)$ is known as the elliptic modulus.

The incomplete elliptic integral of the first kind is defined by

$$x = \mathbf{F}(\phi, k) := \int_0^{\phi} \frac{d\theta}{\sqrt{1 - k^2 \sin^2(\theta)}},$$

where ϕ is called the Jacobi amplitude, and the Jacobi elliptic functions are defined through the inverse of $F(.,k)$:

$$sn(x,k) := \sin(\phi), \quad cn(x,k) := \cos(\phi), \quad dn(x,k) := \sqrt{1 - k^2 \sin^2(\phi)}.$$

The relations

$$1 = sn^2 + cn^2 = k^2 sn^2 + dn^2$$

follow. The period of the elliptic functions can be expressed in terms of the complete elliptic integral of the first kind

$$\mathbf{K}(k) := F\left(\frac{\pi}{2}, k\right), \quad \mathbf{K}(k) \to \begin{cases} \frac{\pi}{2}, & k \to 0 \\ \infty, & k \to 1. \end{cases}$$

Moreover, for $k \in (0,1)$, the incomplete elliptic integral of the second kind is defined by:

$$\mathbf{E}(\phi, k) := \int_0^{\phi} \sqrt{1 - k^2 \sin^2(\theta)} d\theta.$$

The complete elliptic integral of the second kind is defined as

$$\mathbf{E}(k) := \mathbf{E}\left(\frac{\pi}{2}, k\right), \quad \mathbf{E}(0) = \frac{\pi}{2}, \quad \mathbf{E}(1) = 1.$$

The derivatives of elliptic functions (with respect to x) are expressed in terms of elliptic functions. For fixed $k \in (0,1)$, we have:

$$\partial_x sn = cn.dn, \quad \partial_x cn = -sn.dn, \quad \partial_x dn = -k^2 cn.sn.$$

We can easily verify that sn, cn and dn are solutions of (3.1.2):

$$u_{xx} + au + b|u|^2 u = 0,$$

with the coefficients $a, b \in \mathbb{R}$ given by:

$$\begin{aligned} a &= 1 + k^2, \quad b = -2k^2, \quad \text{for } u = sn, \\ a &= 1 - 2k^2, \quad b = 2k^2, \quad \text{for } u = cn, \\ a &= -(2 - k^2), \quad b = 2, \quad \text{for } u = dn. \end{aligned}$$

3.2.2 Analysis of the profile ODE

In this section, we study the bounded solutions of the ordinary differential equation (3.1.2). We distinguish between two different cases depending whether or not $J = 0$ and in each case we study the defocusing and focusing cases. The analysis presented here gathers elements already presented in earlier works such as [38, 46].

3.2.2.1 The case $J \neq 0$

We start with the case $J \neq 0$. By definition of J, this implies in particular that $u(x) \neq 0$ for all $x \in \mathbb{R}$. Hence we can introduce the polar coordinates $u(x) = r(x)e^{i\phi(x)}$, with $r > 0$ and $r, \phi \in C^2(\mathbb{R})$. Moreover $J = r^2\phi_x \neq 0$ and this implies that $\phi_x \neq 0$ so $u(x) \in \mathbb{C}$ with a non-trivial phase. The energy becomes

$$E = \frac{r_x^2}{2} + V_J(r),$$

where $V_J(r)$ is given by

$$V_J(r) = \frac{J^2}{2r^2} + a\frac{r^2}{2} + b\frac{r^4}{4}.$$

We start with the defocusing case, i.e. we assume $b < 0$. We will distinguish between three different cases depending on the values of J. The first case is when $J^2 > \frac{4}{27}\frac{a^3}{b^2}$. Then $V_J'(r) < 0$ for all $r > 0$, hence (3.1.2) has no bounded solution in this case. If $J^2 < \frac{4}{27}\frac{a^3}{b^2}$ (which implies in particular $a > 0$) then we can parametrize J in a unique way as

$$J = q\frac{(q^2 - a)}{b} = Q\frac{(Q^2 - a)}{b}, \quad \text{where } 0 < q^2 < \frac{a}{3} < Q^2 < a.$$

With this parametrization $V_J(r)$ has a unique local minimum at $r_Q = \sqrt{\frac{Q^2-a}{b}}$ and a unique local maximum at $r_q = \sqrt{\frac{q^2-a}{b}}$. We define:

$$E_-(J) = V_J(r_Q) = \frac{1}{4b}(Q^2-a)(3Q^2+a), \quad E_+(J) = V_J(r_q) = \frac{1}{4b}(q^2-a)(3q^2+a).$$

The curves E_+ and E_- delimit the region of the (J, E) plane where there exist bounded solutions to (3.1.2). We have the following description.

1. If $E = E_-(J)$ then u is a plane wave, i.e. $u(x) = r_Q e^{iQx}$ up to phase shift and complex conjugate.
2. If $E = E_+(J)$ then u is a plane wave (i.e. $u(x) = r_q e^{iqx}$ up to phase shift and complex conjugate) or $|u|$ is homoclinic to r_q as $x \to +\infty$.

3. If $E_-(J) < E < E_+(J)$ the modulus $r = |u|$ and the phase derivative ϕ_x are periodic with the same period. If we denote by $r_1 < r_2 < r_3$ the three positive roots of $E - V_J(r)$, the (minimal) period is

$$T(J,E) = 2\int_{r_1}^{r_2} \frac{\mathrm{d}r}{\sqrt{2(E - V_J(r))}}. \tag{3.2.1}$$

Finally the last case is when $J^2 = \frac{4}{27}\frac{a^3}{b^2}$. In this case, the effective potential $V_J(r)$ is strictly decreasing over $\mathbb{R}_+$ with an inflexion point at $r = \sqrt{\frac{-2a}{3b}}$. Since u is bounded we must have $E_-(J) = E_+(J) = \frac{-a^2}{3b}$ hence $u(x) = \sqrt{\frac{q^2-a}{b}}e^{iqx}$ with $q = (a/3)^{\frac{1}{2}} sign(J)$.

Now for the focusing case with a positive (a negative respectively): the potential $V_J(r)$ is strictly convex for any $J \in \mathbb{R}$, and we can parametrize J in a unique way as $J = Q\frac{(Q^2-a)}{b}$, where $Q \in \mathbb{R}$, $Q^2 \geqslant a$, ($Q \in \mathbb{R}$ respectively). Then $V_J(r)$ has a unique critical point at $r_Q = \sqrt{\frac{Q^2-a}{b}}$, where V_J attains its global minimum:

$$E_-(J) = V_J(r_Q) = \frac{1}{4b}(Q^2 - a)(3Q^2 + a).$$

In the case of positive a, the equation (3.1.2) has quasi-periodic solutions for all $E > E_-(J)$. In the case of negative a, the equation (3.1.2) has quasi-periodic solutions for all $E > E_-(J)$ with $E \neq 0$. In both cases, the period T of these solutions is given by (3.2.1).

3.2.2.2 The case $J = 0$

In the case $J = 0$, $u(x) \in \mathbb{R}$ up to a constant phase, so we're in the case of real-valued solutions. The only (non-constant) real-valued, periodic solutions of (3.1.2) are the elliptic functions. We have the following result (see e.g. [46]).

Lemma 3.2.1. Fix a period $T > 0$, $a \in \mathbb{R}$ and $u \in P_T$ a nontrivial real-valued solution of (3.1.2). By invariance under translation, and negation, we may suppose $u(0) = \max u > 0$. There exist $\alpha > 0, \beta > 0$, and $k \in (0,1)$, uniquely determined by T, a, b and $\max u$ such that the following hold.

1. If $b < 0$ (defocusing case) then $0 < |b|u(0)^2 < a$, and $\mathrm{u(x)}=\frac{1}{\alpha} sn(\mathbf{K}(k) + \frac{x}{\beta}, k)$ or $u(0)^2 = \frac{|a|}{b}$ and $u(x) = \sqrt{\frac{-a}{b}}$.
2. If $b > 0$ (focusing case), we have 3 possible cases:
   (a) if $0 \leqslant \min u < u(0)$, then $a < 0$, $|a| < bu(0)^2 < 2|a|$, and $\mathrm{u(x)}=\frac{1}{\alpha} dn(\frac{x}{\beta}, k)$,

(b) if $\min u = u(0)$, then $a < 0$, $u(0)^2 = \frac{|a|}{b}$, and $u(x) = \sqrt{\frac{-a}{b}}$,

(c) if $\min u < 0$, then $\max(0, -2a) < bu(0)^2$, and $u(x) = \frac{1}{\alpha} cn(\frac{x}{\beta}, k)$.

The parameters satisfy the a-independent relation: $b\beta^2 = -2k^2\alpha^2$ for (1), $b\beta^2 = 2\alpha^2$ for (2)-(a) and $b\beta^2 = 2k^2\alpha^2$ for (2)-(b). In addition, there exists $n \in \mathbb{N}$ such that $4\mathbf{K}(k)\beta n = T$ for (1) and (2)-(b) and $2\mathbf{K}(k)\beta n = T$ for (2)-(a).

Remark 3.2.2. In the case of non periodic solution, in the defocusing case if $E = \frac{-a^2}{4b}$ then the solution can be $u(x) = \sqrt{-\frac{a}{b}} \tanh(x\sqrt{\frac{a}{2}})$ and in the focusing case with negative a if $E = 0$ the equation (3.1.2) can have the pulse-like solution $u(x) = \sqrt{-\frac{2a}{b}} \operatorname{sech}(x\sqrt{-a})$.

The graph of E as a function of J for each case is given in Figure 3.1. From left to right we chose $(b = -1, a = 1)$, $(b = 1, a = 1)$ and $(b = 1, a = -1)$.

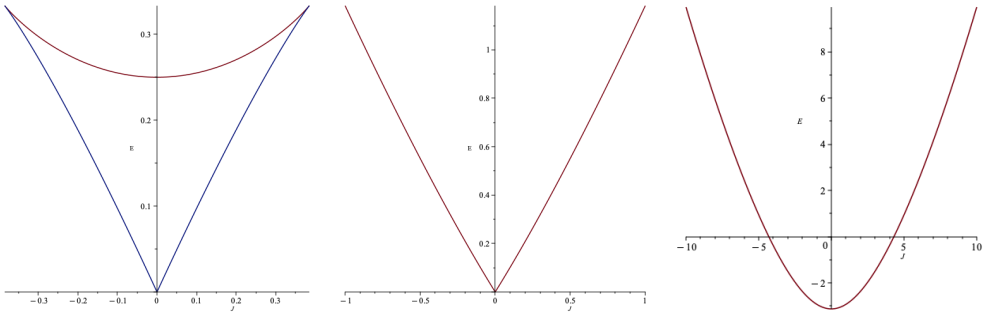

Figure 3.1 – Graphs of E as a function of J.

Given u solution of (3.1.1), the function given by $\bar{u}(-t, x)$ is also solution of (3.1.1). Therefore without loss of generality we restrict our work to the positive case (i.e. $J > 0$). We define the domain of existence of nontrivial quasi-periodic solutions of (3.1.2) for each case as the following: In the defocusing case $b < 0$, let

$$D_1 = \{(J, E) \in \mathbb{R}^2 : 0 < J^2 < \frac{4}{27}\frac{a^3}{b^2},\ E_-(J) < E < E_+(J)\}. \tag{3.2.2}$$

In the focusing case $b > 0$ with $a > 0$, let

$$D_2 = \{(J, E) \in \mathbb{R}^2 : J > 0, E > E_-(J)\}. \tag{3.2.3}$$

In the focusing case $b > 0$ with $a < 0$, let

$$D_3 = \{(J, E) \in \mathbb{R}^2 : J > 0, E > E_-(J)\}. \tag{3.2.4}$$

Lemma 3.2.3. Assume that $(J,E) \in D_1$ (D_2, D_3 respectively) where it is understood that for each case a and b take the corresponding values. We denote by $0 \leqslant y_1 < y_2 < y_3$, ($y_3 < 0 \leqslant y_1 < y_2$, $y_3 \leqslant 0 \leqslant y_1 < y_2$ respectively) with $r = \sqrt{y}$, the roots of the cubic polynomial $P(y) = -by^3 - 2ay^2 + 4Ey - 2J^2$. Then

$$T(J,E) = \sqrt{2}\int_{y_1}^{y_2} \frac{dy}{\sqrt{-b(y-y_1)(y-y_2)(y-y_3)}} = 2\sqrt{2}\int_0^{\frac{\pi}{2}} \frac{d\phi}{\sqrt{b(S(\phi)-y_3)}}, \tag{3.2.5}$$

where $S(\phi) = y_1\cos^2\phi + y_2\sin^2\phi$.

Proof. Notice that $P(r^2) = 4r^2(E - V_J(r))$, therefore $P(y)$ has three roots whenever $(J,E) \in D_1$ (D_2, D_3 respectively). Hence, using the change of variables $r = \sqrt{y}$ in (3.2.1), we obtain the first expression in (3.2.5). Moreover by setting $y = S(\phi)$, we have $dy = 2\sqrt{(y-y_1)(y_2-y)}d\phi$, thus we obtain the last expression. □

3.2.3 Mass and momentum inside the domain and on the boundaries

We start by finding the mass and momentum of the solutions in the domains D_1, D_2 and D_3, where we know that $u(x) = r(x)e^{i\phi(x)}$.Then

$$\begin{aligned} M(u) &= \frac{1}{2}\int_0^{T(E,J)} |u|^2 dx = \frac{1}{2}\int_0^{T(E,J)} (r(x))^2 dx \\ &= \int_{r_1}^{r_2} \frac{r^2 dr}{\sqrt{2(E-V_J)}} = \sqrt{2}\int_0^{\frac{\pi}{2}} \frac{S(\phi)}{\sqrt{b(S(\phi)-y_3)}} d\phi = \tilde{M}(J,E), \end{aligned}$$

and

$$P(u) = \frac{1}{2}\mathcal{I}m\int_0^{T(E,J)} u\overline{u}_x dx = -\frac{1}{2}\int_0^T J dx = -\frac{1}{2}TJ = \tilde{P}(J,E).$$

Note that $\tilde{M}$ and $\tilde{P}$ is used to distinguish P and M as functions of J and E. Next we want to find the mass and momentum of the solutions on the boundaries $E = E_-(J)$ for the focusing/defocusing cases and on $E = E_+(J)$ for the defocusing case.

Proposition 3.2.4. Let $(J,E) \in D_1$ (D_2, D_3 respectively). When $E \to E_-(J)$ the following holds:

$$\lim_{E\to E_-(J)} T(J,E) = \frac{\pi\sqrt{2}}{\sqrt{3Q^2-a}}, \quad \lim_{E\to E_-(J)} \tilde{M}(J,E) = \frac{(Q^2-a)}{2|b|}\frac{\pi\sqrt{2}}{\sqrt{3Q^2-a}},$$

$$\lim_{E\to E_-(J)} \tilde{P}(J,E) = -\frac{1}{2}Q\frac{(Q^2-a)}{b}\frac{\pi\sqrt{2}}{\sqrt{3Q^2-a}}.$$

Proof. We know that $T(J,E) = 2\sqrt{2}\int_0^{\frac{\pi}{2}} \frac{d\phi}{\sqrt{b(S(\phi)-y_3)}}$, where $S(\phi) = y_1\cos^2\phi + y_2\sin^2\phi$. When $E \to E_-(J)$, $y_2 \to y_1$, therefore $\lim_{E\to E_-(J)} T(J,E) = \frac{\pi\sqrt{2}}{\sqrt{b(y_1-y_3)}}$. On the other hand we have $y_1 = r_Q^2 = \frac{Q^2-a}{b}$, and since y_1, y_2, y_3 are solutions of the cubic equation $-by^3 - 2ay^2 + 4Ey - 2J^2 = 0$, we have $y_1+y_2+y_3 = -\frac{2a}{b}$, which implies that $y_3 = -\frac{2a}{b} - 2y_1$ and we can conclude that $\lim_{E\to E_-(J)} T(J,E) = \frac{\pi\sqrt{2}}{\sqrt{3Q^2-a}}$. Recall that $J = Q\frac{(Q^2-a)}{b}$ and on the boundary $E = E_-(J)$, we have $u(x) = \sqrt{\frac{(Q^2-a)}{b}}e^{iQx}$. We can find now the mass on this boundary

$$\begin{aligned}\lim_{E\to E_-(J)} \tilde{M}(J,E) &= \lim_{E\to E_-(J)} \frac{1}{2}\int_0^T |u|^2 dx \\ &= \lim_{E\to E_-(J)} \frac{1}{2}\int_0^T \frac{Q^2-a}{|b|}dx = \frac{(Q^2-a)}{2|b|}\frac{\pi\sqrt{2}}{\sqrt{3Q^2-a}}. \quad (3.2.6)\end{aligned}$$

The momentum is obtained by a direct computation:

$$\lim_{E\to E_-(J)} \tilde{P}(J,E) = -\frac{1}{2}TJ = -\frac{1}{2}Q\frac{(Q^2-a)}{b}\frac{\pi\sqrt{2}}{\sqrt{3Q^2-a}}. \quad (3.2.7)$$

□

Proposition 3.2.5. For the defocusing case, when $E \to E_+(J)$ the following holds:

$$\lim_{E\to E_+(J)} T(J,E) = +\infty, \qquad \lim_{E\to E_+(J)} \frac{\tilde{M}(J,E)}{T(J,E)} = \frac{|1-q^2|}{2},$$

$$\lim_{E\to E_+(J)} \frac{\tilde{P}(J,E)}{T(J,E)} = -\frac{1}{2}q(1-q^2).$$

Proof. Recall that $T(J,E) = 2\sqrt{2}\int_0^{\frac{\pi}{2}} \frac{d\phi}{\sqrt{b(S(\phi)-y_3)}}$. When $E \to E_+(J)$, $y_3 \to y_2$, therefore

$$\lim_{E\to E_+(J)} T(J,E) = \frac{2\sqrt{2}}{\sqrt{b(y_1-y_2)}}\int_0^{\frac{\pi}{2}} \frac{d\phi}{\cos(\phi)} = +\infty.$$

□

Finally the graph of P as a function of M for each case is given in Figure 3.2. From left to right we chose $(b=-1, a=1)$, $(b=1, a=1)$ and $(b=1, a=-1)$.

Note that when $a=-1$ in the focusing case, the behavior of the graph of P as a function of M is determined by the transition of E from negative

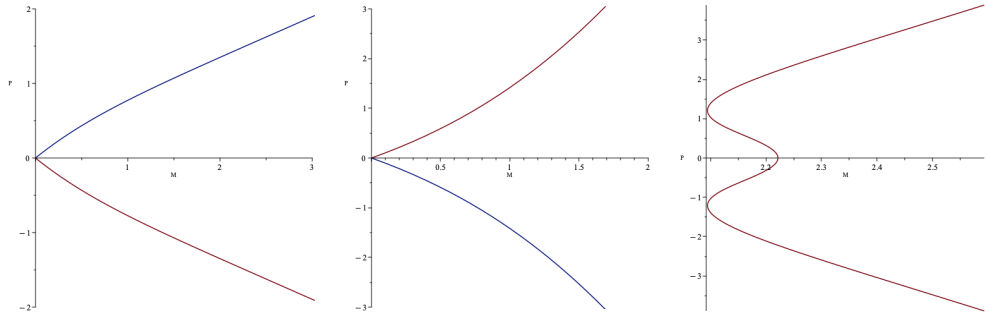

Figure 3.2 – Graphs of P as a function of M.

values to positive values. Specifically, if $Q^2 < \frac{-a}{3}$, then it corresponds to the negative values of E which form the central part of the graph. On the other hand, if $Q^2 > \frac{-a}{3}$, then it corresponds to the positive values of E which form the two side parts of the graph.

3.2.4 Diffeomorphism

In this section we establish a diffeomorphic correspondence between J, E and M, P for the defocusing case only. To this aim, we use a part of the results and methods of [38]. Without loss of generality, we set $b = -1$ and $a = 1$. We start with monotonicity results on T.

Proposition 3.2.6. We have $\frac{\partial T}{\partial E} > 0$ and $\frac{\partial T}{\partial J} < 0$ for all $(J, E) \in D_1$.

Proof. Let $(J, E) \in D_1$. Since y_1, y_2, y_3 are solutions of the cubic equation $y^3 - 2y^2 + 4Ey - 2J^2 = 0$, we have $y_1 + y_2 + y_3 = 2$, and

$$\frac{\partial y_i}{\partial E} = -\frac{4y_i}{3y_i^2 - 4y_i + 4E}, \quad \frac{\partial y_i}{\partial J} = \frac{4J}{3y_i^2 - 4y_i + 4E}, \quad i = 1, 2, 3. \tag{3.2.8}$$

In particular

$$\frac{\partial y_1}{\partial E} < 0, \quad \frac{\partial y_2}{\partial E} > 0, \quad \frac{\partial y_1}{\partial E} + \frac{\partial y_2}{\partial E} = -\frac{\partial y_3}{\partial E} > 0,$$

because $P'(y_1) > 0$, $P'(y_2) < 0$, $P'(y_3) > 0$, where $P(y) = y^3 - 2y^2 + 4Ey - 2J^2$ was defined in Lemma 3.2.3. Similarly, since $J > 0$,

$$\frac{\partial y_1}{\partial J} > 0, \quad \frac{\partial y_2}{\partial J} < 0, \quad \frac{\partial y_1}{\partial J} + \frac{\partial y_2}{\partial J} = -\frac{\partial y_3}{\partial J} < 0.$$

On the other hand, differentiating (3.2.5) with respect to E and J, we find

$$\frac{\partial T}{\partial E} = A_1 \frac{\partial y_1}{\partial E} + A_2 \frac{\partial y_2}{\partial E}, \qquad \frac{\partial T}{\partial J} = A_1 \frac{\partial y_1}{\partial J} + A_2 \frac{\partial y_2}{\partial J},$$

where

$$A_1 = \sqrt{2}\int_0^{\frac{\pi}{2}} \frac{1+\cos^2\phi}{(y_3 - S(\phi))^{\frac{3}{2}}} d\phi, \quad A_2 = \sqrt{2}\int_0^{\frac{\pi}{2}} \frac{1+\sin^2\phi}{(y_3 - S(\phi))^{\frac{3}{2}}} d\phi.$$

We have that

$$A_2 - A_1 = \sqrt{2}\int_0^{\frac{\pi}{2}} \frac{\sin^2\phi - \cos^2\phi}{2(y_3 - S(\phi))^{\frac{3}{2}}} d\phi > 0.$$

Indeed, we have the following results. Let μ be a (Borel) probability measure on some interval $I \subset \mathbb{R}$, and let $f,\ g : I \to \mathbb{R}$ be bounded and measurable functions. If both f and g are strictly increasing or strictly decreasing, and if the support of μ is not reduced to a single point, then

$$\int_I f(x)g(x)d\mu > \left(\int_I f(x)d\mu\right)\left(\int_I g(x)d\mu\right).$$

Therefore $A_2 - A_1 > 0$ follows from the result above, with $I = [0, \frac{\pi}{2}]$, $d\mu = \frac{2}{\pi}d\phi$, $f(\phi) = \sin^2\phi - \cos^2\phi$ and $g(\phi) = (y_3 - S(\phi))^{-\frac{3}{2}}$ (notice that f, g are strictly increasing, and that $\int_0^{\frac{\pi}{2}} f(\phi)d\phi = 0$). Thus, $A_2 > A_1 > 0$. We conclude that

$$\frac{\partial T}{\partial E} = (A_2 - A_1)\frac{\partial y_2}{\partial E} + A_1\left(\frac{\partial y_1}{\partial E} + \frac{\partial y_2}{\partial E}\right) > 0.$$

Similarly,

$$\frac{\partial T}{\partial J} = (A_2 - A_1)\frac{\partial y_2}{\partial J} + A_1\left(\frac{\partial y_1}{\partial J} + \frac{\partial y_2}{\partial J}\right) < 0.$$

This concludes the proof. □

For all $(J, E) \in D_1$, let

$$\Delta = \begin{vmatrix} \frac{\partial \tilde{P}}{\partial E} & \frac{\partial \tilde{M}}{\partial E} \\ \frac{\partial \tilde{P}}{\partial J} & \frac{\partial \tilde{M}}{\partial J} \end{vmatrix}.$$

Proposition 3.2.7. For all $(J, E) \in D_1$ we have $\Delta > 0$.

Proof. We have

$$\begin{aligned}
\frac{\partial \tilde{P}}{\partial E} &= -\frac{1}{2}J\frac{\partial T}{\partial E} = -\frac{1}{2}J\left(A_1\frac{\partial y_1}{\partial E} + A_2\frac{\partial y_2}{\partial E}\right), \\
\frac{\partial \tilde{P}}{\partial J} &= -\frac{1}{2}\left(J\frac{\partial T}{\partial J} + T\right) = -\frac{1}{2}\left(J\left(A_1\frac{\partial y_1}{\partial J} + A_2\frac{\partial y_2}{\partial J}\right) + T\right), \\
\frac{\partial \tilde{M}}{\partial E} &= \frac{\partial \tilde{M}}{\partial y_1}\frac{\partial y_1}{\partial E} + \frac{\partial \tilde{M}}{\partial y_2}\frac{\partial y_2}{\partial E} + \frac{\partial \tilde{M}}{\partial y_3}\frac{\partial y_3}{\partial E}, \\
\frac{\partial \tilde{M}}{\partial J} &= \frac{\partial \tilde{M}}{\partial y_1}\frac{\partial y_1}{\partial J} + \frac{\partial \tilde{M}}{\partial y_2}\frac{\partial y_2}{\partial J} + \frac{\partial \tilde{M}}{\partial y_3}\frac{\partial y_3}{\partial J}.
\end{aligned}$$

We start with

$$\frac{\partial \tilde{M}}{\partial y_1} = \sqrt{2}\int_0^{\frac{\pi}{2}} \frac{\cos^2\phi\sqrt{y_3 - S(\phi)} - \frac{-\cos^2\phi S(\phi)}{2\sqrt{y_3 - S(\phi)}}}{y_3 - S(\phi)} d\phi,$$
$$= \sqrt{2}\int_0^{\frac{\pi}{2}} \frac{2(y_3 - S(\phi))\cos^2\phi + \cos^2\phi S(\phi)}{2(y_3 - S(\phi))^{\frac{3}{2}}} d\phi,$$
$$= \sqrt{2}\int_0^{\frac{\pi}{2}} \frac{2y_3\cos^2\phi - \cos^2\phi S(\phi)}{2(y_3 - S(\phi))^{\frac{3}{2}}} d\phi,$$
$$= \sqrt{2}\int_0^{\frac{\pi}{2}} \frac{2y_3\cos^2\phi + S(\phi)\sin^2\phi - S(\phi)}{2(y_3 - S(\phi))^{\frac{3}{2}}} d\phi.$$

And same for

$$\frac{\partial \tilde{M}}{\partial y_2} = \sqrt{2}\int_0^{\frac{\pi}{2}} \frac{2y_3\sin^2\phi + S(\phi)\cos^2\phi - S(\phi)}{2(y_3 - S(\phi))^{\frac{3}{2}}} d\phi,$$

and

$$\frac{\partial \tilde{M}}{\partial y_3} = \sqrt{2}\int_0^{\frac{\pi}{2}} \frac{-S(\phi)}{2(y_3 - S(\phi))^{\frac{3}{2}}} d\phi.$$

Then

$$\frac{\partial \tilde{M}}{\partial E} = \frac{\partial \tilde{M}}{\partial y_1}\frac{\partial y_1}{\partial E} + \frac{\partial \tilde{M}}{\partial y_2}\frac{\partial y_2}{\partial E} + \frac{\partial \tilde{M}}{\partial y_3}\frac{\partial y_3}{\partial E},$$
$$= \frac{\partial \tilde{M}}{\partial y_1}\frac{\partial y_1}{\partial E} + \frac{\partial \tilde{M}}{\partial y_2}\frac{\partial y_2}{\partial E} + \frac{\partial \tilde{M}}{\partial y_3}\left(-\frac{\partial y_1}{\partial E} - \frac{\partial y_2}{\partial E}\right),$$
$$= \frac{\partial y_1}{\partial E}\left(\frac{\partial \tilde{M}}{\partial y_1} - \frac{\partial \tilde{M}}{\partial y_3}\right) + \frac{\partial y_2}{\partial E}\left(\frac{\partial \tilde{M}}{\partial y_2} - \frac{\partial \tilde{M}}{\partial y_3}\right) = C_1\frac{\partial y_1}{\partial E} + C_2\frac{\partial y_2}{\partial E},$$

with

$$C_1 = \sqrt{2}\int_0^{\frac{\pi}{2}} \frac{2y_3\cos^2\phi + S(\phi)\sin^2\phi}{2(y_3 - S(\phi))^{\frac{3}{2}}} d\phi,$$

and

$$C_2 = \sqrt{2}\int_0^{\frac{\pi}{2}} \frac{2y_3\sin^2\phi + S(\phi)\cos^2\phi}{2(y_3 - S(\phi))^{\frac{3}{2}}} d\phi.$$

Similarly, we have

$$\frac{\partial \tilde{M}}{\partial J} = C_1\frac{\partial y_1}{\partial J} + C_2\frac{\partial y_2}{\partial J}.$$

Therefore,

$$\begin{aligned}\Delta = &\left(-\frac{1}{2}J\left(A_1\frac{\partial y_1}{\partial E}+A_2\frac{\partial y_2}{\partial E}\right)\right)\left(C_1\frac{\partial y_1}{\partial J}+C_2\frac{\partial y_2}{\partial J}\right)\\ &+\frac{1}{2}\left(J\left(A_1\frac{\partial y_1}{\partial J}+A_2\frac{\partial y_2}{\partial J}\right)+T\right)\left(C_1\frac{\partial y_1}{\partial E}+C_2\frac{\partial y_2}{\partial E}\right),\\ =&-\frac{1}{2}\left(JA_1C_1\frac{\partial y_1}{\partial E}\frac{\partial y_1}{\partial J}+JA_1C_2\frac{\partial y_1}{\partial E}\frac{\partial y_2}{\partial J}+JA_2C_1\frac{\partial y_2}{\partial E}\frac{\partial y_1}{\partial J}+JA_2C_2\frac{\partial y_2}{\partial E}\frac{\partial y_2}{\partial J}\right)\\ &+\frac{1}{2}\left(JA_1C_1\frac{\partial y_1}{\partial E}\frac{\partial y_1}{\partial J}+JA_1C_2\frac{\partial y_1}{\partial J}\frac{\partial y_2}{\partial E}+JA_2C_1\frac{\partial y_2}{\partial J}\frac{\partial y_1}{\partial E}+JA_2C_2\frac{\partial y_2}{\partial E}\frac{\partial y_2}{\partial J}\right)\\ &+\frac{1}{2}T\frac{\partial\tilde{M}}{\partial E},\\ =&(A_2C_1-A_1C_2)\left(\frac{1}{2}J\right)\left(\frac{\partial y_1}{\partial E}\frac{\partial y_2}{\partial J}-\frac{\partial y_2}{\partial E}\frac{\partial y_1}{\partial J}\right)+\frac{1}{2}T\frac{\partial\tilde{M}}{\partial E}.\end{aligned}$$

Using the identity (3.2.8)

$$\frac{\partial y_i}{\partial E}=-\frac{y_i}{J}\frac{\partial y_i}{\partial J},$$

we find

$$\Delta=\frac{1}{2}(A_2C_1-A_1C_2)(y_2-y_1)\left(\frac{\partial y_1}{\partial J}\frac{\partial y_2}{\partial J}\right)+\frac{1}{2}T\frac{\partial\tilde{M}}{\partial E}.$$

First we will prove that $C_2>C_1>0$.

Let $f(\phi)=\sin^2\phi-\cos^2\phi$ and $g(\phi)=\frac{2y_3-S(\phi)}{2(y_3-S(\phi))^{\frac{3}{2}}}$. We know that f is increasing. We will prove that g is also increasing.

$$\begin{aligned}g'(\phi)=&\frac{-S'(\phi)(y_3-S(\phi)^{\frac{3}{2}}+\frac{3}{2}(2y_3-S(\phi))S'(\phi)(y_3-S(\phi))^{\frac{1}{2}}}{2(y_3-S(\phi))^3}\\ =&\frac{S'(\phi)\big(-(y_3-S(\phi))+3y_3-\frac{3}{2}S(\phi)\big)}{2(y_3-S(\phi))^{\frac{5}{2}}}\\ =&\frac{S'(\phi)(2y_3-\frac{1}{2}S(\phi))}{2(y_3-S(\phi))^{\frac{5}{2}}}\\ =&\frac{(\sin\phi\cos\phi)(y_2-y_1)(2y_3-\frac{1}{2}S(\phi))}{(y_3-S(\phi))^{\frac{5}{2}}}>0,\end{aligned}$$

because $\sin\phi\cos\phi>0,\ y_2-y_1>0,\ y_3-S(\phi)>0$ and $2y_3-\frac{1}{2}S(\phi)>0$. Then g is strictly increasing and same as before, as we have two strictly increasing functions, we have $C_2>C_1>0$. Therefore

$$\begin{aligned}\frac{\partial\tilde{M}}{\partial E}&=C_1\frac{\partial y_1}{\partial E}+C_2\frac{\partial y_2}{\partial E}\\ &=(C_2-C_1)\frac{\partial y_2}{\partial E}+C_1(\frac{\partial y_1}{\partial E}+\frac{\partial y_2}{\partial E})>0.\end{aligned}$$

Now we will prove that $A_1C_2 - A_2C_1 > 0$.

Let $\sigma(\phi) = (1 - y_3^{-1}S(\phi))^{\frac{1}{2}}$. Then

$$A_1 = \sqrt{2}\int_0^{\frac{\pi}{2}} \frac{1+\cos^2\phi}{(y_3 - S(\phi))^{\frac{3}{2}}}d\phi = 2\sqrt{2}y_3^{-\frac{3}{2}}A_1^{'}, \quad A_1^{'} = \int_0^{\frac{\pi}{2}} \frac{1+\cos^2\phi}{2\sigma(\phi)^3}d\phi,$$

$$A_2 = \sqrt{2}\int_0^{\frac{\pi}{2}} \frac{1+\sin^2\phi}{(y_3 - S(\phi))^{\frac{3}{2}}}d\phi = 2\sqrt{2}y_3^{-\frac{3}{2}}A_2^{'}, \quad A_2^{'} = \int_0^{\frac{\pi}{2}} \frac{1+\sin^2\phi}{2\sigma(\phi)^3}d\phi,$$

$$C_1 = \sqrt{2}\int_0^{\frac{\pi}{2}} \frac{2y_3\cos^2\phi + S(\phi)\sin^2\phi}{2(y_3 - S(\phi))^{\frac{3}{2}}}d\phi = \sqrt{2}y_3^{-\frac{1}{2}}C_1^{'},$$

$$C_1^{'} = \int_0^{\frac{\pi}{2}} \frac{2\cos^2\phi + (1-\sigma(\phi)^2)\sin^2\phi}{2\sigma(\phi)^3}d\phi,$$

$$C_2 = \sqrt{2}\int_0^{\frac{\pi}{2}} \frac{2y_3\sin^2\phi + S(\phi)\cos^2\phi}{2(y_3 - S(\phi))^{\frac{3}{2}}}d\phi = \sqrt{2}y_3^{-\frac{1}{2}}C_2^{'},$$

$$C_2^{'} = \int_0^{\frac{\pi}{2}} \frac{2\sin^2\phi + (1-\sigma(\phi)^2)\cos^2\phi}{2\sigma(\phi)^3}d\phi.$$

Therefore

$$\begin{aligned} A_1C_2 - A_2C_1 &= (2\sqrt{2}y_3^{-\frac{3}{2}}A_1^{'})(\sqrt{2}y_3^{-\frac{1}{2}}C_2^{'}) - (2\sqrt{2}y_3^{-\frac{3}{2}}A_2^{'})(\sqrt{2}y_3^{-\frac{1}{2}}C_1^{'}) \\ &= 4y_3^{-2}(A_1^{'}C_2^{'} - A_2^{'}C_1^{'}). \end{aligned}$$

We want to prove that $A_1^{'}C_2^{'} - A_2^{'}C_1^{'} > 0$. In fact,

$$C_1^{'} = A_1^{'} - \tilde{C}_1 \quad \text{with} \quad \tilde{C}_1 = \int_0^{\frac{\pi}{2}} \frac{\sin^2\phi}{2\sigma(\phi)}d\phi,$$

$$C_2^{'} = A_2^{'} - \tilde{C}_2 \quad \text{with} \quad \tilde{C}_2 = \int_0^{\frac{\pi}{2}} \frac{\cos^2\phi}{2\sigma(\phi)}d\phi,$$

which implies that

$$\begin{aligned} A_1^{'}C_2^{'} - A_2^{'}C_1^{'} &= A_1^{'}(A_2^{'} - \tilde{C}_2) - A_2^{'}(A_1^{'} - \tilde{C}_1) \\ &= A_1^{'}A_2^{'} - A_1^{'}\tilde{C}_2 - A_2^{'}A_1^{'} + A_2^{'}\tilde{C}_1 \\ &= A_2^{'}\tilde{C}_1 - A_1^{'}\tilde{C}_2 \end{aligned}$$

We know that $A_2^{'} > A_1^{'} > 0$ and $\tilde{C}_1 > \tilde{C}_2 > 0$ so $A_1^{'}C_2^{'} - A_2^{'}C_1^{'} > 0$ and then $A_2C_1 - A_1C_2 < 0$. Finally from $A_2C_1 - A_1C_2 < 0$, $y_2 - y_1 > 0$, $\frac{\partial y_1}{\partial J}\frac{\partial y_2}{\partial J} < 0$ and $\frac{1}{2}T\frac{\partial \tilde{M}}{\partial E} > 0$, we conclude that

$$\Delta > 0,$$

which concludes the proof. □

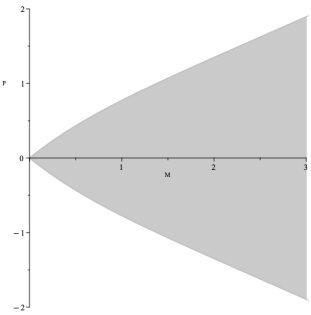

Figure 3.3 – Domain $\tilde{D}$.

Let $\tilde{D} = \{(\tilde{M}, \tilde{P}) \in \mathbb{R}^2 : \tilde{M} > 0,\ |\tilde{P}| < \frac{\sqrt{3\tilde{M}^2+\pi^2-\sqrt{9\tilde{M}^4+4\tilde{M}^2\pi^2}}}{\pi}\}$.

Theorem 3.2.8. The map $\Psi : D_1 \to \tilde{D}$, defined by $\Psi(J, E) = (\tilde{M}(J, E), \tilde{P}(J, E))$ is a diffeomorphism.

Proof. We know from Section 3.2.3 that $\lim_{E\to E_-(J)} T(J, E) = \frac{\pi\sqrt{2}}{\sqrt{3Q^2-1}}$, and $\lim_{E\to E_+(J)} T(J, E) = +\infty$. Moreover we have

$$\lim_{E\to E_-(J)} \tilde{M}(J, E) = \frac{(1-Q^2)}{2}\frac{\pi\sqrt{2}}{\sqrt{3Q^2-1}}, \qquad \lim_{E\to E_+(J)} \tilde{M}(J, E) = +\infty,$$

and

$$\lim_{E\to E_-(J)} \tilde{P}(J, E) = -\frac{1}{2}Q(1-Q^2)\frac{\pi\sqrt{2}}{\sqrt{3Q^2-1}}, \qquad \lim_{E\to E_+(J)} \tilde{P}(J, E) = -\infty.$$

The range of the map $\tilde{M} : D_1 \to \mathbb{R}$ is exactly the interval $(0, +\infty)$ since $\frac{\partial\tilde{M}}{\partial E} > 0$. We fix $\tilde{M}_0 > 0$, and let $\Sigma = \{(J, E) \in D_1 : \tilde{M}(J, E) = \tilde{M}_0\}$.

By the implicit Function Theorem, Σ is a smooth curve in D_1 which can be represented as a graph over the J-axis. Moreover, we know that Σ connects the boundary points $(0, E_0)$ and $(J_0, E_-(J_0))$ is determined by the relation

$$\frac{(1-Q_0^2)}{2}\frac{\pi\sqrt{2}}{\sqrt{3Q_0^2-1}} = \tilde{M}_0,$$

where $J_0 = Q_0(1-Q_0^2)$, $Q_0 \in (\frac{1}{\sqrt{3}}, 1)$ and E_0 the corresponding energy for $J = 0$ and $\tilde{M} = \tilde{M}_0$. We know that $\Delta > 0$ which implies that the restriction of $\tilde{P}$ to the curve Σ is a strictly decreasing function of J, because

$$\frac{d}{dJ}\tilde{P}_{|\Sigma} = \left(\frac{\partial\tilde{M}}{\partial E}\right)^{-1}\left(\frac{\partial\tilde{M}}{\partial E}\frac{\partial\tilde{P}}{\partial J} - \frac{\partial\tilde{M}}{\partial J}\frac{\partial\tilde{P}}{\partial E}\right) < 0.$$

Thus $\tilde{P}$ varies from 0 to $-\tilde{P}_0$ on the curve Σ, where

$$\tilde{P}_0 = -\frac{1}{2}Q_0(1-Q_0^2)\frac{\pi\sqrt{2}}{\sqrt{3Q_0^2-1}} = \frac{\sqrt{3\tilde{M}_0^2+\pi^2-\sqrt{9\tilde{M}_0^4+4\tilde{M}_0^2\pi^2}}}{\pi}.$$

This proves that Ψ is onto and therefore Ψ is a diffeomorphism. □

For the focusing case we recall the results of [38] on the monotonicity of the period T.

Proposition 3.2.9. Let $b = 1$, $a = 1$. We have

$$\frac{\partial T}{\partial E} < 0, \quad \frac{\partial T}{\partial J} < 0 \quad \text{for all } (J,E) \in D_2.$$

Proposition 3.2.10. Let $b = 1$, $a = -1$. Unlike in the previous cases, the period T is no longer a monotone function of the energy E. In fact the period $T(J,E)$ satisfies

$$\frac{\partial T}{\partial E}(0,E) > 0 \quad \text{for } -\frac{1}{4} < E < 0, \quad \text{and} \quad \frac{\partial T}{\partial E}(0,E) < 0 \quad \text{for } E > 0.$$

On the other hand, sine $J > 0$, the period T is still a monotone function of J and it satisfies

$$\frac{\partial T}{\partial J}(J,E) < 0.$$

3.3 From the minimization problem to the ordinary differential equation

In this section, we aim to study the minimizing problem and establish the link between the minimizer and the solution of the ordinary differential equation (3.1.2). One of the difficulties in this problem is identifying the minimizer as a solution of the ODE. The existence of the minimizer can be proven by taking a sequence that minimizes the energy and showing that it is bounded in H_T^θ, which implies that it has a weakly convergent subsequence in H_T^θ. The weak convergence of the subsequence, along with the compactness of the embedding of H_T^θ into L^p for $p \in (1,\infty)$, implies the convergence of the subsequence in L^p. Therefore, the minimizing sequence converges to a function that minimizes the energy. In the cubic case, it was further shown in [46] that the minimizer is a stationary wave, which is a periodic solution of the NLS equation with a special form of the profile function. Specifically, the minimizer was identified as a Jacobi elliptic function *cn* or *dn* depending

on the value of the mass parameter. Moreover it was conjectured that the minimizer of the energy with fixed mass and momentum is a snoidal periodic wave. In the complex-valued case we need to identify the minimizer as a solution of the ODE (3.1.2).

3.3.1 Variational problems

We start by recalling the result of Gustafson, Le Coz and Tsai [46] on the global variational characterizations of the elliptic function periodic waves as constrained-mass energy minimizers among periodic functions. Later on, we use these results to compare our numerical method with the theoretical results.

For $m > 0$, we consider the following minimization problem with fixed mass

$$\min\{\mathcal{E}(u) : u \in H_T^\theta,\ M(u) = m\}, \tag{3.3.1}$$

and the minimization problem with fixed mass and momentum

$$\min\{\mathcal{E}(u) : u \in H_T^\theta,\ M(u) = m, P(u) = 0\}. \tag{3.3.2}$$

Theorem 3.3.1. Assume $b > 0$ (focusing case). We have the following properties:

1. Let $\theta = 0$, we are in the periodic case:
   (a) If $0 < m \leqslant \frac{\pi^2}{bT}$ then there exists a unique (up to phase shift) minimizer for (3.3.1) and (3.3.2), which is the constant function $u_{min} = \sqrt{\frac{2m}{T}}$
   (b) If $\frac{\pi^2}{bT} < m < \infty$ then there exists a unique minimizer (up to translations and phase shift) for (3.3.1) and (3.3.2), which is the rescaled function $dn_{\alpha,\beta,k} = \frac{1}{\alpha} dn\left(\frac{\cdot}{\beta}, k\right)$, where the parameters α, β, k are uniquely determined. In particular given $k \in (0,1)$, if $b = 2$, $T = 2\mathbf{K}(k)$ and $m = \mathbf{E}(k)$, then the unique minimizer is $dn(., k)$.
2. If $\theta = \pi$, we are in the anti-periodic case, then there exists a unique minimizer (up to translations and phase shift) for (3.3.1) and (3.3.2), which is the rescaled function $cn_{\alpha,\beta,k} = \frac{1}{\alpha} cn\left(\frac{\cdot}{\beta}, k\right)$, where the parameters α, β, k are uniquely determined. In particular given $k \in (0,1)$, if $b = 2k^2$, $T = 2\mathbf{K}(k)$ and $m = \frac{(\mathbf{K}-\mathbf{E})}{k^2}$, then the unique minimizer is $cn(., k)$.

Proof. First we start with the periodic case by proving that (3.3.1) and (3.3.2) share the same minimizer. Without loss of generality we can restrict the

minimization problem to real-valued non negative functions. Indeed, if $u \in H^1_{loc} \cap P_T$, then $|u| \in H^1_{loc} \cap P_T$ and we have $\|\partial_x |u|\|_{L^2} \leqslant \|\partial_x u\|_{L^2}$. This implies that (3.3.1) and (3.3.2) share the same minimizers. Next we prove that the minimal energy is finite and negative. To prove the negativity, let $\phi_{m,0} \equiv \sqrt{\frac{2m}{T}}$ be a test function. We have $M(\phi_{m,0}) = m, \quad \mathcal{E}(\phi_{m,0}) < 0$. To prove that it is finite, we consider a minimizing sequence $(u_n) \subset H^1_{loc} \cap P_T$ for (3.3.1). It is bounded in $H^1_{loc} \cap P_T$. We observe that by Gagliardo-Nirenberg inequality: for any $u \in H^1_{loc} \cap P_T$, we have

$$\|u\|^4_{L^4} \lesssim \|u\|^3_{L^2} \|u_x\|_{L^2} + \|u\|^4_{L^2}.$$

Consequently, for any $u \in H^1_{loc} \cap P_T$, such that $M(u) = m$, we have

$$\mathcal{E}(u) \gtrsim \|u_x\|_{L^2}(\|u_x\|_{L^2} - m^{\frac{3}{2}}) - m^2.$$

The previous inequality implies the boundedness of $\|\partial_x u_n\|_{L^2}$. Indeed, by contradiction, let's suppose that $\|\partial_x u_n\|_{L^2} \to \infty$, therefore $\mathcal{E}(u_n) \to \infty$, which is a contradiction with the minimizing nature of (u_n). Hence the sequence (u_n) is bounded in $H^1_{loc} \cap P_T$, hence $\mathcal{E}(u)$ is bounded from below. Therefore up to a subsequence, (u_n) converges weakly in $H^1_{loc} \cap P_T$ and strongly in $L^2_{loc} \cap P_T$ and $L^4_{loc} \cap P_T$ towards $u_\infty \in H^1_{loc} \cap P_T$. By weak convergence, we have

$$\|\partial_x u_\infty\|^2_{L^2} \leqslant \lim_{n \to +\infty} \|\partial_x u_n\|^2_{L^2}.$$

Hence $\mathcal{E}(u_\infty) \leqslant \lim\limits_{n \to +\infty} \mathcal{E}(u_n)$. On the other hand $M(u_\infty) = m$, so by the definition of the minimizer $\mathcal{E}(u_\infty) = \lim\limits_{n \to +\infty} \mathcal{E}(u_n)$. Therefore the convergence from (u_n) to u_∞ is also strong in $H^1_{loc} \cap P_T$. Since u_∞ is a minimizer of (3.3.1), there exists a Lagrange multiplier $a \in \mathbb{R}$ such that

$$-\mathcal{E}'(u_\infty) + aM'(u_\infty) = 0$$

that is

$$\partial_{xx} u_\infty + a u_\infty + b u^3_\infty = 0. \tag{3.3.3}$$

Multiplying by u_∞ and integrating (recall that the functions considered are assumed to be real), we find that

$$a = \frac{\|\partial_x u_\infty\|^2_{L^2} - b\|u_\infty\|^4_{L^4}}{\|u_\infty\|^2_{L^2}}.$$

Note that

$$\|\partial_x u_\infty\|^2_{L^2} - b\|u_\infty\|^4_{L^4} = 2\mathcal{E}(u_\infty) - \frac{b}{2}\|u_\infty\|^4_{L^4},$$

therefore

$$a < 0.$$

We know from Lemma 3.2.1 that the solutions of (3.3.3) are either the constant function or the $dn_{\alpha,\beta,k}$ function, where $dn_{\alpha,\beta,k}(x) = \frac{1}{\alpha} dn(\frac{x}{\beta}, k)$. We start by proving that if $m > \frac{\pi^2}{bT}$ then $u_\infty = dn_{\alpha,\beta,k}$. By contradiction we suppose that $u_\infty = \sqrt{\frac{2m}{T}}$. Therefore $a = -\frac{2bm}{T}$. Since u_∞ is a constrained minimizer, the operator

$$-\partial_{xx} - a - 3bu_\infty^2 = -\partial_{xx} - \frac{4bm}{T}$$

must have at most 1 negative eigenvalue, where the eigenvalues are given by: $\left(\frac{2\pi n}{T}\right)^2 - \frac{4bm}{T}$. For $n = 0$, the eigenvalue is negative. For $n = 1$, $\left(\frac{2\pi n}{T}\right)^2 - \frac{4bm}{T} \geqslant 0$ if and only if $m \leqslant \frac{\pi^2}{bT}$, which gives the contradiction. Now we prove that if $u_\infty = dn_{\alpha,\beta,k}$ then $m > \frac{\pi^2}{bT}$. We find the mass of $dn_{\alpha,\beta,k}$ which is equal to $M(dn_{\alpha,\beta,k}) = \frac{4}{bT}\mathbf{E}(k)\mathbf{K}(k)$. We have $\partial_k \mathbf{EK}(k) > 0$ therefore for $k \in (0,1)$, $M(dn_{\alpha,\beta,k})$ is a strictly increasing function of k from $\left(\frac{\pi^2}{bT}, \infty\right)$, which concludes the proof. Thus u_∞ must be constant when $0 < m \leqslant \frac{\pi^2}{bT}$. Finally we will prove that given $k \in (0,1)$, if $b = 2$, $T = 2\mathbf{K}(k)$ and $m = \mathbf{E}(k)$, then the unique minimizer is $dn(., k)$. In this case $m > \frac{\pi^2}{bT}$ since $\mathbf{EK} > \frac{\pi^2}{4}$ and therefore from before we know that $u_\infty = dn_{\alpha,\beta,s}$ for $s \in (0,1)$. By Sturm-Liouville, the fundamental period of u_∞ is $T = 2\mathbf{K}(s)\beta$. So $M(dn_{\alpha,\beta,s}) = \mathbf{E}(s)\mathbf{K}(s) = \mathbf{E}(k)\mathbf{K}(k)$ and by the monotonicity of $\mathbf{EK}$ we have $k = s$. Thus $\alpha = \beta = 1$ and $u_\infty = dn(x, k)$.

For the anti-periodic case, from [46] we have the following result: Let $v \in H^1_{loc} \cap A_T$. There exists $\tilde{v} \in H^1_{loc} \cap A_T$ such that:

$$\tilde{v}(x) \in \mathbb{R}, \quad \|\tilde{v}\|_{L^2} = \|v\|_{L^2}, \quad \|\partial_x \tilde{v}\|_{L^2} = \|\partial_x v\|_{L^2}, \quad \|\tilde{v}\|_{L^4} \geqslant \|v\|_{L^4}.$$

Therefore we can restrict the minimization problem to real valued functions, and this implies the equivalence between the two minimization problems (3.3.1) and (3.3.2). Same as for the periodic case we consider a minimizing sequence $(u_n) \subset H^1_{loc} \cap A_T$ and the convergence from (u_n) to u_∞ is also strong in $H^1_{loc} \cap P_T$. Since u_∞ is a minimizer of (3.3.1), there exists a Lagrange multiplier $a \in \mathbb{R}$ such that

$$-\mathcal{E}'(u_\infty) + aM'(u_\infty) = 0$$

that is

$$\partial_{xx} u_\infty + a u_\infty + b u_\infty^3 = 0.$$

We assume that $\max u = u(0) > 0$ and therefore $u_\infty = c n_{\alpha,\beta,k}$. Moreover with the same method as before, using the monotonicity of m with respect to k,

we prove that given $k \in (0,1)$, if $b = 2k^2$, $T = 2\mathbf{K}(k)$ and $m = \frac{(\mathbf{K}-\mathbf{E})}{k^2}$, then the unique minimizer is $cn(.,k)$. This concludes the proof. □

Theorem 3.3.2. Assume $b < 0$ (defocusing case). We have the following properties:

1. If $\theta = 0$, we are in the periodic case, then there exists a unique minimizer (up to phase shift) for (3.3.1) and (3.3.2), which is the constant function $u_{min} = \sqrt{\frac{2m}{T}}$.
2. If $\theta = \pi$, we are in the anti-periodic case: There exists a unique minimizer (up to phase shift) for (3.3.1) which is the plane wave $u_{min} = \sqrt{\frac{2m}{T}} e^{\frac{2i\pi x}{T}}$.

Proof. For the periodic case we know that for all $f \in L^4(0,T)$, we have by Hölder's inequality: $\|f\|_{L^2} \leqslant T^{\frac{1}{4}} \|f\|_{L^4}$, with equality if and only if $|f|$ is constant. We want to prove that $\phi_{m,0} = \sqrt{\frac{2m}{T}}$ is the minimizer. Let $v \in H^1_{loc} \cap P_T$ such that $M(v) = m$, and $v \neq e^{i\theta}\phi_{m,0}$, $(\theta \in \mathbb{R})$. We have:

$$0 = \|\partial_x \phi_{m,0}\|^2_{L^2} < \|\partial_x v\|^2_{L^2},$$

and

$$\|\phi_{m,0}\|^4_{L^4} = 4T^{-1}M^2(\phi_{m,0}) = 4T^{-1}M^2(v) \leqslant \|v\|^4_{L^4},$$

therefore $\mathcal{E}(\phi_{m,0}) < \mathcal{E}(v)$ which concludes the proof of the first part of the theorem.

For the anti-periodic case we denote $w(x) = \sqrt{\frac{2m}{T}} e^{\frac{2i\pi x}{T}}$. Let $v \in H^1_{loc} \cap A_T$ such that $M(v) = m$ and $v \neq e^{i\theta} w$ $(\theta \in \mathbb{R})$. We have

$$\|w\|^4_{L^4} = 4T^{-1}M^2(w) = 4T^{-1}M^2(v) \leqslant \|v\|^4_{L^4}.$$

Since $v \in A_T$, v must have 0 mean value. Therefore by Poincaré-Wirtinger inequality we have

$$\|v\|^2_L \leqslant \frac{T}{2\pi} \|v'\|_{L^2}.$$

Moreover

$$\|\partial_x w\|^2_{L^2} = \frac{8\pi^2}{T} M(w) = \frac{8\pi^2}{T} M(w) < \|\partial_x v\|^2_{L^2},$$

therefore $\mathcal{E}(\phi_{m,0}) < \mathcal{E}(v)$ which concludes the proof. □

Conjecture 3.3.3. There exists a unique minimizer (up to translations and phase shift) of (3.3.2) which is the rescaled function $sn_{\alpha,\beta,k} = \frac{1}{\alpha} sn\left(\frac{\cdot}{\beta}, k\right)$, where the parameters α, β, k are uniquely determined. In particular given $k \in (0,1)$, if $b = -2k^2$, $T = 2\mathbf{K}(k)$ and $m = \frac{8}{bT}\mathbf{K}(\mathbf{K}-\mathbf{E})$, then the unique minimizer is $sn(.,k)$.

3.3.2 Numerical solutions of the ordinary differential equation

In this section we explain how we proceeded to compute numerically the solution of the ordinary differential equation (3.1.2):

$$u_{xx} + au + b|u|^2u = 0.$$

The Python function *odeintw* has been used to find the numerical solution. In order to use this function we need to find the period T and the initial data at a fixed (J, E). Recall that

$$V_J(r) = \frac{J^2}{2r^2} + a\frac{r^2}{2} + b\frac{r^4}{4}.$$

We start our numerical experiments by fixing a value of J in the domain D_1 (D_2, D_3 respectively) for each defocusing and focusing case. Recall that when $J \neq 0$, u is of the form $u(x) = r(x)e^{i\phi(x)}$. If we are in the defocusing case we find the minimum r_Q and the maximum r_q of $V_J(r)$. We know that $E_- = V_J(r_Q)$ and $E_+ = V_J(r_q)$. Then we choose E such that $E_- \leqslant E < E_+$. Note that we chose $E < E_+$ since $\lim\limits_{E\to E_+(J)} T(J, E) = +\infty$. Moreover we find the three positive roots $r_1 < r_2 < r_3$ of $E - V_J(r)$. If we are in the focusing case we find the minimum r_Q of $V_J(r)$ and we have $E_- = V_J(r_Q)$. Then we choose E such that $E_- \leqslant E$. Moreover we find the two positive roots $r_1 < r_2$ of $E - V_J(r)$. Recall that the period T is given by (3.2.1)

$$T(J, E) = 2\int_{r_1}^{r_2} \frac{1}{\sqrt{2(E - V_J(r))}}dr.$$

Furthermore, the Floquet multiplier is given by

$$\begin{aligned}\theta(J, E) = \phi(x + T) - \phi(x) &= \int_0^T \phi_x(x)dx \\ &= \int_0^T \frac{J}{r(x)^2}dx = 2\int_{r_1}^{r_2} \frac{J}{r^2\sqrt{2(E - V_J(r))}}dr,\end{aligned}$$

the mass is given by

$$M(J, E) = \frac{1}{2}\int_0^T |u|^2dx = \frac{1}{2}\int_0^T r(x)^2dx = \int_{r_1}^{r_2} \frac{r^2}{\sqrt{2(E - V_J(r))}}dr,$$

and the momentum is given by

$$\begin{aligned}P(J, E) = \frac{1}{2}\mathcal{I}m\int_0^T u\overline{u}_x dx &= -\frac{1}{2}\int_0^T \phi_x r(x)^2dx \\ &= -\frac{1}{2}\int_0^T Jdx = -\int_{r_1}^{r_2} \frac{J}{\sqrt{2(E - V_J(r))}}dr.\end{aligned}$$

Recall that on the boundary $E = E_-$ the period T is given by the limit when E tends to E_-, which is given in Proposition (3.2.4).

To use the function *odeintw*, we set $y = \begin{pmatrix} u \\ v \end{pmatrix}$, where $v = u'$, therefore $y' = \begin{pmatrix} v \\ -au - b|u|^2u \end{pmatrix}$. For the initial data, we suppose that $u(0) = r(0) = r_1$ and $u'(0) = i\phi'(0)r(0) = \frac{J}{r_1}i$, therefore we find the numerical solution.

The results of the numerical experiments are presented in Section 3.3.5.

3.3.3 Continuous gradient flow with discrete normalization

The variational problem that we consider is the following:

$$\min\{\mathcal{E}(u) : u \in H^\theta_T,\ M(u) = m, P(u) = p\}, \tag{3.3.4}$$

where $m > 0$ and $p \in \mathbb{R}$. Our goal in this section is to compute the minimizer of the energy at fixed mass m and momentum p. The approach that we use is the normalized gradient flow: at each step we evolve in the direction of the gradient of the energy and renormalize the mass and the momentum of the outcome. One of the earliest mathematical analysis was performed by Bao and Du [13]. They proved the energy diminishing property of a normalized gradient flow and compared several discretization methods. In the case of the nonlinear Schrödinger equation on the line $\mathbb{R}$ with focusing cubic non linearity, Faou and Jezequel [34] performed a theoretical analysis of the various level of the discretization of the method, from the continuous one to the fully discrete scheme. In the periodic setting Gustafson, Le Coz and Tsai [46] developed a numerical method to obtain the minimizer of the energy with fixed mass $m > 0$ and fixed momentum $p = 0$. More recently Besse, Duboscq and Le Coz [20] implemented a method based on normalized gradient flow of the energy to compute ground states of nonlinear Schrödinger equations on metric graphs.

Define an increasing sequence of time $0 = t_0 < ... < t_n$ and take an initial data u_0. Between each time step, let $u(t, x)$ evolve along the gradient flow

$$\begin{cases} u_t = -\mathcal{E}'(u) = u_{xx} + b|u|^2u, \\ u(t_n, x) = u_n(x), \end{cases} \tag{3.3.5}$$

where $x \in \mathbb{R}$, $t_n < t < t_{n+1}$, $n \geqslant 0$. At each time step t_n, the function is renormalized so as to have the desired mass m and momentum p. Recall that, as noted in [13], the renormalization of the mass is equivalent to solving

exactly the following ordinary differential equation:

$$u_t = \mu_n u, \quad t_n < t < t_{n+1}, \quad n \geqslant 0, \quad \mu_n = \frac{1}{t_{n+1} - t_n} \ln \left(\frac{\sqrt{2m}}{\|u(t_n)\|_{L^2}} \right). \tag{3.3.6}$$

Inspired by this remark, we consider the following numerical algorithm which gives the desired mass m and momentum p simultaneously by one flow. Suppose $\tilde{u}_{n+1}$ has been computed from u_n using the semi-implicit Euler scheme. To normalize $\tilde{u}_{n+1}$ we proceed in the following way. Let

$$m_0 = M(\tilde{u}_{n+1}), \quad p_0 = P(\tilde{u}_{n+1}), \quad k_0 = \frac{1}{2} \int_0^T |\partial_x \tilde{u}_{n+1}|^2 dx.$$

Consider the following flow

$$\partial_t u = (\mu + i\omega \partial_x) u.$$

We have at $(t = t_{n+1})$

$$\frac{d}{dt} M(u) = Re \int_0^T \bar{u} u_t dx = 2m_0 \mu + 2p_0 \omega,$$

$$\frac{d}{dt} P(u) = Im \int_0^T \bar{u}_x u_t dx = 2p_0 \mu + 2k_0 \omega.$$

We want to choose $\mu_n = \mu \delta t$ and $\omega_n = \omega \delta t$ so that

$$2m_0 \mu_n + 2p_0 \omega_n = m - m_0,$$

$$2p_0 \mu_n + 2k_0 \omega_n = p - p_0.$$

Note that by Cauchy-Schwarz

$$p_0^2 = \left(\frac{1}{2} \mathcal{I}\mathcal{m} \int_0^T u \bar{u}_x dx \right)^2 \leqslant \left(\frac{1}{2} \int_0^T |u|^2 dx \right) \left(\frac{1}{2} \int_0^T |u_x|^2 dx \right) = m_0 k_0.$$

In the case $m_0 k_0 - p_0^2 > 0$, we can solve

$$\mu_n = \frac{k_0(m - m_0) - p_0(p - p_0)}{2(m_0 k_0 - p_0^2)},$$

$$\omega_n = \frac{m_0(p - p_0) - p_0(m - m_0)}{2(m_0 k_0 - p_0^2)}.$$

In the case $m_0 k_0 - p_0^2 = 0$, we have Cauchy-Schwarz equality. To be periodic, $\tilde{u}_{n+1}$ is a plane wave and for some real constants r, α for the Cauchy-Schwarz equality we have

$$\tilde{u}_{n+1} = r e^{i\alpha x}.$$

We choose

$$u_{n+1} = \sqrt{\frac{2m}{T}} e^{-i \frac{p}{m} x}.$$

3.3.4 Discretization

Several numerical methods can be considered for discretizing (3.3.5). For example, a standard Crank-Nicolson scheme would consist in

$$\frac{u_{n+1}-u_n}{\delta_t} = \partial_{xx}\left(\frac{u_{n+1}+u_n}{2}\right) + b|u_n|^2\left(\frac{u_{n+1}+u_n}{2}\right).$$

This method can be proved to be energy diminishing. However in the above discretization, we need to solve a fully nonlinear system at every time step, which is time and resource consuming in practical computation. A more efficient method is the Gradient Flow with Discrete Normalization (GFDN) which consists into one step of classical gradient flow followed by a mass and momentum normalization step. The discretized problem is of the form

$$\begin{cases} \dfrac{\tilde{u}_{n+1}-u_n}{\delta_t} = \partial_{xx}\tilde{u}_{n+1} + b|u_n|^2\tilde{u}_{n+1}, \\ \dfrac{u_{n+1}-\tilde{u}_{n+1}}{\delta_t} = (\mu + i\omega\partial_x)u_{n+1}. \end{cases}$$

Note that in the first equation, we used Euler explicit for the nonlinear term, and Euler implicit for the linear terms. Therefore we obtain a semi-implicit Euler scheme and the first equation becomes linear. Finally we present the fully discretized problem. We discretize the space interval $[0,T]$ by setting

$$x^0 = 0, \quad x^l = x^0 + l\delta x, \quad \delta x = \frac{T}{N}, \quad N \in \mathbb{N}.$$

We denote by u_n^l the numerical approximation of $u(t_n, x^l)$. Using the (Backward Euler) semi-implicit scheme for time discretization and second-order centered finite difference for the second spatial derivatives, and the first centered finite difference for the first spatial derivatives, we obtain the following scheme:

$$\begin{cases} \dfrac{\tilde{u}_{n+1}^l - u_n^l}{\delta_t} = \dfrac{\tilde{u}_{n+1}^{l-1} - 2\tilde{u}_{n+1}^l + \tilde{u}_{n+1}^{l+1}}{\delta x^2} + b|u_n^l|^2\tilde{u}_{n+1}^l, \\ \dfrac{u_{n+1}^l - \tilde{u}_{n+1}^l}{\delta_t} = \mu u_{n+1}^l + i\omega\dfrac{u_{n+1}^{l-1} - u_{n+1}^{l+1}}{2\delta x}. \end{cases}$$

Recall that as we are in the space H_T^θ, we know that $u(x+T) = e^{i\theta}u(x)$, therefore with the discretization on the space interval $[0,T]$, we have

$$u_{n+1}^L = e^{i\theta}u_{n+1}^0$$

Remark 3.3.4. Since the problem is invariant under phase multiplication and spatial translation, at each step we shift u_j so that the minimum of its modulus is at the boundary, and is real. We do the same for the numerical solutions of the ordinary differential equation.

3.3.5 Experiments

Our main observation is the following.

Observation 3.3.5. Let $(J, E) \in D_1$ (D_2, D_3 respectively) for each defocusing and focusing case, u_{ode} be the associated solution of the ordinary differential equation (3.1.2). Then (up to phase shift and translation) the minimizer of the problem

$$\min\{\mathcal{E}(u) : u \in H^{\theta}_{T},\ M(u) = M(u_{ode}), P(u) = P(u_{ode}), u \in H^{\theta}_{T}\},$$

is given by u_{ode}.

We performed different tests using the schemes described above. In every test we were comparing the minimizer that we obtained from the normalized gradient flow with the numerical solution of the ordinary differential equation. The choice of the initial data was arbitrary and equal to $u_0(x) = 1 + i + \cos\left(\frac{2\pi x}{T}\right)$. Other initial data lead to similar results. We use $N = 1000$ grid points for the interval $[0, T]$. We run the algorithm until a maximal difference of $\epsilon = 10^{-6}$ between the absolute values of the moduli of u^l_j. For the time discretization we take $\delta_t = 10^{-3}$.

Minimization among periodic functions is completely covered by theoretical results (see Theorems 3.3.2, 3.3.1). Therefore we started the experiments by testing the conjecture on these cases: the dnoidal, the cnoidal and the snoidal functions. We have chosen to fix $k = 0.9$. Recall that to run the algorithm we have to fix a, b, J and E. For these three cases we fix $J = 0$.

We start with the periodic case. Let

$$E = -0.095, \quad b = 2, \quad a = -(2 - k^2).$$

As mentioned in Section 3.3.2, after fixing J and E we can now find the period T, the Floquet multiplier θ , the mass m and the momentum p. We found the following quantities:

$$T = 2\mathbf{K}(k), \quad \theta = 0, \quad m = \mathbf{E}(k), \quad p = 0,$$

which are exactly the period, mass and momentum of the dnoidal function. We start by plotting u_{ode} the numerical solution of the ordinary differential equation (3.1.2) and the function $dn(x, k)$. We can see on the left of Figure 3.4 that u_{ode} is very close to the exact solution dn. The second step is to run the algorithm and find the minimizer u_{min} which we compare to the solution of the ODE u_{ode}. We observe convergence towards dnoidal functions as we see on the right of Figure 3.4 with a maximum difference between the solutions of 3×10^{-3}.

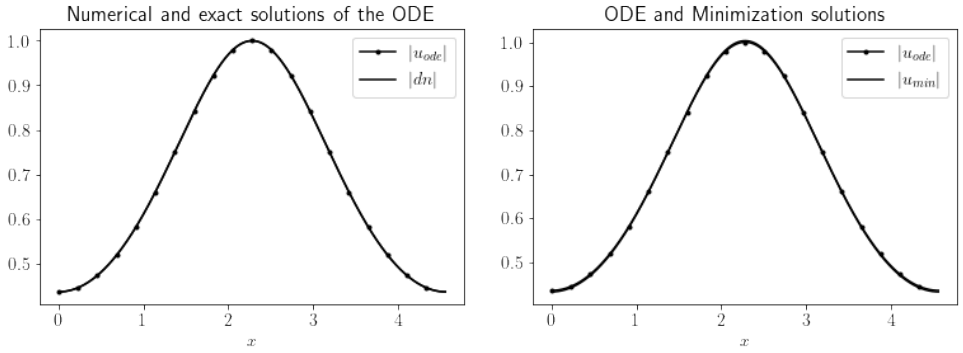

Figure 3.4 – Comparison of the dn function and the solutions of the ODE and the minimization problem.

The second case is the anti-periodic functions. We fix

$$E = 0.095, \quad b = 2k^2, \quad a = 1 - 2k^2.$$

Same as before we find the period T, the mass m and the momentum p. For the Floquet multiplier θ, we impose $\theta = \pi$ and therefore we have:

$$T = 2\mathbf{K}(k), \quad \theta = \pi, \quad m = \frac{(\mathbf{K} - \mathbf{E})}{k^2}, \quad p = 0.$$

We start by comparing the numerical solution of the ODE with the exact solution. We can see on the left of Figure of 3.5 that the numerical solution of the ODE is the exact solution cn. Then we compare it to the solution of the minimization problem. We observe convergence towards cnoidal functions as we see on the right of Figure 3.5 with a maximum difference between the solutions of 3×10^{-4}.

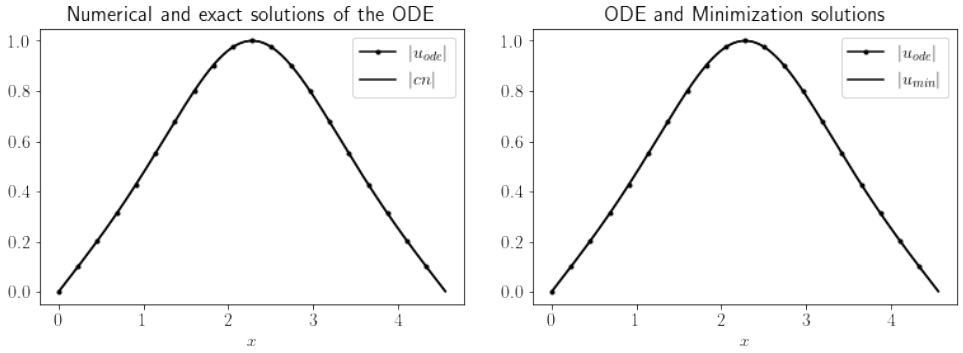

Figure 3.5 – Comparison of the cn function and the solutions of the ODE and the minimization problem.

For the third case, let

$$E = 0.5, \quad b = -2k^2, \quad a = 1 + k^2.$$

With the same method as before we have

$$T = 2\mathbf{K}(k), \quad \theta = \pi, \quad m = \frac{8}{bT}\mathbf{K}(\mathbf{K} - \mathbf{E}), \quad p = 0.$$

First we can see on the left of Figure of 3.6 that the numerical solution of the ODE is the exact solution sn. Then we compare it to the solution of the minimization problem. We observe convergence towards snoidal functions as we see on the right of Figure 3.6 with a maximum difference between the solutions of 1×10^{-2}. This case is not covered by the theoretical result. Our observation here is similar to the one of [46]: snoidal functions minimize the energy on fixed mass and 0 momentum among anti-periodic functions.

Now we will test the conjecture on the other cases where we do not know the theoretical results i.e. for complex valued solutions of (3.1.2). To do so we fix different values of J and for each of these values, we choose E such that $(J, E) \in D_1$, $((D_2), (D_3))$ defined in (3.2.2), (3.2.3), (3.2.4). We plot the numerical solution of the ODE and the solution of the minimization problem and we do the comparison.

We start with the defocusing case, and we fix $b = -1$ and $a = 1$. We choose $J = 0.2$ arbitrarily. For other values of $(J, E) \in D_1$ that we tested, we obtain the same result. Then we fix three values of E such that: the first one corresponds to $E = E_-(J) = V(J, r_Q)$, where we know that the solution is a plane wave, the second is strictly between $E_-(J)$and $E_+(J)$ and the third is very close to $E_+(J)$. For each value of E we plot the numerical solution of the ODE and the solution of the minimization problem. As we can see in Figure 3.7, we obtain a very good agreement with the conjecture. For the first value of E we have a maximum difference between the solutions of 5×10^{-8}, for the second value of E a maximum difference of 1×10^{-2} and for the third value of E a maximum difference of 3×10^{-2}.

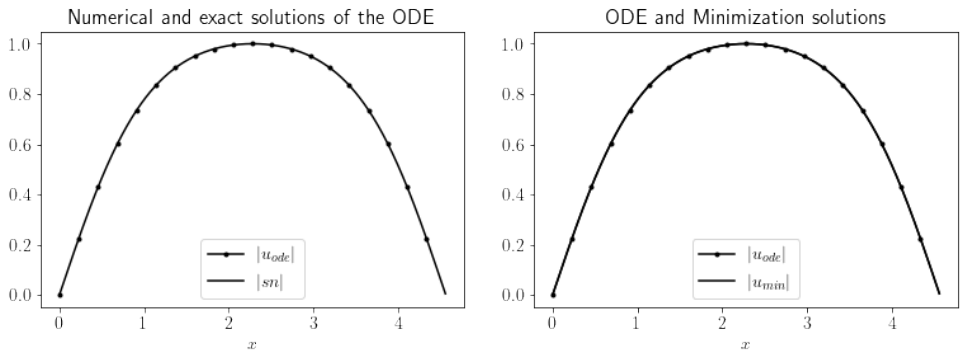

Figure 3.6 – Comparison of the sn function and the solutions of the ODE and the minimization problem.

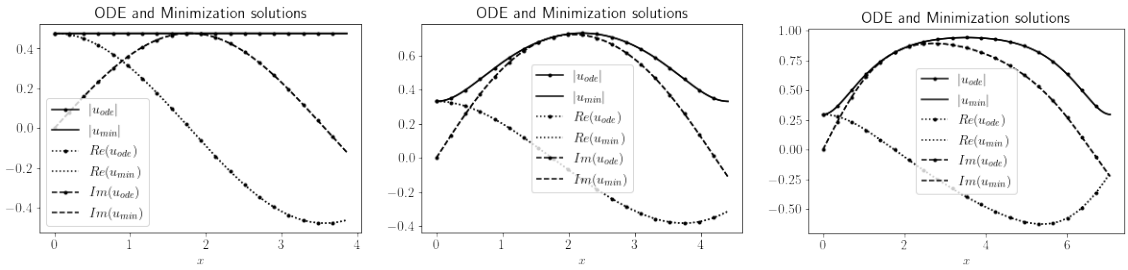

Figure 3.7 – Comparison between u_{min} and u_{ode} for the defocusing case.

We do the same for the focusing case, with positive a. We fix $b = 1$ and $a = 1$ and an arbitrary $J = 1$. We choose two values for E. The first one $E = E_{-}(J) = V(J, r_Q)$ and the second such that $E_{-}(J) < E = 5$. We plot the solutions and we can see in Figure 3.8 that the solution of the ODE is the minimizer with a maximum difference of 1.2×10^{-7} for the first value of E and 1×10^{-2} in the second.

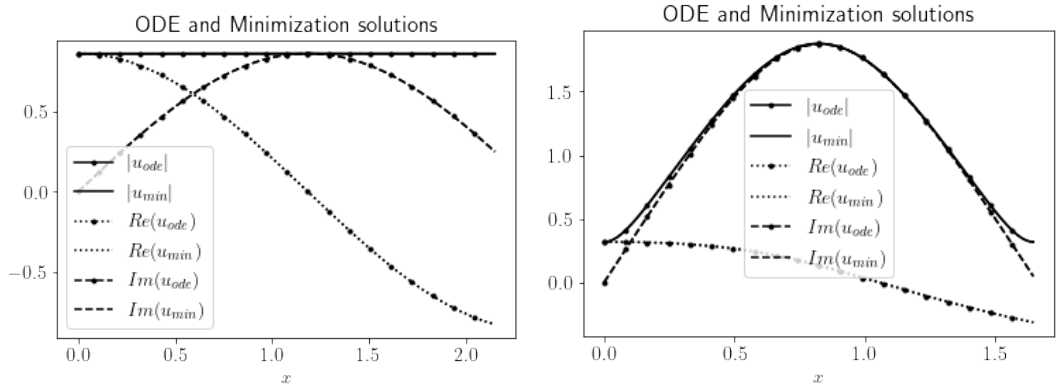

Figure 3.8 – Comparison between u_{min} and u_{ode} for the focusing case with $a = 1$.

Finally the focusing case with negative a. We fix $b = 1$ and $a = -1$ and an arbitrary $J = 4$. We choose two values for E. The first one $E = E_{-}(J) = V(J, r_Q)$ and the second $E_{-}(J) < E = 7$. We plot the solutions and we can see in Figure 3.9 that the solution of the ODE is the minimizer. For the first value of E we have a maximum difference between the solutions of 6×10^{-8}, for the second value of E a maximum difference of 2×10^{-3}.

3.3.6 Order of the scheme

Using the numerical solution of the ODE and the solution of minimization problem, we were able to evaluate the order of the scheme which is of order

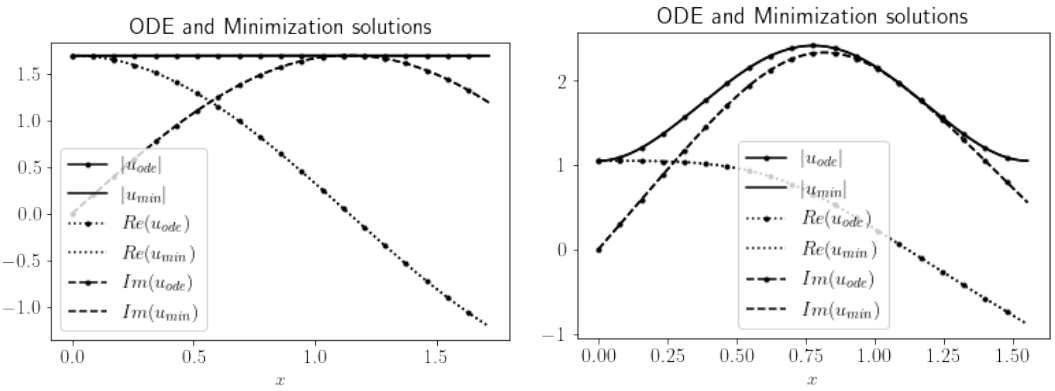

Figure 3.9 – Comparison between u_{min} and u_{ode} for the focusing case with $a = -1$.

1. To confirm this we make various simulations for different mesh sizes δ_x and present the results below. We tried to change the Laplacien and the matrix of the derivative to order 4 in order to obtain a better order of the scheme but the observed order of the scheme was still 1.

For the defocusing case, we choose to fix $(J, E) = (0.15, 0.25)$ and $(J, E) = (0.3, 0.29)$ arbitrarily. We present the results in Figure 3.10. For the focusing case with positive $a = 1$, we choose to fix $(J, E) = (1, 2)$ and $(J, E) = (2, 5)$ arbitrarily. We present the results in Figure 3.11. For $a = -1$ we fix $(J, E) = (2, 6)$ and $(J, E) = (3, 6)$. We can see in Figure 3.12 that the scheme is of order 1.

Remark 3.3.6. When we minimize the energy without the momentum constraint, for the dnoidal function the scheme is of order 2. For the cnoidal function it is of order 1.

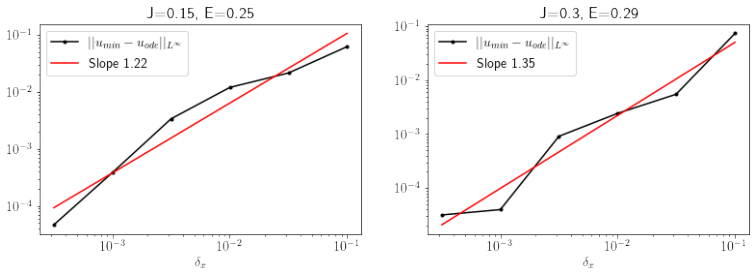

Figure 3.10 – Defocusing case.

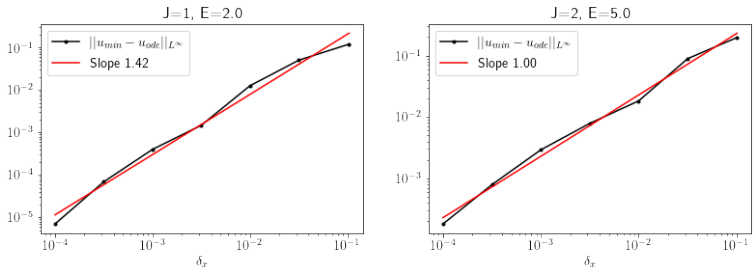

Figure 3.11 – Focusing case with $a = 1$.

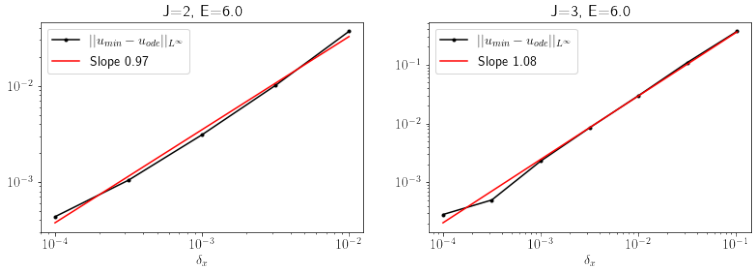

Figure 3.12 – Focusing case with $a = -1$.

3.4 Surfaces

3.4.1 The conserved quantities surfaces

In this section we plot the surfaces of the conserved quantities of the ordinary differential equation with respect to the period T, the Floquet multiplier θ and the conserved mass and momentum of the nonlinear Schrödinger equation (3.1.1). We start with the defocusing case. Let $b = -1$ and $a = 1$. We take 25 values of J between 0.1 and $\frac{4}{27}\frac{a^3}{b^2}$. For each value of J we take 40 value of E such that $E_-(J) \leqslant E < E_+(J) - 0.001$. For each couple (J, E) we find the period T, the Floquet multiplier θ, the mass M and the momentum P. Recall that from Section 3.2.4 we know that in the defocusing case the period T is strictly increasing in function of E and strictly decreasing in function of J for all $J > 0$. We represent each of the surfaces in Figures 3.13 and 3.14 .

For the focusing case let $b = 1$. For each positive or negative a, we take 50 values of J between 0.1 and 10. For each value of J we take 40 value of E such that $E_-(J) \leqslant E \leqslant 30$. For each couple (J, E) we find the period T, the Floquet multiplier θ, the mass M and the momentum P. Recall that from Section 3.2.4 we know that in the focusing case with positive a the period T is strictly decreasing in function of E and strictly decreasing in function of J for all $J > 0$. Unlike the other cases for the focusing case with a negative T is no longer a monotonic function of E (see Proposition 3.2.10). We represent

each of the surfaces in Figures 3.15 and 3.16 for $a = 1$ and in Figures 3.17 and 3.18 for $a = -1$.

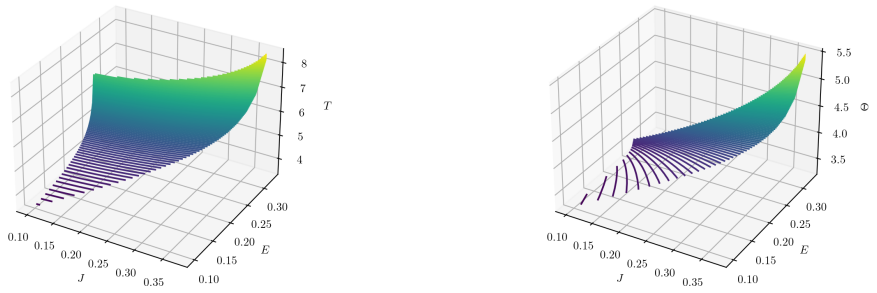

Figure 3.13 – Surfaces (J, E, T) and (J, E, θ) for the defocusing case.

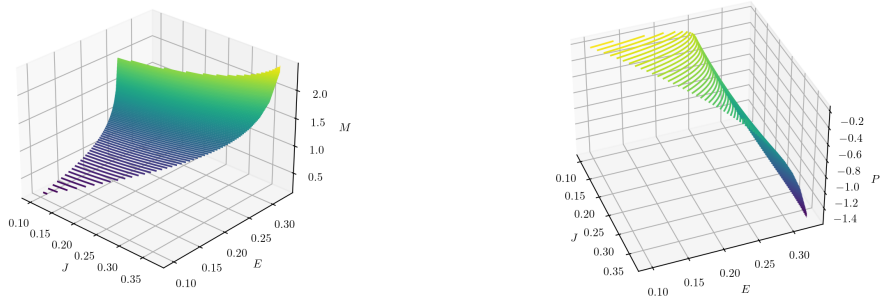

Figure 3.14 – Surfaces (J, E, M) and (J, E, P) for the defocusing case.

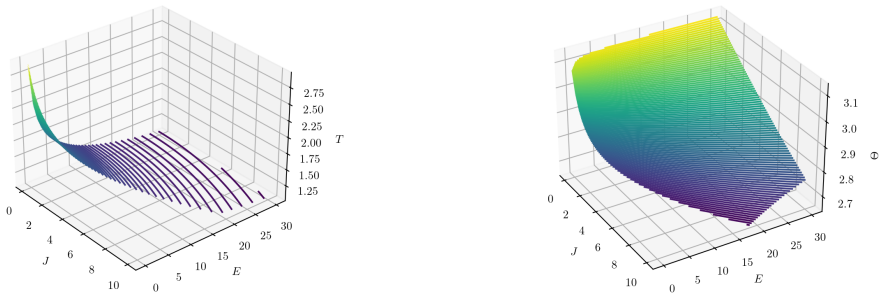

Figure 3.15 – Surfaces (J, E, T) and (J, E, θ) for the focusing case with $a = 1$.

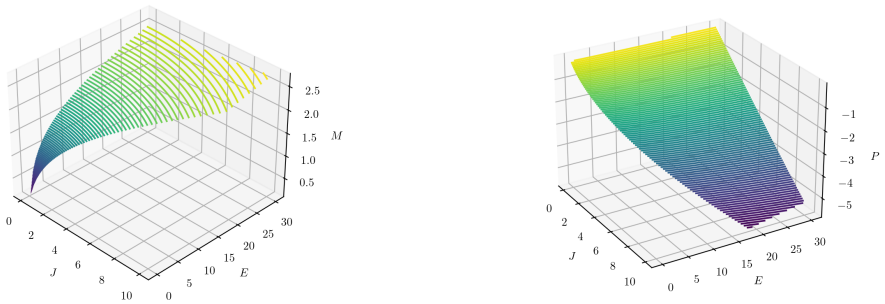

Figure 3.16 – Surfaces (J, E, M) and (J, E, P) for the focusing case with $a = 1$.

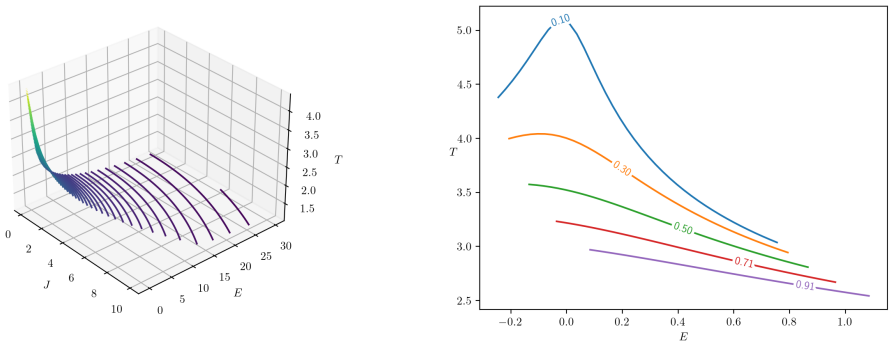

Figure 3.17 – Surface (J, E, T) for the focusing case with $a = -1$.

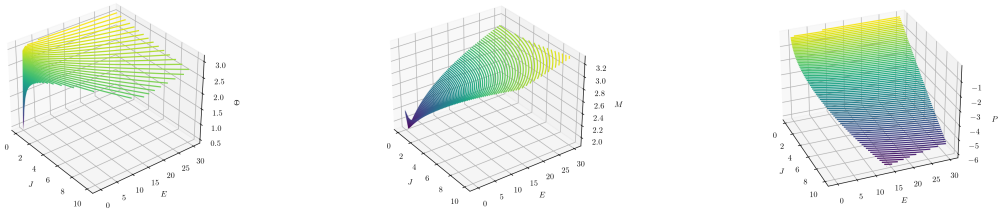

Figure 3.18 – Surfaces (J, E, θ), (J, E, M) and (J, E, P) for the focusing case with $a = -1$.

3.4.2 The energy surfaces

In this section we will represent the surface in $(M, P, \mathcal{E})$ for each of the focusing/defocusing case. We fix $N = 500$, $T = \pi$ and we will take 2 values of θ which are 0 and π. We start with the defocusing case. Let $b = -1$ and $a = 1$. Let $\theta = 0$. We choose the mass such that it varies from 1 to 3 with $r = 17$ values. Then for each value of M we let P varies in $(0, 2M)$ with $k = 11$ values. Using the gradient flow algorithm we find the solution for every fixed (M, P) and we calculate the energy $\mathcal{E}$ of every solution and we represent the surface $(M, P, \mathcal{E})$. As we can see in Figure 3.19, for the defocusing case with $\theta = 0$ the energy is increasing as a function of P and the minimum of the energy is at $P = 0$ which is consistent with the fact that in the defocusing case with periodic solutions the minimizer of the energy with fixed mass is the constant function. Now we fix $\theta = \pi$. In this case and same as before we represent the surface in $(M, P, \mathcal{E})$ in Figure 3.20. We can see that the energy starts decreasing from $P = 0$ to $P = M$ and then increases. This is consistent with the fact that in the anti-periodic case the minimizer is a plane wave which occurs at $P = M$.

Finally, for the focusing case let $b = 1$ and $a = -1$. In this case the surface $(M, P, \mathcal{E})$ is represented in Figure 3.21. We can see that the energy is an increasing function of P.

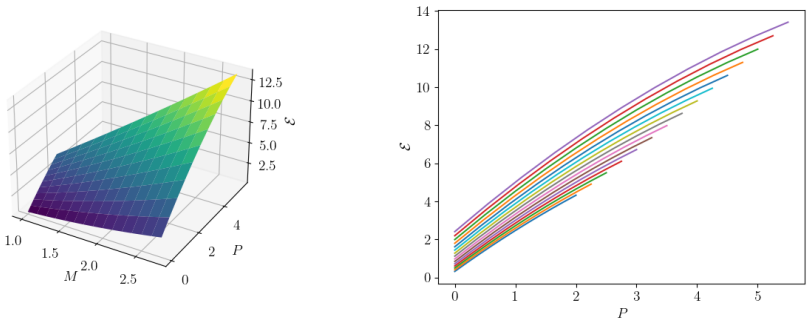

Figure 3.19 – Defocusing case with $\theta = 0$.

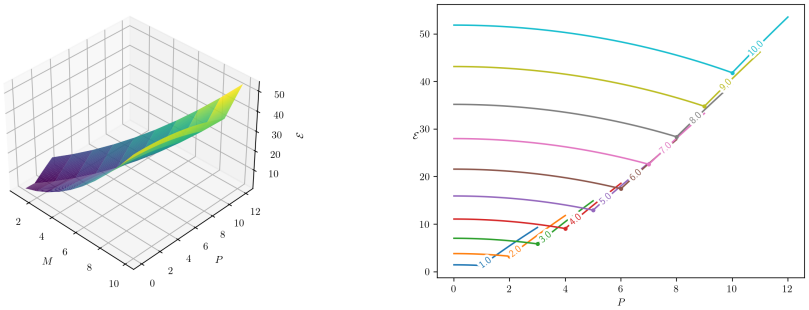

Figure 3.20 – Defocusing case with $\theta = \pi$.

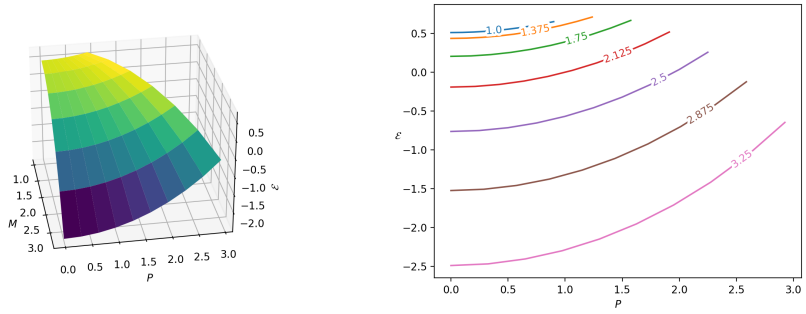

Figure 3.21 – Focusing case with $a = -1$ and $\theta = \pi$.

3.5 Notebook

This section includes the Python code that we have developed to demonstrate our findings. Our goal is to compute the minimizer of the energy at a fixed mass m and momentum p using the normalized gradient flow approach. Furthermore, we compare the obtained minimizer with the solution of the ordinary differential equation, which we also compute.

[1]:
```
import matplotlib.pyplot as plt
import numpy as np
import numpy.linalg as nl
import math
import functools
import scipy as sp
import scipy.optimize
import scipy.integrate as integrate
import scipy.sparse as scs
import scipy.sparse.linalg as scl

from scipy.integrate import odeint
from odeintw import odeintw

from IPython.display import display, clear_output
```

[2]:
```
TeXFont = True
#plt.rcParams['figure.figsize']=[6,(3/4)*6]
if TeXFont:
    plt.rcParams['font.size'] = 14.0          # font size
    plt.rcParams['mathtext.fontset'] = 'cm'   # computer moder math font
    plt.rcParams['text.usetex'] = True        # use tex engine for␣
 ↪everything (useful for the axes labels)
else:
    plt.rcParams['text.usetex'] = False

FontSize = 14
```

[3]:
```
N=1000
```

[15]:
```
b=-1 #fix b
a=1  #fix a
```

[16]:
```
#In the case of the Jacobi elliptic functions, we fix a,b,k and m

#k=0.9
#m=k**2

#b=2  #dn
#a=-(2-k**2) #dn

#b=2*k**2  #cn
#a=1-2*k**2  #cn

#b=-2*k**2  #sn
#a=1+k**2 #sn

#u0=1
```

```
#E=a*(u0)**2/2+b*(u0)**4/4
#print(E)
```

The effective potential

$$V_J(r) = \frac{J^2}{2r^2} + a\frac{r^2}{2} + b\frac{r^4}{4}. \tag{1}$$

[17]:
```
def V(J,r):
    return (J**2)/(2*r**2)+a*(r**2)/2+b*(r**4)/4
```

We start our numerical experiments by fixing a value of J in the domain D for each focusing/defocusing case.

[18]:
```
print(math.sqrt(abs(4*a**3/(27*b**2))))
```

```
0.3849001794597505
```

[21]:
```
J=0.2 #fix J
if b<0 and (J**2)>(4*a**3/(27*b**2)):
    print('J is not in the admissible range for existence of solutions')
```

[22]:
```
r = np.linspace(0.02,3,200)
plt.plot(r,V(J,r))
```

[22]:
```
[<matplotlib.lines.Line2D at 0x7f9d0fd8e520>]
```

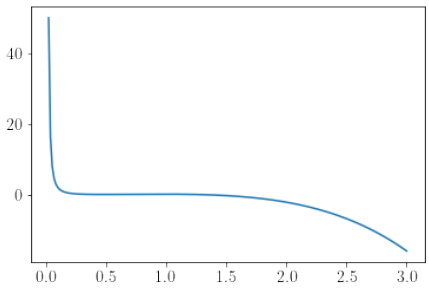

If we are in the defocusing case we find r_Q and r_q where the minimum and the maximum of $V_J(r)$ occurs. We know that $E_- = V_J(r_Q)$ and $E_+ = V_J(r_q)$. If we are in the focusing case we find r_Q where the minimum of $V_J(r)$ occurs and we have $E_- = V_J(r_Q)$.

[23]:
```
def v(J,r):   #derivative of V(J,r) to find the minimum and the maximum
    return -(J**2)/(r**3)+a*r+b*r**3
```

[24]:
```
coeff= [b,0,a,0,0,0,-J**2]
s=np.roots(coeff)
real_valued = s.real[abs(s.imag)<1e-8] # where I chose 1-e5 as a␣
 ↪threshold
roots=real_valued[real_valued>=0]
```

```
if b<0:
    rQ=roots[1]
else:
    rQ=roots[0]
rq=roots[0]
print(rQ,rq)
print(V(J,rQ),V(J,rq))
```

```
0.4770335840617313 0.9778838168185794
0.18872302001819116 0.2704365170651153
```

[25]:
```
# Keep for non polynomial V
# For polynomial V, use the roots
#vv=functools.partial(v,J)
#rQ=scipy.optimize.fsolve(vv,0.01)  #rQ where the minimum of V(J,r) occurs
#rq=scipy.optimize.fsolve(vv,1)     #rq where the maximum of V(J,r) occurs
#print(rQ,rq)
#print(V(J,rQ),V(J,rq))
```

[28]:
```
Q=math.sqrt(abs(a+b*rQ**2))
q=math.sqrt(abs(a+b*rq**2))
print(Q,q)
```

```
0.8788850662499729 0.20914884844131254
```

We know that $E_- = V_J(r_Q)$ and $E_+ = V_J(r_q)$. Then in the defocusing case, we choose E such that $E_- \leq E < E_+$. And in the focusing case we choose E such that $E_- \leq E$.

[29]:
```
n=10
if J==0:
    E=np.linspace(E,E,n) # To keep the values used for dn, cn, sn
elif b<0:
    E=np.linspace(V(J,rQ),V(J,rq)-0.001,n) #should be between V(J,rQ)<E<V(J,rq)
    #E=np.linspace(V(J,rQ),0.29,n)
else:
    E=np.linspace(V(J,rQ),7,n) #should be V(J,rQ)<E, 7 arbitrary value

print(E)
```

```
[0.18872302 0.19769119 0.20665935 0.21562752 0.22459569 0.23356385
 0.24253202 0.25150018 0.26046835 0.26943652]
```

We find the positive roots of $E - V_J(r)$.

[30]:
```
R=[]                # we solve E-V(J,r)=0 to find the roots r1,r2 and r3
for i in range(n):
```

```
    print(i)
    c=[-b,0,-2*a,0,4*E[i],0,-2*J**2]
    l=np.roots(c)
    real_valued = l.real[abs(l.imag)<1e-5]  #where I chose 1-e5 as a␣
↪threshold
    roots= real_valued[real_valued>0]
    roots.sort()
    print(roots)
    R+=[roots]
```

```
0
[0.47703357 0.4770336  1.24293118]
1
[0.4032382  0.57043643 1.22963459]
2
[0.37717092 0.61704513 1.21531782]
3
[0.35871481 0.6572121  1.19974828]
4
[0.34412042 0.69502394 1.18259159]
5
[0.33194925 0.73243323 1.16333626]
6
[0.32146987 0.77102879 1.1411274 ]
7
[0.31225131 0.81288612 1.11432278]
8
[0.304015   0.86236914 1.07883935]
9
[0.29656889 0.94321343 1.01113566]
```

On the boundary $E = E_-$ the period T is given by the limit when E tends to E_-. The period T is given by

$$T(J,E) = 2\int_{r_1}^{r_2} \frac{1}{\sqrt{2(E - V_J(r))}} dr.$$

The Floquet multiplier is given by

$$\theta(J,E) = \phi(x+T) - \phi(x) = \int_0^T \phi_x(x)dx$$
$$= \int_0^T \frac{J}{r^2(x)}dx = 2\int_{r_1}^{r_2} \frac{J}{r^2\sqrt{2(E - V_J(r))}} dr.$$

The mass is given by

$$M(J,E) = \frac{1}{2}\int_0^T |u|^2 dx = \frac{1}{2}\int_0^T r^2(x)dx = \int_{r_1}^{r_2} \frac{r^2}{\sqrt{2(E - V_J(r))}} dr.$$

And the momentum is given by

$$P(J,E) = \frac{1}{2}\Im\int_0^T u\bar{u}_x dx = -\frac{1}{2}\int_0^T \phi_x r^2 dx$$
$$= -\frac{1}{2}\int_0^T J dx = -\frac{JT}{2} = -\int_{r_1}^{r_2} \frac{J}{\sqrt{2(E-V_J(r))}} dr.$$

When $E \to E_-(J)$ the following holds:

$$\lim_{E\to E_-(J)} T(J,E) = \frac{\pi\sqrt{2}}{\sqrt{3Q^2-a}}, \quad \lim_{E\to E_-(J)} M(J,E) = \frac{|Q^2-a|}{2|b|}\frac{\pi\sqrt{2}}{\sqrt{3Q^2-a}},$$

$$\lim_{E\to E_-(J)} P(J,E) = -\frac{1}{2}Q\frac{(Q^2-a)}{b}\frac{\pi\sqrt{2}}{\sqrt{3Q^2-a}}.$$

For the defocusing case, when $E \to E_+(J)$ the following holds:

$$\lim_{E\to E_+(J)} T(J,E) = +\infty, \quad \lim_{E\to E_+(J)} M(J,E) = +\infty,$$

$$\lim_{E\to E_+(J)} P(J,E) = -\infty.$$

[32]:
```
# Warning: does not take J=0 into account
T=[]
Theta=[]
Mass=[]
P=[]
for i in range(n):
    if E[i]==V(J,rQ):      #plane wave on the boundary E=E_
        t=(math.pi* math.sqrt(2))/math.sqrt(abs((3*Q**2-a)))
        theta=Q*t
        mass=abs((Q**2-a)/b)*t/2
        p=-Q*abs((Q**2-a)/b)*t/2

    else:
        t=integrate.quad(lambda r: 2/(math.
↪sqrt(2*(E[i]-V(J,r)))),R[i][0],R[i][1])[0]
        theta=integrate.quad(lambda r: 2*J/(r**2*math.
↪sqrt(2*(E[i]-V(J,r)))),R[i][0],R[i][1])[0]
        mass=integrate.quad(lambda r: r**2/(math.
↪sqrt(2*(E[i]-V(J,r)))),R[i][0],R[i][1])[0]
        p=integrate.quad(lambda r: -J/(math.
↪sqrt(2*(E[i]-V(J,r)))),R[i][0],R[i][1])[0]

    T+=[t]
    Theta+=[theta]
    Mass+=[mass]
```

```
    P+=[p]

print(T)
print(Theta)
print(Mass)
print(P)
```

```
[3.8709694357533957, 3.9485816232601585, 4.037153071335709, 4.
↪140091496655486,
4.262662811923297, 4.413637390919369, 4.6092835723471905, 4.
↪8853781622577745,
5.350452558101836, 7.063792023604424]
[3.4021372289937433, 3.4143576837487988, 3.4285582296326544, 3.
↪445388344853337,
3.4658617612291454, 3.4916848623211587, 3.526059027086435, 3.
↪5761123703181696,
3.6637750705155403, 4.007528305825266]
[0.44044091592886525, 0.4843078001338, 0.5337798144019222, 0.
↪5905526075453051,
0.6572345919189245, 0.7381494793422435, 0.8412772233349577, 0.
↪9840726921022922,
1.2191687539643439, 2.0559075637909263]
[-0.38709694357533947, -0.3948581623260117, -0.40371530713356835,
-0.414009149665553, -0.4262662811923308, -0.4413637390919343,
-0.46092835723471903, -0.4885378162257671, -0.5350452558101829,
-0.7063792023640353]
```

[34]:
```
j=0 # take a value inside E
```

[35]:
```
#Theta=np.linspace(np.pi,np.pi,n)
# case J=0 to be treated
```

[36]:
```
def D(delta_x,N):
    A=scs.identity(N,dtype = 'complex_')
    A=A.tolil()
    for i in range(N):
        A[i,i]=0
    for i in range(N-1):
        A[i+1,i]=-1
        A[i,i+1]=1
    A[0,N-1]=-np.exp(-1j*Theta[j])
    A[N-1,0]=np.exp(1j*Theta[j])
    A=A/(2*delta_x)
    return A
def Lap(delta_x,N):
    A=scs.identity(N,dtype = 'complex_')
    A=A.tolil()
    for i in range(N):
```

```
        A[i,i]=-2
    for i in range(N-1):
        A[i,i-1]=1
        A[i+1,i]=1
        A[i,i+1]=1
    A[0,N-1]=np.exp(-1j*Theta[j])
    A[N-1,0]=np.exp(1j*Theta[j])
    A=A/(delta_x**2)
    return A
```

[37]:
```
delta_t=10**(-3)
Epsilon=10**(-6)
IterMax=10**(5)
x=np.linspace(0,T[j],N,endpoint=False)
delta_x=x[1]-x[0]
u=1+np.cos(2*math.pi*x/T[j])+1j # futur initial data
#u=sol[:,0]
plt.plot(x,np.abs(u))
```

[37]:
```
[<matplotlib.lines.Line2D at 0x7f9d1016d220>]
```

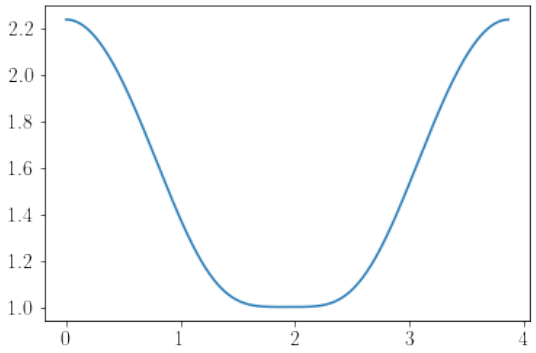

[38]:
```
#In the case of the Jacobi elliptic functions
#sn, cn, dn, ph=sp.special.ellipj(x, m)

#if J==0:
#    if b==2:
#        y0= [dn[0],-k**2*cn[0]*sn[0]]
#    elif b==2*k**2:
#        y0= [cn[0],-sn[0]*dn[0]]
#    elif b==-2*k**2:
#        y0= [sn[0],cn[0]*dn[0]]
#z=sn
#zmin=np.argmin(np.abs(z))
#z=np.concatenate((np.exp(-1j*Theta[j])*z[zmin:],z[:zmin]),axis=0)
```

```
#z=(np.conjugate(z[np.int(0)])/np.abs(z[np.int(0)]))*z
```

[40]:
```
#Numerical solution of the ordinary differential equation
def fun(y, x):
    # x is space/time and y the vector solution of the first order ODE
    u, v = y
    dydx = [v,-a*u-b*abs(u)**2*u]
    return dydx

y0=[R[j][0],1j*J/(R[j][0])]

sol =odeintw(fun, y0, x)
```

[41]:
```
solmin=np.argmin(np.abs(sol[:, 0]))
sol[:, 0]=np.concatenate((np.exp(-1j*Theta[j])*sol[:, 0][solmin:],sol[:
 ↪, 0][:solmin]),axis=0)
sol[:, 0]=(np.conjugate(sol[:, 0][np.int(0)])/np.abs(sol[:, 0][np.
 ↪int(0)]))*sol[:, 0]
sol[:, 0]=sol[:, 0]*np.sign(np.real(sol[:, 0][0]))
```

[42]:
```
#Compare the fixed Mass m with the mass of the ODE solution
#same for the momentum P
print(1/2*(nl.norm(sol[:, 0])*math.sqrt(delta_x))**2-Mass[j])
print(1/2*(delta_x*sum((sol[:, 0])*(D(delta_x,N)*(sol[:, 0])).
 ↪conjugate())).imag-P[j])
```

```
-2.4082479843645643e-08
7.679099551793911e-07
```

[43]:
```
plt.plot(x,abs(sol[:, 0]),'k',marker='.
 ↪',markevery=50,label='$|u_{ode}|$')
plt.plot(x, (np.real(sol[:, 0])),'k:',marker='.
 ↪',markevery=50,label='$Re(u_{ode})$')
plt.plot(x, np.imag(sol[:, 0]),'k--',marker='.
 ↪',markevery=50,label='$Im(u_{ode})$')

#plt.plot(x,abs(z),'k',label='$|sn|$')
#plt.plot(x,np.real(z),'r--',label='Real(dn)')#
#plt.plot(x, np.imag(z),'g--',label='Imag(dn)')

#plt.plot(x,(np.sqrt(1-Q**2))*np.real(np.exp(1j*Q*x)),'r-.
 ↪',label='plane wave')

plt.xlabel('$x$')
#plt.ylabel('y label')
plt.title("Numerical and exact solutions of the ODE")
plt.legend()
plt.show()
```

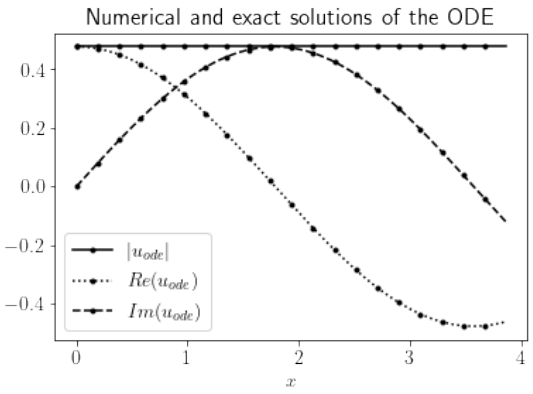

[44]:
```
def Energie(u):
    return 1/2*(nl.norm(D(delta_x,N)*u))**2*delta_x-b/4*(nl.
 ↪norm(u**2))**2*delta_x
```

[46]:
```
def cngf(u,Mass,P,b,delta_t,delta_x,Epsilon,IterMax):
    N=np.size(u)
    M_1 = scs.identity(N) - delta_t*Lap(delta_x,N)
    for n in range(IterMax):
        u_old = u
        M = M_1 - b*delta_t*scs.diags(abs(u)**2)
        u = scl.spsolve(M,u)

        m0= 1/2*(nl.norm(u)*math.sqrt(delta_x))**2
        p0= 1/2*(delta_x*sum(u*(D(delta_x,N)*u).conjugate())).imag
        k0= 1/2*(nl.norm(D(delta_x,N)*u)*math.sqrt(delta_x))**2

        print(p0**2-m0*k0)
        if abs(m0*k0-p0**2)>10**(-2):
            mu= (k0*(Mass[j]-m0)-p0*(P[j]-p0))/(delta_t*2*(m0*k0-p0**2))
            om= (m0*(P[j]-p0)-p0*(Mass[j]-m0))/(delta_t*2*(m0*k0-p0**2))
            K=(1-delta_t*mu)*scs.csr_matrix(scs.
 ↪identity(N))-delta_t*1j*om*D(delta_x,N)
            u=scl.spsolve(K,u)

        else:
            u= np.sqrt(2*Mass[j]/T[j])*np.exp(1j*(-P[j]/Mass[j])*x)
            break

        umin=np.argmin(abs(u))
        u=np.concatenate((np.exp(-1j*Theta[j])*u[umin:],u[:
 ↪umin]),axis=0)

        u=(np.conjugate(u[np.int(0)])/np.abs(u[np.int(0)]))*u
```

```
        u=u*np.sign(np.real(u[0]))

        clear_output(wait=True)
        print('iteration',n,'stop-crit',nl.norm(u-u_old)/nl.norm(u_old))


        Stop_crit = nl.norm(u-u_old)/nl.norm(u_old)<Epsilon
        if Stop_crit:
            break

    print(f'End at iteration {n+1} on {IterMax}')
    return u
```

[47]:
```
v=cngf(u,Mass,P,b,delta_t,delta_x,Epsilon,IterMax)
```

```
iteration 880 stop-crit 0.0006650850053313828
-0.009981388128428997
End at iteration 882 on 100000
```

[50]:
```
print(Energie(sol[:,0])-Energie(v))
print(1/2*(nl.norm(v)*math.sqrt(delta_x))**2-Mass[j])
print(1/2*(delta_x*sum((v)*(D(delta_x,N)*(v)).conjugate())).imag-P[j])
```

```
-2.4082360494670496e-08
-5.551115123125783e-17
7.467442608155572e-07
```

[51]:
```
plt.subplots(figsize=(15, 5))

plt.subplot(1, 2, 1)
plt.plot(x,np.abs(v),'g')
plt.plot(x,np.real(v),'r')
plt.plot(x,np.imag(v),'b')

plt.subplot(1, 2, 2)
plt.plot(x, np.abs(sol[:, 0]),'g--')
plt.plot(x, np.real(sol[:, 0]),'r--')
plt.plot(x, np.imag(sol[:, 0]),'b--')
```

[51]:
```
[<matplotlib.lines.Line2D at 0x7f9d1051d3d0>]
```

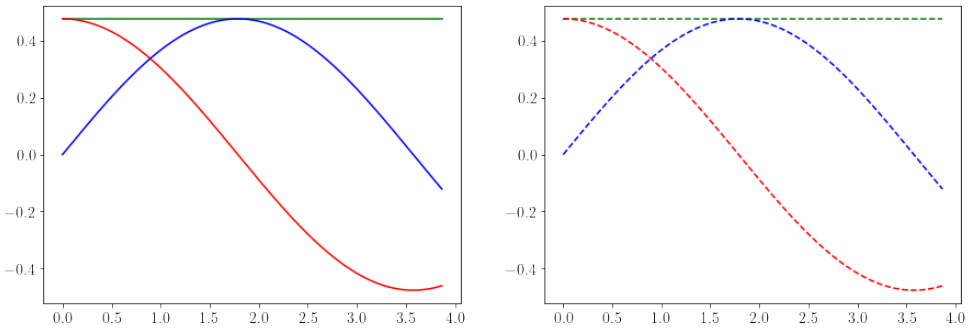

[52]:
```
plt.plot(x, np.abs(sol[:, 0]),'k',marker='.
  ↪',markevery=50,label='$|u_{ode}|$')
plt.plot(x, np.abs(v),'k',label='$|u_{min}|$')

plt.plot(x, np.real(sol[:, 0]),'k:',marker='.
  ↪',markevery=50,label='$Re(u_{ode})$')
plt.plot(x,np.real(v),'k:',label='$Re(u_{min})$')

plt.plot(x, np.imag(sol[:, 0]),'k--',marker='.
  ↪',markevery=50,label='$Im(u_{ode})$')
plt.plot(x,np.imag(v),'k--',label='$Im(u_{min})$')


plt.xlabel('$x$')
plt.title("ODE and Minimization solutions")


plt.legend()
plt.show()
```

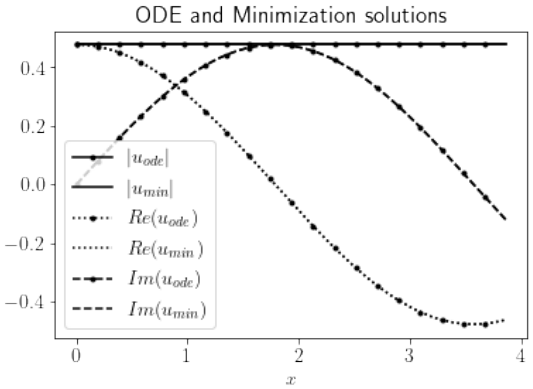

[53]:
```
plt.subplots(figsize=(15, 5))


plt.subplot(1,3,1)
plt.plot(x,abs(v-sol[:, 0]),'g')

plt.subplot(1,3,2)
plt.plot(x,np.real(v)-np.real(sol[:, 0]),'r')

plt.subplot(1, 3, 3)
plt.plot(x,np.imag(v)-np.imag(sol[:, 0]),'b')
```

[53]:
```
[<matplotlib.lines.Line2D at 0x7f9d10a25790>]
```

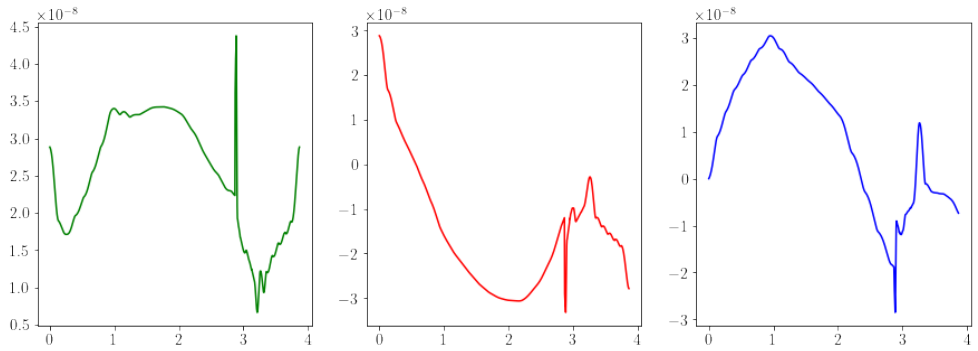

CHAPTER 4

General nonlinearity

4.1 Introduction

We consider in one space dimension the nonlinear Schrödinger equation

$$i\psi_t + \psi_{xx} + bf(\psi) = 0, \tag{4.1.1}$$

where $\psi : \mathbb{R}_t \times \mathbb{R}_x \to \mathbb{C}$, the nonlinearity $f : \mathbb{C} \to \mathbb{C}$ is defined for any $z \in \mathbb{C}$ by $f(z) = g(|z|^2)z$ with $g \in C^0([0, +\infty), \mathbb{R}) \cap C^2((0, +\infty), \mathbb{R})$ and $b \in \mathbb{R} \setminus \{0\}$. For simplicity, we denote by f' the derivative of $f_{|\mathbb{R}}$. We make the following assumptions on the nonlinearity:

- The function
$$h(s) := (sf(s) - 2F(s))s^{-2}, \tag{4.1.2}$$
is strictly increasing on $(0, +\infty)$, where $F(z) = \int_0^{|z|} f(s)ds = \frac{1}{2}G(|z|^2)$, with $G' = g$ and $G(0) = 0$. Also $\lim_{s\to 0} h(s) = 0$ and $\lim_{s\to 0} \frac{f(s)}{s} = 0$.
- There exist $M > 0$, $1 < p < 5$ and s_0 such that for all $s \geqslant s_0$ we have $|f(s)| \leqslant Ms^p$.

Under these assumptions, the functions $s \to \frac{F(s)}{s^2}$ and $s \to \frac{f(s)}{s}$ are increasing functions that grow to infinity. We also assume that f satisfies the inequality:

$$s^2 f''(s) > sf'(s) - f(s). \tag{4.1.3}$$

Finally, to avoid linear behavior of f at infinity, we assume that:

$$\lim_{s\to\infty} \left(\frac{f(s)}{s} - f'(s) \right) = -\infty. \tag{4.1.4}$$

Note that these assumptions hold for nonlinearities of the form of sum of powers with positive coefficients, for example.

We are particularly interested in the spatially periodic solutions $\psi(t, .) \in H^1_{loc} \cap P_T$, and anti-periodic solutions $\psi(t, .) \in H^1_{loc} \cap A_T$ where

$$P_T = \{f \in L^2_{loc}(\mathbb{R}) : f(x + T) = f(x)\},$$

and

$$A_T = \{f \in L^2_{loc}(\mathbb{R}) : f(x + T) = -f(x)\}.$$

The Cauchy problem (4.1.1) is known to be globally well posed in $H^1_{loc} \cap P_T$ (see [24]). Solutions to (4.1.1) conserve the mass M, the momentum P, and energy $\mathcal{E}$:

$$M(\psi) = \frac{1}{2}\int_0^T |\psi|^2 dx, \qquad P(\psi) = \frac{1}{2}\mathcal{I}m \int_0^T \psi\overline{\psi}_x dx$$

$$\mathcal{E}(\psi) = \frac{1}{2}\int_0^T |\psi_x|^2 dx - b\int_0^T F(\psi) dx.$$

The simplest non-trivial solutions of (4.1.1) are the *standing waves*. They are solutions of the form

$$\psi(t,x) = e^{-iat}u(x), \quad a \in \mathbb{R}.$$

The profile function $u(x)$ satisfies the ordinary differential equation

$$u_{xx} + au + bf(u) = 0. \tag{4.1.5}$$

It is an integrable ordinary differential equation, whose conserved quantities (on $\mathbb{C}$) are the momentum J and the energy E, given by

$$J = \mathcal{I}m(u_x\overline{u}), \qquad E = \frac{1}{2}|u_x|^2 + \frac{a}{2}|u|^2 + bF(u).$$

In the work of Gustafson, Le Coz and Tsai [46] they provided a global variational characterization of the cnoidal, snoidal, and dnoidal elliptic functions for the cubic case, and proved some orbital stability results for the corresponding solutions of the nonlinear Schrödinger equation.

In this work, we aim to generalize their results to the case of a general nonlinearity. Specifically, we start with the analysis of the profile equation (4.1.5), which describes the behavior of stationary solutions to (4.1.1). We will consider the real and complex-valued solutions and represent their phase portraits for various parameter regimes. We will then study the minimization problems for the energy functional with fixed mass and momentum constraints for the periodic and anti-periodic cases, extending the previous results to this more general setting. We will analyze the existence, uniqueness, and stability of the minimizers for each case, and investigate their properties in detail using variational methods. Finally, we will consider the minimization problem on the Nehari manifold. The ground state solutions for the minimization problem lie on the Nehari manifold, and we can characterize them by minimizing the energy functional subject to the Nehari constraint. The analysis of these problems is expected to provide a better understanding of the dynamics of the nonlinear Schrödinger equation.

4.2 Preliminaries

When dealing with functions in P_T, we will denote norms such $L^q(0,T)$ by

$$\|u\|_{L^q} = \|u\|_{L^q(0,T)} = \left(\int_0^T |u|^q\right)^{\frac{1}{q}},$$

and the complex L^2 inner product by

$$(f,g) = \int_0^T f\bar{g}dx.$$

4.2.1 Orbital stability

Recall that we say that the standing wave $\psi(t,x) = e^{-iat}u(x)$ is orbitally stable for the flow of (4.1.1) in the function space X if for all $\epsilon > 0$, there exists $\delta > 0$ such that the following holds: if $\psi_0 \in X$ verifies

$$\|\psi_0 - u\|_X \leqslant \delta,$$

then the solution ψ of (4.1.1) with initial data $\psi(0,x) = \psi_0$ verifies for all $t \in \mathbb{R}$ the estimate

$$\inf_{\theta\in\mathbb{R}, y\in\mathbb{R}} \|\psi(t,.) - e^{i\theta}u(.-y)\|_X < \epsilon.$$

4.3 Analysis of the profile equation

In this section, we study the bounded solutions of the profile equation (4.1.5). We will distinguish between two different cases depending whether or not $J = 0$. We introduce the polar coordinates

$$u(x) = r(x)e^{i\phi(x)},$$

with $r > 0$ and $r, \phi \in C^2(\mathbb{R})$. The invariants become

$$J = r^2\phi_x, \quad E = \frac{{r_x}^2}{2} + \frac{J^2}{2r^2} + a\frac{r^2}{2} + bF(r).$$

If $J = 0$, then replacing $r(x)e^{i\phi(x)}$ with $r(x)e^{i\phi}$ for some $\phi \in [0, 2\pi]$ we can assume that $u(x) \in \mathbb{R}$ up to a constant phase. If $J \neq 0$, then $u(x) \neq 0$ for all $x \in \mathbb{R}$, and $\phi_x \neq 0$. Define the effective potential by

$$V_J(r) = \frac{J^2}{2r^2} + a\frac{r^2}{2} + bF(r).$$

By elementary calculations, we have

$$V_J'(r) = -\frac{J^2}{r^3} + ar + bf(r).$$

In what follows, we describe the potential V_J. We start with the case $J = 0$. Then

$$V(r) = a\frac{r^2}{2} + bF(r), \quad V'(r) = ar + bf(r).$$

If $V'(r) = 0$, then $\frac{f(r)}{r} = -\frac{a}{b}$. We know that $\frac{f(r)}{r}$ is an increasing function for all $r > 0$ therefore there exists at most one value $r_0 > 0$ such that

$$ar_0 + bf(r_0) = 0.$$

We now discuss what happens depending on the values of a and b. We know that $\lim_{r\to 0} \frac{f(r)}{r} = 0$ and then $sign(V'(r)) = sign(a)$, when r approaches 0. And we know that $\lim_{r\to+\infty} V(r) = sign(b)\infty$, because we have $\lim_{r\to+\infty} \frac{F(r)}{r^2} = +\infty$. We start with the defocusing case where $b < 0$, and assume $a > 0$. Then $V'(r) = 0$ has exactly one solution. Therefore the graph of V as a function of r is given on the left of Figure 4.1. The second case is the focusing case where $b > 0$ with $a > 0$. Then $V'(r)$ has always the same sign. The graph of V as a function of r is represented on the center of Figure 4.1. The last case is the focusing case where $b > 0$ with $a < 0$, then $V'(r) = 0$ has again exactly one solution, and the graph of V as a function of r is represented on the right of Figure 4.1.

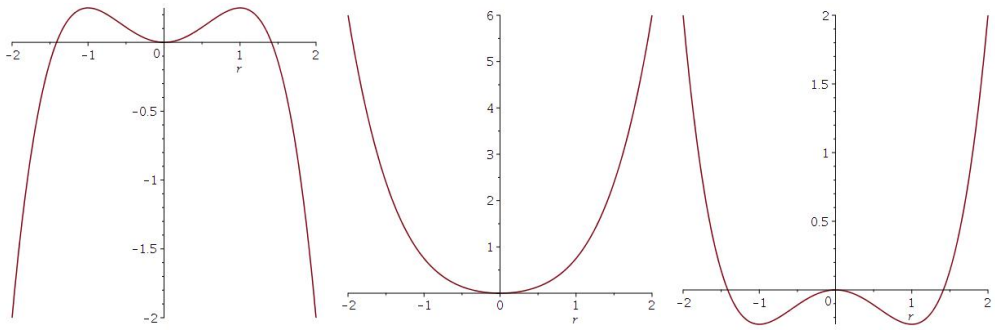

Figure 4.1 – $V(r)$ as a function of r with $J = 0$.

Now we suppose that $J \neq 0$. If $V_J'(r) = 0$, then $-J^2 + r^4\left(a + b\frac{f(r)}{r}\right) = 0$. Let

$$h(r) = r^4\left(a + b\frac{f(r)}{r}\right).$$

We will study the variations of the function h, which will give us the graph of the potential. We have

$$h'(r) = 4ar^3 + bf'(r)r^3 + 3br^2 f(r) = r^3 \left(4a + bf'(r) + 3b\frac{f(r)}{r}\right).$$

We start with the defocusing case where $b < 0$ and $a > 0$. In this case the graph of $h(r)$ as a function of r is presented on the left of Figure 4.2. Hence $V_J'(r) = 0$ has 2 solutions for $J^2 < r_c$ where $h'(r_c) = 0$ and the maximum occurs. Then the graph of V_J as function of r is presented on the left of Figure 4.3. The second case is the focusing case where $b > 0$ and $a > 0$. We know that $h(r)$ is a strictly increasing function presented on the center of Figure 4.2. Hence $V_J'(r) = 0$ has a unique solution. Then the graph of V_J as function of r is given on the center of Figure 4.3. The last case is the focusing case where $b > 0$ and $a < 0$. The graph of h as a function of r is represented on the right of Figure 4.2. Hence $V_J'(r) = 0$ has a unique solution. Then the graph of V_J as function of r is represented on the right of Figure 4.3.

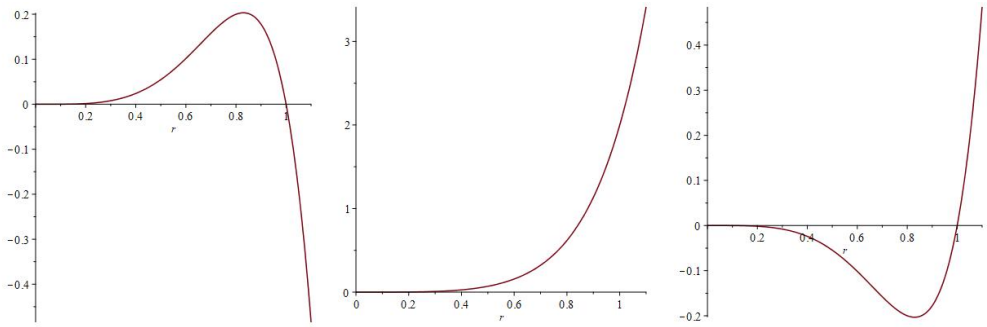

Figure 4.2 – $h(r)$ as a function of r.

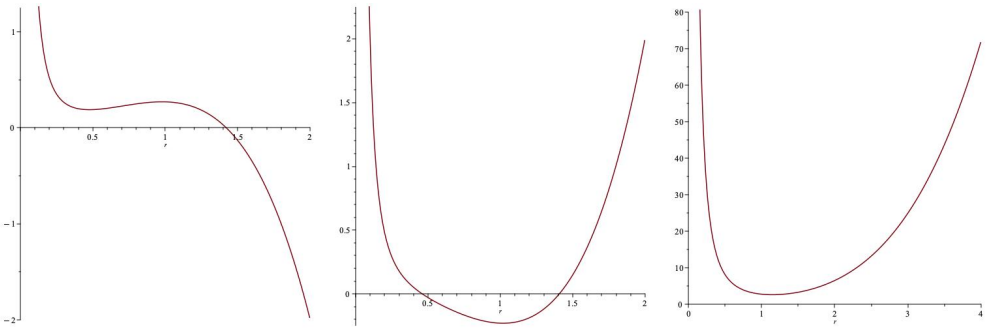

Figure 4.3 – $V_J(r)$ as a function of r with $J \neq 0$.

4.3.1 Phase portraits

In this section we will represent the phase portraits for each focusing and defocusing cases and depending whether or not $J = 0$. In polar coordinates, the equation (4.1.5) becomes

$$r_{xx} - \frac{J^2}{r^3} + ar + bf(r) = 0.$$

We rewrite this second order differential equation in the form of a first order system by introducing new coordinates

$$y = \begin{pmatrix} y_1 \\ y_2 \end{pmatrix} = \begin{pmatrix} r \\ r_x \end{pmatrix}.$$

Then the differential system is the following

$$y' = G(y) = \begin{pmatrix} y_2 \\ \frac{J^2}{y_1^3} - ay_1 - bf(y_1) \end{pmatrix} = \begin{pmatrix} f_1(y_1, y_2) \\ f_2(y_1, y_2) \end{pmatrix}.$$

We start by finding the equilibrium points y such that $G(y) = 0$. Then we find the isoclines I_0 and I_∞, where

$$I_\alpha = \left\{ (y_1, y_2) \in \mathbb{R}^2 : \frac{f_2(y_1, y_2)}{f_1(y_1, y_2)} = \alpha \right\}.$$

We start with the case $J = 0$. We have

$$I_0 = \{(y_1, y_2) \in \mathbb{R}^2 : y_2 \neq 0, ay_1 + bf(y_1) = 0\},$$

and

$$I_\infty = \{(y_1, y_2) \in \mathbb{R}^2 : -ay_1 - bf(y_1) \neq 0, \quad y_2 = 0\}.$$

These isoclines I_0 and I_∞ meet at the equilibrium points of the system and determine the regions where the trajectories are monotone:

$$\begin{aligned} Q_{++} &= \{y \in \mathbb{R}^2, \quad f_1(y) > 0, \quad f_2(y) > 0\}. \\ Q_{+-} &= \{y \in \mathbb{R}^2, \quad f_1(y) > 0, \quad f_2(y) < 0\}. \\ Q_{-+} &= \{y \in \mathbb{R}^2, \quad f_1(y) < 0, \quad f_2(y) > 0\}. \\ Q_{--} &= \{y \in \mathbb{R}^2, \quad f_1(y) < 0, \quad f_2(y) < 0\}. \end{aligned}$$

Then we study the stability of the equilibrium points. The Jacobian matrix of F is of the form

$$J_F = \begin{pmatrix} 0 & 1 \\ -a - bf'(y_1) & 0 \end{pmatrix}.$$

Classification of equilibrium points is determined by the eigenvalues λ_1 and λ_2 of the Jacobian matrix J_F. There are 4 different types of equilibrium points:

1. If λ_1, λ_2 are real numbers of the same sign the point is called a node.
2. If λ_1, λ_2 are real numbers and non-zero of opposite sign the point is called a saddle.
3. If λ_1, λ_2 are complex numbers, the real parts are equal and non-zero the point is called focus.
4. If λ_1, λ_2 are purely imaginary numbers the point is called center.

Let's start with the defocusing case where $b < 0$ and $a > 0$. We know that $\frac{f(r)}{r}$ is an increasing function on $(0, \infty)$ therefore in this case there exists a unique $r_0 > 0$ such that $ar_0 + bf(r_0) = 0$. Thus we have three equilibrium points $(0, 0)$, $(r_0, 0)$ and $(-r_0, 0)$. Hence

$$I_0 = \{(y_1, y_2) \in \mathbb{R}^2 : y_1 \in \{0, \pm r_0\}, y_2 \neq 0\},$$

and

$$I_\infty = \{(y_1, y_2) \in \mathbb{R}^2 : y_1 \notin \{0, \pm r_0\}, y_2 = 0\}.$$

The characteristic polynomial of the Jacobian matrix J_F is given by $P(\lambda) = \lambda^2 + a + bf'(y_1)$. At the equilibrium point $(0, 0)$ the eigenvalues are $\lambda = \pm i\sqrt{a}$ (recall that $a > 0$). Since the eigenvalues are purely imaginary, the equilibrium point $(0, 0)$ is a center. At the equilibrium points $(\pm r_0, 0)$ we have $a + bf'(r_0) < 0$, therefore the eigenvalues are non-zero real numbers of opposite signs and the equilibrium point is a saddle point. The phase portrait is given in Figure 4.4.

For the focusing case where $b > 0$ with $a > 0$ we have one equilibrium point $(0, 0)$ satisfying the equation $ar_0 + bf(r_0) = 0$. The eigenvalues are given at the equilibrium point $(0, 0)$ by $\lambda = \pm i\sqrt{a}$ and the equilibrium point $(0, 0)$ is a center. The phase portrait is given on the left of Figure of 4.5.

The last case is the focusing case with $b > 0$ and $a < 0$. There exists a unique $r_0 > 0$ such that $ar_0 + bf(r_0) = 0$ and we have three equilibrium points $(0, 0)$, $(r_0, 0)$ and $(-r_0, 0)$. Same as before we have the iscolines I_0 and I_∞. At the equilibrium point $(0, 0)$ the eigenvalues are $\lambda = \pm\sqrt{-a}$ and the equilibrium point $(0, 0)$ is a saddle. At the equilibrium points $(\pm r_0, 0)$ the eigenvalues are purely imaginary numbers hence the equilibrium point is a center. The phase portrait is given on the right of Figure 4.5.

The second case is when $J \neq 0$. We have

$$I_0 = \{(y_1, y_2) \in \mathbb{R}^2 : \frac{J^2}{y_1^3} - ay_1 - bf(y_1) = 0, y_2 \neq 0\},$$

and

$$I_\infty = \{(y_1, y_2) \in \mathbb{R}^2 : \frac{J^2}{y_1^3} - ay_1 - bf(y_1) \neq 0, y_2 = 0\}.$$

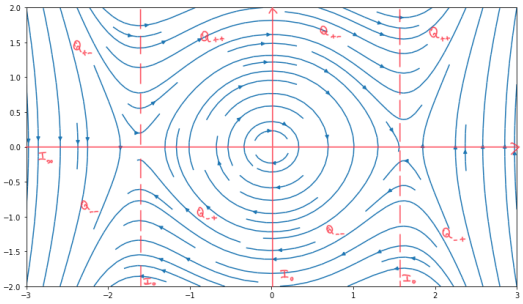

Figure 4.4 – Phase portraits of the solutions for the defocusing when $J = 0$.

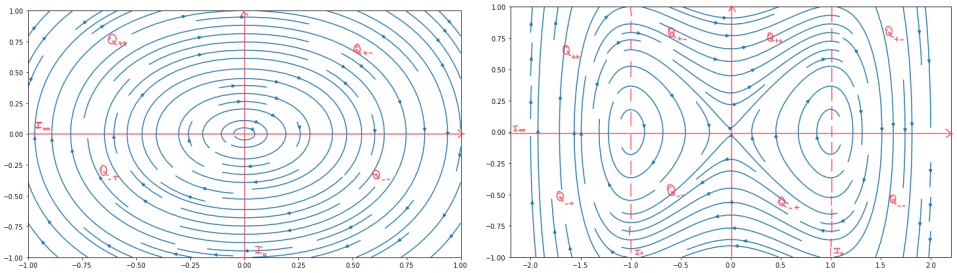

Figure 4.5 – Phase portraits of the solutions for the focusing case when $J = 0$.

The Jacobian matrix of $F(y)$ is of the form

$$J_F = \begin{pmatrix} 0 & 1 \\ -3\frac{J^2}{y_1^4} - a - bf'(y_1) & 0 \end{pmatrix}.$$

We start with the defocusing case where $b < 0$ and $a > 0$. In this case the equation $\frac{J^2}{y_1^4} - ay_1 - bf(y_1) = 0$ has 2 solutions r_Q and r_q such that $0 < r_Q < r_q$. Thus we have two equilibrium points $(r_Q, 0)$ and $(r_q, 0)$. The characteristic polynomial of the Jacobian matrix J_F is given by $P(\lambda) = \lambda^2 + \frac{3J^2}{y_1^4} + a + bf'(y_1)$. On the first equilibrium point $(r_Q, 0)$ we have $\lambda^2 = -\frac{3J^2}{r_Q^4} - 1 + f'(r_Q) = -V_J''(r_Q) < 0$, because $V_J(r)$ is convex at r_Q and therefore the eigenvalues are purely imaginary and the equilibrium point $(r_Q, 0)$ is a center. On the second equilibrium point $(r_q, 0)$ we have $\lambda^2 = -\frac{3J^2}{r_q^4} - 1 + f'(r_q) = -V_J''(r_q) > 0$, because $V_J(r)$ is concave at r_q and therefore the eigenvalues are non-zero real numbers of opposite signs hence the equilibrium point is a saddle. The phase portrait is given on the left of Figure 4.6.

For the focusing case where $b > 0$, with both cases $a > 0$ or $a < 0$, the equation $\frac{J^2}{y_1^3} - ay_1 - bf(y_1) = 0$ has 1 solution r_Q. On the equilibrium point $(r_Q, 0)$ we have $\lambda^2 = -\frac{3J^2}{r_Q^4} - a - f'(r_Q) < 0$, therefore the eigenvalues are purely imaginary and the equilibrium point $(r_Q, 0)$ is a center. The phase

portrait for these two cases is given on the right of Figure 4.6.

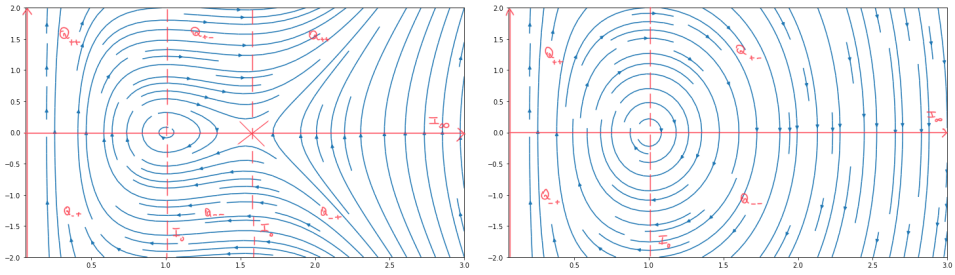

Figure 4.6 – Phase portraits of the solutions when $J \neq 0$.

4.3.2 Triple power nonlinearity

In this section we treat a special case not included in the general case we treated before. Let $f(u) = a_1|u|u + a_2|u|^2u + a_3|u|^3u = 0$, where $a_1, a_3 > 0$ and $a_2 < 0$. After using the symmetry of (4.1.1), we may assume $a_1 = a_3 = 1$ and $a_2 = -\gamma < 0$. Let

$$f(\phi) = |\phi|\phi - \gamma|\phi|^2\phi + |\phi|^3\phi.$$

Denote also

$$F(\phi) = \frac{1}{3}|\phi|^3 - \frac{\gamma}{4}|\phi|^4 + \frac{1}{5}|\phi|^5.$$

We study the critical points of V. Since f is gauge-invariant, V is even in r and we may restrict the study to positive critical points. Let $\omega = -a$, we have

$$V'(r) = -\omega r + f(r).$$

Define

$$f_1(r) = \frac{f(r)}{r}.$$

The difference between this case and the case we treated before is that $f_1(r)$ is not strictly increasing. A positive zero of V' is a positive solution of

$$0 = -\omega + f_1(r) = -\omega + r - \gamma r^2 + r^3. \tag{4.3.1}$$

To determine the number of zeros of V', we analyze the variations of f_1. We have

$$f_1'(r) = 1 - 2\gamma r + 3r^2,$$

which has constant sign when $\gamma < \sqrt{3}$ and otherwise has two (positive) zeros given by

$$r_\pm = \frac{1}{3}\left(\gamma \pm \sqrt{\gamma^2 - 3}\right).$$

As a consequence, when $0 < \gamma \leqslant \sqrt{3}$, the function f_1 is strictly increasing on $[0, \infty)$ and there exists a (unique) positive solution of (4.3.1) if and only if $\omega > 0$.

When $\gamma > \sqrt{3}$, we have $f_1'(r) > 0$ for $r \in (0, r_-) \cup (r_+, \infty)$ and $f_1'(r) < 0$ for $r \in (r_-, r_+)$. In this case, (4.3.1) has between 0 and 3 solutions. In particular, (4.3.1) has three positive solutions if and only if $\omega > 0$ and

$$\frac{1}{27}\left(\gamma(-2\gamma^2+9) - 2(\gamma^2-3)^{\frac{3}{2}}\right) = f_1(r_+) < \omega < f(r_-) = \frac{1}{27}\left(\gamma(-2\gamma^2+9) + 2(\gamma^2-3)^{\frac{3}{2}}\right).$$

The $\gamma - \omega$ regions of existence of solutions for (4.3.1) is represented in the figure below (zero solution, one solution, two solutions, three solutions).

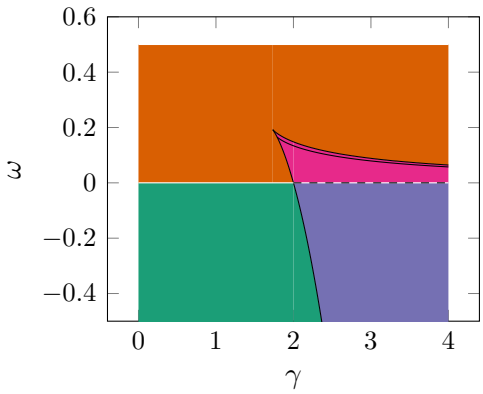

Whenever they exist, we denote the solutions of (4.3.1) by

$$0 < c_1 < r_- < c_2 < r_+ < c_3,$$

with the convention that when $r_\pm$ do not exist the solution is called c_1.

Let us now distinguish the various possibles phase portraits depending on γ and ω.

4.3.2.1 Case $\omega < \min\{0, f_1(r_+)\}$

In this case the only critical point of V is 0, which is a center. Solutions of (4.1.5) are all of sn/cn type. The phase portrait is given in Figure 4.7.

4.3.2.2 Case $\omega > 0$, $\omega \notin \{(f_1(r_+), f_1(r_-))\}$

In this case, V has two non-negative critical points: 0 and c_1. The point 0 is a saddle point. The other critical point c_1 is a center. The phase portrait

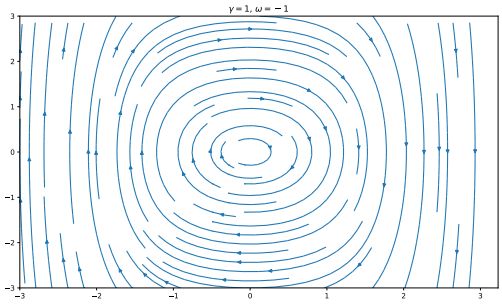

Figure 4.7 – Phase portrait 0 solution.

is similar to the one of the single focusing power. We have dn type solutions close to the center and cn type solutions for higher first integrals. The phase portrait is given in Figure 4.8.

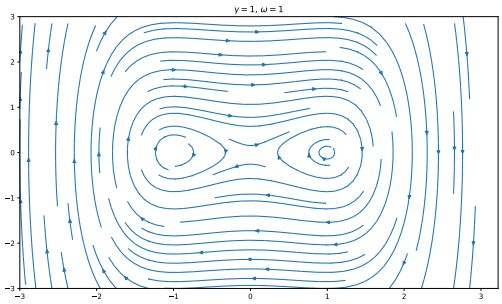

Figure 4.8 – Phase portrait 1 solution.

4.3.2.3 Case $f_1(r_+) < \omega < 0$

In this case, V has three non-negative critical points: 0 and c_2, c_3. The points 0 and c_3 are centers. The other critical point c_2 is a saddle point. Only one possible phase portrait with discussion about the co-existence of periodic solutions for same values of the first integral. The phase portrait is given in Figure 4.9.

4.3.2.4 Case $\max(0, f_1(r_+)) < \omega < f_1(r_-)$

In this case, V has four non-negative critical points: 0 and c_1, c_2, c_3. The points 0 and c_2 are saddle points. The other critical point c_1 and c_3 are centers. Three possible phase portraits depending on the value of $V(c_2)$. If $V(c_2) > 0$, then we have a homoclinic solution connecting 0 to itself without passing through c_2 and an heteroclinic solution connecting c_2 to $-c_2$. If $V(c_2) < 0$, then the heteroclinic solution connecting 0 to itself passes through c_2 and c_3

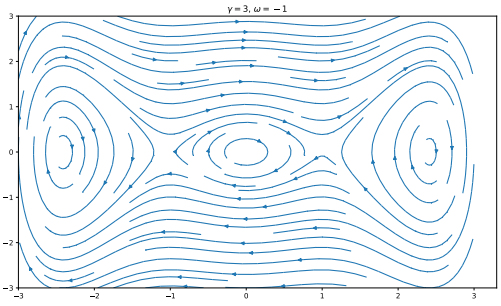

Figure 4.9 – Phase portrait 3 solution.

and there are two homoclinic solutions at c_2 (one by lower values and the other by upper values). Finally, at the borderline case $V(c_2) = 0$ the main distinguishing feature is a half-kink solution connecting 0 to c_2. In the plane (γ, ω), the half-kink line corresponds to the curve

$$\gamma \to -\frac{5\gamma\left(5\gamma^2 - 24\right)}{432} + \frac{\sqrt{5}\sqrt{\left(5\gamma^2 - 16\right)^3}}{432},$$

starting at the point $\left(\frac{4}{\sqrt{5}}, \frac{2\sqrt{5}}{27}\right)$ (observe that this is nothing but the line of non-existence of solitons found in [58]). The phase portraits are given in Figure 4.10.

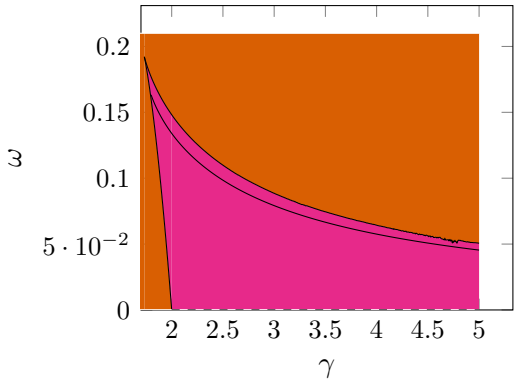

4.4 The minimization problems

In the work of Gustafson, Le Coz and Tsai [46], the authors gave global variational characterizations of the cnoidal, snoidal, and dnoidal elliptic functions for the cubic nonlinear Schrödinger equation. Specifically, they showed that these functions arise as minimizers of the energy functional subject to

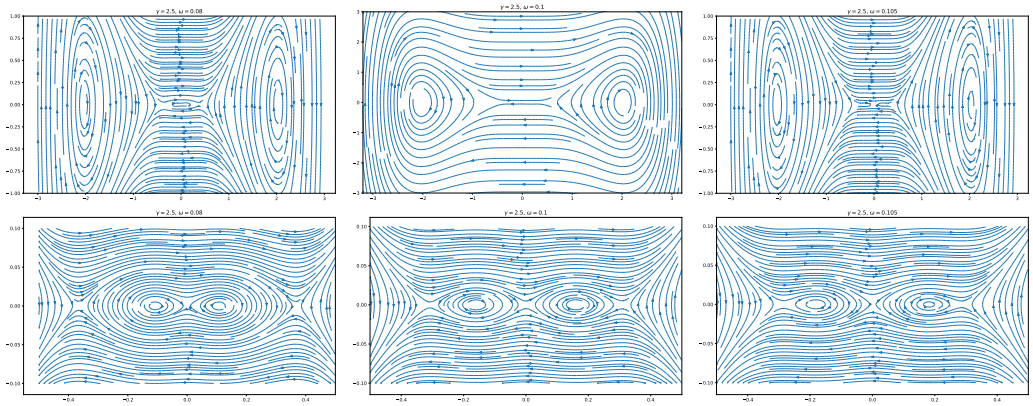

Figure 4.10 – Phase portrait 3 solution, $V(c_2) > 0$, $V(c_2) = 0$, $V(c_2) < 0$, bottom line is a zoom of the top one.

appropriate mass and momentum constraints. Their work built upon earlier results in [25], which established the stability of the minimizers of the energy functional subject to fixed mass constraints. By combining the variational characterization of stability with the existence of minimizers for the mass-constrained problem, the authors of [46] were able to prove the stability of the cnoidal, snoidal, and dnoidal elliptic functions.

In this section, we are looking to study the minimization problems where we minimize the energy to fixed mass and momentum constraints for the nonlinear Schrödinger equation (4.1.1). We shall provide some stability results on the minimizer.

4.4.1 Minimization among the periodic functions

Let $m > 0$. The basic variational problem is to minimize the energy at fixed mass:

$$\min\{\mathcal{E}(u) : u \in H^1_{loc} \cap P_T,\ M(u) = m\}. \tag{4.4.1}$$

Since the momentum is also conserved for (4.1.1), it is natural to consider the problem with a further momentum constraint:

$$\min\{\mathcal{E}(u) : u \in H^1_{loc} \cap P_T,\ M(u) = m,\ P(u) = 0\}. \tag{4.4.2}$$

The minimization problems (4.4.1) and (4.4.2) seek to find functions u which minimize the energy subject to the constraint that the mass is fixed and, in the case of (4.4.2), the momentum is also zero. Note that when we minimize the energy with fixed mass and fixed momentum $p \neq 0$ the problem is more complicated. It is known that there exists u_∞ minimizer, and there exist Lagrange-multipliers ω and σ such that

$$-\mathcal{E}'(u_\infty) + \omega M'(u_\infty) + \sigma P'(u_\infty) = 0,$$

that is

$$-\partial_{xx}u_\infty + \omega u_\infty - b|u_\infty|^2 u_\infty \pm i\sigma\partial_x u_\infty = 0.$$

In this chapter we will only focus on the case $p = 0$.

4.4.1.1 The focusing case in P_T

Assume that $b > 0$.

Proposition 4.4.1. For all $m > 0$, the minimization problem (4.4.1) admits a minimizer which is also a minimizer of the minimization problem (4.4.2). The minimal energy is finite and negative.

Proof. Without loss of generality, we can restrict the minimization to real valued non-negative functions. Indeed, if $u \in H^1_{loc} \cap P_T$, then $|u| \in H^1_{loc} \cap P_T$ and we have $\|\partial_x|u|\|_{L^2} \leqslant \|\partial_x u\|_{L^2}$. This implies that (4.4.1) and (4.4.2) share the same minimizers.

Let us prove that the minimal energy is negative. To do so, let $\phi_{m,0} \equiv \sqrt{\frac{2m}{T}}$ be a test function. We have

$$M(\phi_{m,0}) = m, \quad \mathcal{E}(\phi_{m,0}) = -\int_0^T F\left(\sqrt{\frac{2m}{T}}\right) dx = -TF\left(\sqrt{\frac{2m}{T}}\right) < 0,$$

where the last inequality holds because $F(z) > 0$ for any $z \in \mathbb{C}$ by the assumptions on f.

Consider now a minimizing sequence $(u_n) \subset H^1_{loc} \cap P_T$ for (4.4.1). We first prove that it is bounded in $H^1_{loc} \cap P_T$. To this aim, we rely on the Gagliardo-Nirenberg inequality: for any $u \in H^1_{loc} \cap P_T$, we have

$$\|u\|^{p+1}_{L^{p+1}} \lesssim \|u_x\|^{\alpha(p+1)}_{L^2} \|u\|^{(1-\alpha)(p+1)}_{L^2} + \|u\|^{p+1}_{L^2},$$

where $\alpha = \frac{1}{2} - \frac{1}{p+1}$. We also know that there exists $p > 1$ such that

$$F(u) \leqslant |F(u)| \lesssim |u|^2 + |u|^{p+1}.$$

Consequently, for any $u \in H^1_{loc} \cap P_T$, such that $M(u) = m$, we have

$$\begin{aligned}
\mathcal{E}(u) &= \frac{1}{2}\|u_x\|^2_{L^2} - \int_0^T F(u)dx, \\
&\gtrsim \frac{1}{2}\|u_x\|^2_{L^2} - \|u\|^2_{L^2} - \|u\|^{p+1}_{L^{p+1}}, \\
&\gtrsim \frac{1}{2}\|u_x\|^2_{L^2} - m - \|u_x\|^{\alpha(p+1)}_{L^2} m^{\frac{(1-\alpha)(p+1)}{2}} - m^{\frac{p+1}{2}}, \\
&= \|u_x\|^2_{L^2}\left(\frac{1}{2} - \|u_x\|^{\alpha(p+1)-2} m^{\frac{(1-\alpha)(p+1)}{2}}\right) - m^{\frac{p+1}{2}} - m.
\end{aligned}$$

The previous inequality implies the boundedness of $\|\partial_x u_n\|_{L^2}$ when $1 < p < 5$. Indeed, by contradiction, we suppose that $\|\partial_x u_n\|_{L^2} \to \infty$. Since $1 < p < 5$, we have $\alpha(p+1) - 2 < 0$, and this implies that $\|\partial_x u_n\|_{L^2}^{\alpha(p+1)-2} \to 0$, and therefore $\mathcal{E}(u_n) \to \infty$, which is a contradiction with the minimizing nature of (u_n). Moreover, the same arguments show that if $1 < p < 5$, then the minimal energy is finite. Hence the sequence (u_n) is bounded in $H^1_{loc} \cap P_T$. Therefore up to a subsequence, (u_n) converges weakly in $H^1_{loc} \cap P_T$ and strongly in $L^2_{loc} \cap P_T$ and $L^{p+1}_{loc} \cap P_T$ towards $u_\infty \in H^1_{loc} \cap P_T$. We now show that (u_n) converges strongly towards u_∞ in $H^1_{loc} \cap P_T$. By weak convergence, we have

$$\|\partial_x u_\infty\|_{L^2}^2 \leqslant \lim_{n \to +\infty} \|\partial_x u_n\|_{L^2}^2.$$

Up to a subsequence, we also have $F(u_n) \to F(u_\infty)$ almost everywhere. Moreover, we have

$$\begin{aligned} |F(u_n)| &\lesssim |u_n|^2 + |u_n|^{p+1} \\ &\lesssim \|u_n\|_{L^\infty}^2 + \|u_n\|_{L^\infty}^{p+1} \\ &\lesssim \|u_n\|_{H^1}^2 + \|u_n\|_{H^1}^{p+1} \leqslant \max_{n \in \mathbb{N}} \{\|u_n\|_{H^1}^2 + \|u_n\|_{H^1}^{p+1}\} < \infty. \end{aligned}$$

then by the dominated convergence theorem we have

$$\lim_{n \to +\infty} \int_0^T F(u_n) dx = \int_0^T F(u) dx.$$

Combining the previous arguments, we obtain

$$\mathcal{E}(u_\infty) \leqslant \lim_{n \to +\infty} \mathcal{E}(u_n), \quad M(u_n) = m,$$

which in turn implies

$$\|\partial_x u_\infty\|_{L^2}^2 = \lim_{n \to +\infty} \|\partial_x u_n\|_{L^2}^2.$$

Therefore the convergence from (u_n) to u_∞ is also strong in $H^1_{loc} \cap P_T$. □

Proposition 4.4.2. If $m > \tilde{m}$, then the minimizer is not a constant, the associated Lagrange multiplier verifies $a < 0$, the minimizer is positive, it is a solution of the ordinary differential equation (4.1.5).

Remark 4.4.3. In the cubic case, it is known that for small enough values of m, the minimizer of the energy functional in this case is the constant function. However, in our work, we do not provide a rigorous proof of this conjecture, but we believe it to be true based on the known result in the cubic case.

Proof. Since u_∞ is a minimizer of (4.4.1), there exists a Lagrange multiplier $a \in \mathbb{R}$ such that

$$-\mathcal{E}'(u_\infty) + aM'(u_\infty) = 0$$

that is

$$\partial_{xx} u_\infty + a u_\infty + b f(u_\infty) = 0.$$

Multiplying by u_∞ and integrating (recall that the functions considered are assumed to be real), we find that

$$a = \frac{\|\partial_x u_\infty\|_{L^2}^2 - b\int_0^T f(u_\infty) u_\infty dx}{\|u_\infty\|_{L^2}^2}.$$

Note that

$$\begin{aligned}\|\partial_x u_\infty\|_{L^2}^2 - b\int_0^T f(u_\infty) u_\infty dx &= 2\mathcal{E}(u_\infty) + 2b\int_0^T F(u_\infty) dx - \int_0^T b f(u_\infty) u_\infty dx \\ &= 2\mathcal{E}(u_\infty) + b\int_0^T (2F(u_\infty) - f(u_\infty) u_\infty) dx,\end{aligned}$$

where $\mathcal{E}(u_\infty) < 0$ and $2F(u_\infty) - f(u_\infty)u_\infty < 0$, by the assumption on (4.1.2). Therefore, we have

$$a < 0.$$

We introduce an auxiliary function

$$A(s) = \frac{4\pi^2}{T^2} + b\left(\frac{f(s)}{s} - f'(s)\right).$$

By assumption (4.1.3), we have

$$A'(s) = b\left(\frac{f'(s)s - f(s)}{s^2} - f''(s)\right) < 0.$$

Therefore A is a decreasing function, from $\frac{4\pi^2}{T^2}$ to $-\infty$ from assumption (4.1.4). Let m^* be such that $A(m^*) = 0$ and define

$$\tilde{m} = \frac{T m^{*2}}{2}$$

We want to prove that if $m > \tilde{m}$, then u_∞ is not constant.

By contradiction, we assume that u_∞ is constant for $m > \tilde{m}$. Then we necessarily have $u_\infty \equiv \sqrt{\frac{2m}{T}}$. The Lagrange multiplier can also be computed and we find

$$a = \frac{-b\int_0^T f\left(\sqrt{\frac{2m}{T}}\right)\sqrt{\frac{2m}{T}} dx}{2m} = -bf\left(\sqrt{\frac{2m}{T}}\right)\sqrt{\frac{T}{2m}}.$$

Since u_∞ is supposed to be a constrained minimizer for (4.4.1), the operator

$$-\partial_{xx} - a - bf'(u_\infty) = -\partial_{xx} + b\sqrt{\frac{T}{2m}} f\left(\sqrt{\frac{2m}{T}}\right) - bf'\left(\sqrt{\frac{2m}{T}}\right),$$

must have Morse Index at most 1, i.e, at most 1 negative eigenvalue. The eigenvalues are given for $n \in \mathbb{Z}$ by the following formula:

$$\left(\frac{2\pi n}{T}\right)^2 + b\sqrt{\frac{T}{2m}} f\left(\sqrt{\frac{2m}{T}}\right) - bf'\left(\sqrt{\frac{2m}{T}}\right), \qquad n \in \mathbb{Z}.$$

If $n = 0$, the eigenvalue is negative:

$$b\sqrt{\frac{T}{2m}} f\left(\sqrt{\frac{2m}{T}}\right) - bf'\left(\sqrt{\frac{2m}{T}}\right) < 0.$$

Indeed as $\frac{f(s)}{s}$ is an increasing function we have that for all $s > 0$, $\left(\frac{f(s)}{s}\right)' = \frac{f'(s)s - f(s)}{s^2} > 0$. If $n = 1$ the eigenvalue is of the form:

$$\frac{4\pi^2}{T^2} + b\sqrt{\frac{T}{2m}} f\left(\sqrt{\frac{2m}{T}}\right) - bf'\left(\sqrt{\frac{2m}{T}}\right) = A\left(\sqrt{\frac{2m}{T}}\right).$$

Recall that $A\left(\sqrt{\frac{2m}{T}}\right)$ is non-negative if and only if $\sqrt{\frac{2m}{T}} \leqslant m^*$ which is equivalent to $m \leqslant \tilde{m}$ which gives the contradiction. Therefore when $m > m^*$ the minimizer u_∞ is not constant, which concludes the proof.

□

4.4.1.2 The defocusing case in P_T

Assume that $b < 0$.

Proposition 4.4.4. For all $m \in (0, \infty)$ the constrained minimization problems (4.4.1) and (4.4.2) have the same unique (up to phase shift) minimizer, which is the constant function $u_\infty \equiv \sqrt{\frac{2m}{T}}$.

Proof. Consider a minimizing sequence $(u_n) \subset H^1_{loc} \cap P_T$ for (4.4.1). We first prove that it is bounded in $H^1_{loc} \cap P_T$. We have

$$\mathcal{E}(u_n) = \frac{1}{2}\|\partial_x u_n\|^2_{L^2} + \int_0^T F(u_n)dx.$$

By contradiction, we suppose that $\|\partial_x u_n\|_{L^2} \to \infty$. Therefore $\mathcal{E}(u_n) \to \infty$, which is a contradiction with the minimizing nature of (u_n). Moreover, the

same argument show that the minimal energy is finite. Hence the sequence (u_n) is bounded in $H^1_{loc} \cap P_T$. Therefore up to a subsequence, (u_n) converges weakly in $H^1_{loc} \cap P_T$ and strongly in $L^2_{loc} \cap P_T$ and $L^{p+1}_{loc} \cap P_T$ towards $u_\infty \in H^1_{loc} \cap P_T$. As in the proof of Proposition 4.4.1 we have that (u_n) converges strongly towards u_∞ in $H^1_{loc} \cap P_T$.

As in the proof of Proposition 4.4.2, we know that there exists a Lagrange multiplier a such that

$$-\mathcal{E}'(u_\infty) + aM'(u_\infty) = 0, \tag{4.4.3}$$

i.e. u_∞ satisfies the ordinary differential equation (4.1.5). Hence a might be explicitly expressed in the following way:

$$a = \frac{\|\partial_x u_\infty\|^2_{L^2} - b\int_0^T f(u_\infty)u_\infty dx}{\|u_\infty\|^2_{L^2}}.$$

Since $b < 0$, we have $a > 0$. In this case we know that the phase portrait for real valued solutions of (4.1.5) is given in Figure 4.4.

As for the focusing case, for any $v \in H^1_{loc} \cap P_T$, we have

$$M(|v|) = M(v), \quad \mathcal{E}(|v|) \leqslant \mathcal{E}(v),$$

therefore we may assume that $u_\infty \geqslant 0$. The only solutions of (4.1.5) that do not change sign are the constant functions $\pm\sqrt{\frac{2m}{T}}$. As a consequence, there exists $\theta \in \mathbb{R}$ such that

$$u_\infty = e^{i\theta}\sqrt{\frac{2m}{T}},$$

which concludes the proof. □

Remark 4.4.5. Under the assumptions of Proposition 4.4.4, the minimizer is $u_\infty \equiv \sqrt{\frac{2m}{T}}$ (up to phase shift), and therefore the associated Lagrange multiplier is given by

$$a = -bf\left(\sqrt{\frac{2m}{T}}\right)\sqrt{\frac{T}{2m}}.$$

Therefore, the eigenvalues of the associated linearized operator

$$-\partial_{xx} - a - bf'(u_\infty) = -\partial_{xx} + b\sqrt{\frac{T}{2m}}f\left(\sqrt{\frac{2m}{T}}\right) - bf'\left(\sqrt{\frac{2m}{T}}\right)$$

are given for $n \in \mathbb{Z}$ by the following formula:

$$\left(\frac{2\pi n}{T}\right)^2 + b\left(\sqrt{\frac{T}{2m}}f\left(\sqrt{\frac{2m}{T}}\right) - f'\left(\sqrt{\frac{2m}{T}}\right)\right).$$

Since $b < 0$ and $f(s)s^{-1} - f'(s) < 0$ (see assumption (4.1.2)), we remark that the eigenvalues are all positive.

4.4.2 Minimization among anti-periodic functions

We will also consider variational problems restricted to anti-symmetric functions:

$$\min\{\mathcal{E}(u) : u \in H^1_{loc} \cap A_{\frac{T}{2}},\ M(u) = m\}, \tag{4.4.4}$$

$$\min\{\mathcal{E}(u) : u \in H^1_{loc} \cap A_{\frac{T}{2}},\ M(u) = m,\ P(u) = 0\}. \tag{4.4.5}$$

4.4.2.1 The defocusing case for anti-periodic functions

Assume $b < 0$. In this section, we restrict ourselves to the sum of two powers to use the Hölder inequality that cannot be used in the general case. Moreover we can generalize to the sum of several powers.

Proposition 4.4.6. Let $f(u) = |u|^{p-1}u + |u|^{q-1}u$, with $p, q > 1$. There exists a unique (up to phase shift and complex conjugate) minimizer of (4.4.4). It is the plane wave $u_\infty \equiv \sqrt{\frac{2m}{T}} e^{\frac{i\pi x}{T}}$.

Proof. Denote the supposed minimizer by $w(x) = \sqrt{\frac{2m}{T}} e^{\pm\frac{i\pi x}{T}}$. Let $v \in H^1_{loc} \cap A_{\frac{T}{2}}$ such that: $M(v) = m$ and $v \not\equiv e^{i\theta} w$ ($\theta \in \mathbb{R}$). Since $v \in H^1_{loc} \cap A_{\frac{T}{2}}$, v must have 0 mean value. Recall that in this case v verifies the Poincaré-Wirtinger inequality

$$\|v\|_{L^2} \leqslant \frac{T}{2\pi} \|v'\|_{L^2},$$

and that the optimizers of the Poincaré-Wirtinger inequality are of the form $ce^{\pm\frac{i\pi x}{T}}, c \in \mathbb{C}$. This implies that

$$\|\partial_x w\|^2_{L^2} = \frac{8\pi^2}{T^2} M(w) = \frac{8\pi^2}{T^2} M(v) < \|\partial_x v\|^2_{L^2}.$$

We will prove now that $\int_0^T F(w)dx \leqslant \int_0^T F(v)dx$. We have

$$\begin{aligned}
&\int_0^T \left(\frac{1}{p+1}|w|^{p+1} + \frac{1}{q+1}|w|^{q+1} \right) dx, \\
&= \int_0^T \left(\left(\frac{1}{p+1}\right) \left|\sqrt{\frac{2m}{T}}\right|^{p+1} + \left(\frac{1}{q+1}\right) \left|\sqrt{\frac{2m}{T}}\right|^{q+1} \right) dx, \\
&= T\left(\left(\frac{1}{p+1}\right) \left(T^{-\frac{p+1}{2}} 2^{\frac{p+1}{2}} m^{\frac{p+1}{2}} \right) + \left(\frac{1}{q+1}\right) \left(T^{-\frac{q+1}{2}} 2^{\frac{q+1}{2}} m^{\frac{q+1}{2}} \right) \right), \\
&= T\left(\left(\frac{1}{p+1}\right) \left(T^{-\frac{p+1}{2}} \|v\|^{p+1}_{L^2} \right) + \left(\frac{1}{q+1}\right) \left(T^{-\frac{q+1}{2}} \|v\|^{q+1}_{L^2} \right) \right), \\
&\leqslant T\left(\left(\frac{1}{p+1}\right) \left(T^{-\frac{p+1}{2}} T^{\frac{p-1}{2}} \|v\|^{p+1}_{L^{p+1}} \right) + \left(\frac{1}{q+1}\right) \left(T^{-\frac{q+1}{2}} T^{\frac{q-1}{2}} \|v\|^{q+1}_{L^{q+1}} \right) \right),
\end{aligned}$$

where the last inequality came from Hölder inequality:

$$\|v\|_{L^2}^{p+1} \leqslant T^{\frac{p-1}{2}} \|v\|_{L^{p+1}}^{p+1}, \quad \frac{1}{\frac{p+1}{2}} + \frac{1}{\frac{p+1}{p-1}} = 1.$$

Therefore we have

$$\frac{1}{p+1}\|w\|_{L^{p+1}}^{p+1} + \frac{1}{q+1}\|w\|_{L^{q+1}}^{q+1} \leqslant \frac{1}{p+1}\|v\|_{L^{p+1}}^{p+1} + \frac{1}{q+1}\|v\|_{L^{q+1}}^{q+1}$$

which implies that

$$\mathcal{E}(w) < \mathcal{E}(v),$$

which concludes the proof. □

4.5 A Fourier rearrangement inequality

Lemma 4.5.1. Let $v \in H^1_{loc} \cap A_{\frac{T}{2}}$ and p an odd integer. Then there exists $\tilde{v} \in H^1_{loc} \cap A_{\frac{T}{2}}$ such that:

$$\tilde{v}(x) \in \mathbb{R}, \quad \|\tilde{v}\|_{L^2} = \|v\|_{L^2}, \quad \|\partial_x \tilde{v}\|_{L^2} = \|\partial_x v\|_{L^2}, \quad \|\tilde{v}\|_{L^{p+1}} \geqslant \|v\|_{L^{p+1}}.$$

Proof. Since $v \in H^1_{loc} \cap A_{\frac{T}{2}}$, its Fourier series expansion contains only terms indexed by odd integers:

$$v(x) = \sum_{\substack{j \in \mathbb{Z} \\ j odd}} v_j e^{ij\frac{2\pi}{T}x}.$$

We define $\tilde{v}$ by its Fourier series expansion

$$\tilde{v}(x) = \sum_{\substack{j \in \mathbb{Z} \\ j odd}} \tilde{v}_j e^{ij\frac{2\pi}{T}x}, \quad \tilde{v}_j := \sqrt{\frac{|v_j|^2 + |v_{-j}|^2}{2}}.$$

It is clear that $\tilde{v}(x) \in \mathbb{R}$, and by Plancherel formula, we have

$$\|\tilde{v}\|_{L^2} = \|v\|_{L^2}, \quad \|\partial_x \tilde{v}\|_{L^2} = \|\partial_x v\|_{L^2},$$

so all we have to prove is that $\|\tilde{v}\|_{L^{p+1}} \geqslant \|v\|_{L^{p+1}}$. We have

$$|v(x)|^2 = \sum_{\substack{j \in \mathbb{Z} \\ j odd}} |v_j|^2 + \sum_{\substack{n \in 2\mathbb{N} \\ n \geqslant 2}} w_n e^{in\frac{2\pi}{T}x} + \bar{w}_n e^{in\frac{2\pi}{T}x},$$

where we have defined

$$w_n = \sum_{\substack{j>k, j+k=n \\ j,k odd}} v_j \bar{v}_{-k} + v_k \bar{v}_{-j}.$$

Let $N = \frac{p+1}{2}$. We start with

$$\begin{aligned}
|v|^{p+1} &= \left(|v|^2\right)^{\frac{p+1}{2}} \\
&= \left(\sum_{\substack{j\in\mathbb{Z}\\ j odd}} |v_j|^2 + \sum_{\substack{n\in 2\mathbb{N}\\ n\geqslant 2}} w_n e^{in\frac{2\pi}{T}x} + \bar{w}_n e^{in\frac{2\pi}{T}x} \right)^N, \\
&= \sum_{k=0}^{N} \binom{N}{k} \left(\sum_{\substack{j\in\mathbb{Z}\\ j odd}} |v_j|^2 \right)^{N-k} \left(\sum_{\substack{n\in 2\mathbb{N}\\ n\geqslant 2}} w_n e^{in\frac{2\pi}{T}x} + \bar{w}_n e^{in\frac{2\pi}{T}x} \right)^k.
\end{aligned}$$

We have

$$\begin{aligned}
&\left(\sum_{\substack{n\in 2\mathbb{N}\\ n\geqslant 2}} w_n e^{in\frac{2\pi}{T}x} + \bar{w}_n e^{in\frac{2\pi}{T}x} \right)^k \\
&= \sum_{s=0}^{k} \binom{k}{s} \sum_{p_1} \cdots \sum_{p_k} \bar{w}_{p_1} \cdots \bar{w}_{p_s} \cdot w_{p_s} w_{p_{s+1}} \cdots w_{p_k} e^{i(-p_1-\cdots-p_s+p_{s+1}+\cdots+p_k)\frac{2\pi}{T}x}, \\
&= \sum_{s=0}^{k} \binom{k}{s} \sum_{p_1} \cdots \sum_{p_k} \left(\prod_{l=1}^{s} \bar{w}_{p_l} e^{-ip_l\frac{2\pi}{T}x} \right) \left(\prod_{l=s+1}^{k} w_{p_l} e^{ip_l\frac{2\pi}{T}x} \right),
\end{aligned}$$

where

$$\prod_{l=1}^{0} \bar{w}_{p_l} e^{-ip_l\frac{2\pi}{T}x} = 1, \quad \prod_{l=k+1}^{k} w_{p_l} e^{ip_l\frac{2\pi}{T}x} = 1.$$

Then we have

$$\begin{aligned}
&\frac{1}{T}\int_0^T |v|^{p+1}dx \\
&\quad = \frac{1}{T}\int_0^T \sum_{k=0}^{N}\binom{N}{k}\left(\sum_{\substack{j\in\mathbb{Z}\\ jodd}}|v_j|^2\right)^{N-k}\left(\sum_{\substack{n\in 2\mathbb{N}\\ n\geqslant 2}} w_n e^{in\frac{2\pi}{T}x}+\bar{w}_n e^{in\frac{2\pi}{T}x}\right)^k dx \\
&\qquad\qquad = \sum_{k=0}^{N}\binom{N}{k}\left(\sum_{\substack{j\in\mathbb{Z}\\ jodd}}|v_j|^2\right)^{N-k}\cdot \\
&\frac{1}{T}\int_0^T \sum_{s=0}^{k}\binom{k}{s}\sum_{p_1}\cdots\sum_{p_k}\left(\prod_{l=1}^{s}\bar{w}_{p_l}e^{-ip_l\frac{2\pi}{T}x}\right)\left(\prod_{l=s+1}^{k} w_{p_l}e^{ip_l\frac{2\pi}{T}x}\right)dx \\
&= \sum_{k=0}^{N}\binom{N}{k}\left(\sum_{\substack{j\in\mathbb{Z}\\ jodd}}|v_j|^2\right)^{N-k}\sum_{s=0}^{k}\binom{k}{s}\sum_{p_1,\ldots,p_n\in\sigma}\left(\prod_{l=1}^{s}\bar{w}_{p_l}\right)\left(\prod_{l=s+1}^{k} w_{p_l}\right),
\end{aligned}$$

where $\sigma = \{(p_1,...,p_n) : \exists\alpha\in\{0,1\}^n : \sum_j (-1)^{\alpha_j}p_j = 0\}$, and where we have used the fact that for $n\in\mathbb{N}, n\neq 0$, we have

$$\int_0^T e^{in\frac{2\pi}{T}x}dx = 0.$$

On the other hand, we observe that

$$w_n = \sum_{\substack{j>k, j+k=n\\ j,kodd}}\begin{pmatrix} v_j\\ \tilde{v}_{-j}\end{pmatrix}.\begin{pmatrix} v_k\\ \tilde{v}_k\end{pmatrix}, \tag{4.5.1}$$

where the . denotes the complex vector scalar product. Therefore,

$$\begin{aligned}
|w_n| &\leqslant \sum_{\substack{j>k, j+k=n\\ j,kodd}}\left|\begin{pmatrix} v_j\\ \tilde{v}_{-j}\end{pmatrix}\right|\left|\begin{pmatrix} v_k\\ \tilde{v}_k\end{pmatrix}\right| = \sum_{\substack{j>k, j+k=n\\ j,kodd}}\sqrt{2\tilde{v}_j^2}\sqrt{2\tilde{v}_k^2} \\
&= 2\sum_{\substack{j>k, j+k=n\\ j,kodd}}\tilde{v}_j\tilde{v}_k = \tilde{w}_n,
\end{aligned}$$

where by $\tilde{w}_n$, we denote the quantity defined similarly as in (4.5.1) for $(\tilde{v}_j)$.

Therefore,

$$\begin{aligned}
&\frac{1}{T}\int_0^T |v|^{p+1}dx \\
&\leqslant \sum_{k=0}^{N}\binom{N}{k}\left(\sum_{\substack{j\in\mathbb{Z}\\ jodd}}|v_j|^2\right)^{N-k}\sum_{s=0}^{k}\binom{k}{s}\sum_{p_1,\dots,p_n\in\sigma}\left(\prod_{l=1}^{s}|\bar{w}_{p_l}|\right)\left(\prod_{l=s+1}^{k}|w_{p_l}|\right), \\
&\leqslant \sum_{k=0}^{N}\binom{N}{k}\left(\sum_{\substack{j\in\mathbb{Z}\\ jodd}}|v_j|^2\right)^{N-k}\sum_{s=0}^{k}\binom{k}{s}\sum_{p_1,\dots,p_n\in\sigma}\left(\prod_{l=1}^{s}\tilde{w}_{p_l}\right)\left(\prod_{l=s+1}^{k}\tilde{w}_{p_l}\right), \\
&= \sum_{k=0}^{N}\binom{N}{k}\left(\sum_{\substack{j\in\mathbb{Z}\\ jodd}}|v_j|^2\right)^{N-k}\cdot \\
&\frac{1}{T}\int_0^T\sum_{s=0}^{k}\binom{k}{s}\sum_{p_1}\cdots\sum_{p_k}\left(\prod_{l=1}^{s}\tilde{w}_{p_l}e^{-ip_l\frac{2\pi}{T}x}\right)\left(\prod_{l=s+1}^{k}\tilde{w}_{p_l}e^{ip_l\frac{2\pi}{T}x}\right)dx, \\
&= \frac{1}{T}\int_0^T|\tilde{v}|^{p+1}dx,
\end{aligned}$$

which concludes the proof. □

4.6 Minimizing problem on the Nehari manifold

In this section we restrict ourselves to the nonlinearity of the form $f(u) = |u|^{p-1}u$, with $p > 1$. We define the functional $S : H^1_{loc} \to \mathbb{R}$ by setting for $u \in H^1_{loc}$

$$S(u) := \frac{1}{2}\|\partial_x u\|^2_{L^2} - \frac{a}{2}\|u\|^2_{L^2} - \frac{b}{p+1}\|u\|^{p+1}_{L^{p+1}}.$$

It is standard that S is of class C^2. The Fréchet derivative of S at u is given by

$$S'(u) = -u_{xx} - au - b|u|^{p-1}u.$$

Therefore, u is a solution of the ordinary differential equation (4.1.5) if and only if $S'(u) = 0$. Let $I(u) = \|\partial_x u\|^2_{L^2} - a\|u\|^2_{L^2} - b\|u\|^{p+1}_{L^{p+1}}$. The set

$$\{u \in H^1_{loc} : u \neq 0, I(u) = 0\}$$

is called Nehari manifold. We are interested in the minimization problem on the Nehari manifold:

$$\min\{S(u) : u \in H^1_{loc} \cap P_T, u \neq 0, I(u) = 0\}, \tag{4.6.1}$$

and

$$\min\{S(u) : u \in H^1_{loc} \cap A_{\frac{T}{2}}, u \neq 0, I(u) = 0\}. \tag{4.6.2}$$

The minimization problem on the Nehari manifold has been studied in numerous works. In this regard, we mention the work of Szulkin and Weth [6], the work of Pankov [64] and Pankov and Zhang [74] for the discrete nonlinear Schrödinger equation. We also mention the work of Hayashi [47] on the nonlinear Schrödinger equation of derivative type and the work of Colin and Watanabe [28] on the nonlinear Klein-Gordon-Maxwell type system.

4.6.1 Periodic case

4.6.1.1 Focusing case

Let $b > 0$ and $a < 0$. We have the following lemma.

Lemma 4.6.1. The minimum of (4.6.1) is finite and there exists a minimizer solution of (4.1.5).

Proof. Consider a minimizing sequence $(u_n) \subset H^1_{loc} \cap P_T$ for (4.6.1). We have $I(u_n) = 0$, therefore

$$S(u_n) = S(u_n) - \frac{1}{p+1} I(u_n) = \left(\frac{1}{2} - \frac{1}{p+1}\right) \left(\|\partial_x u_n\|^2_{L^2} - a\|u_n\|^2_{L^2}\right). \tag{4.6.3}$$

We have the boundedness of the sequence (u_n) in $H^1_{loc} \cap P_T$. Indeed, by contradiction we suppose that $\|u_n\|^2_{L^2} \to \infty$, or $\|\partial_x u_n\|^2_{L^2} \to \infty$, therefore $S(u_n) \to \infty$, which is a contradiction with the minimizing nature of (u_n). Therefore up to a subsequence, (u_n) converges weakly in $H^1_{loc} \cap P_T$ and strongly in $L^2_{loc} \cap P_T$ and $L^{p+1}_{loc} \cap P_T$ towards $u_\infty \in H^1_{loc} \cap P_T$. By the weak convergence we have

$$\|u_\infty\|_{H^1} \leqslant \liminf_{n\to\infty} \|u_n\|_{H^1},$$

then

$$\|\partial_x u_\infty\|^2_{L^2} - a\|u_\infty\|^2_{L^2} \leqslant \liminf_{n\to\infty} \left(\|\partial_x u_n\|^2_{L^2} - a\|u_n\|^2_{L^2}\right).$$

Therefore

$$S(u_\infty) - \frac{1}{p+1} I(u_\infty) \leqslant \liminf_{n\to\infty} S(u_n).$$

On the other hand we have

$$\begin{aligned} I(u_\infty) &= \|\partial_x u_\infty\|^2_{L^2} - a\|u_\infty\|^2_{L^2} - b\|u_\infty\|^{p+1}_{L^{p+1}} \\ &\leqslant \liminf_{n\to\infty} \left(\|\partial_x u_n\|^2_{L^2} - a\|u_n\|^2_{L^2}\right) - b \lim_{n\to\infty} \|u_n\|^{p+1}_{L^{p+1}} \\ &\leqslant \lim_{n\to\infty} I(u_n) = 0. \end{aligned}$$

Then

$$I(u_\infty) \leqslant 0,$$

and this implies that

$$S(u_\infty) \leqslant S(u_\infty) - \frac{1}{p+1} I(u_\infty) \leqslant \lim_{n\to\infty} \inf S(u_n).$$

The graph of $I(tu)$ is given in the figure 4.11. We know that $I(t_1 u_\infty) \leqslant 0$, there exists $t_0 < 1$ such that $I(t_0 u_\infty) = 0$. We have

$$\begin{aligned} S(t_0 u_\infty) &= S(t_0 u_\infty) - \frac{1}{p+1} I(t_0 u_\infty), \\ &= \left(\frac{1}{2} - \frac{1}{p+1}\right) \|t_0 u_\infty\|^2_{H^1}, \\ &\leqslant \left(\frac{1}{2} - \frac{1}{p+1}\right) \|u_\infty\|^2_{H^1}, \\ &= S(u_\infty) - \frac{1}{p+1} I(u_\infty) \leqslant \lim_{n\to\infty} \inf S(u_n). \end{aligned}$$

Therefore

$$S(t_0 u_\infty) \leqslant \lim_{n\to\infty} \inf S(u_n), \quad I(t_0 u_\infty) = 0,$$

which implies the existence of the minimizer.

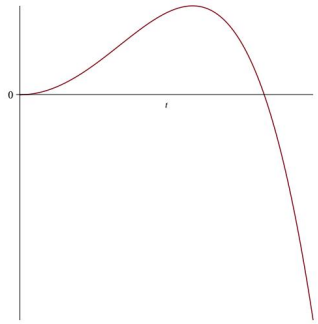

Figure 4.11 – $I(tu)$ in function of t.

We have $I(u) = \|\partial_x u\|^2_{L^2} - a\|v\|^2_{L^2} - b\|v\|^{p+1}_{L^{p+1}}$. Therefore

$$\begin{aligned} I'(u) &= -2u_{xx} - 2au - b(p+1)|u|^{p-1}u, \\ &= -2u_{xx} - 2au - 2b|u|^{p-1}u + b(2-(p+1))|u|^{p-1}u, \\ &= 2S'(u) - b(p-1)|u|^{p-1}u. \end{aligned}$$

Moreover $I(u) =< S'(u), u >$, therefore

$$\begin{aligned} < I'(u), u > &= 2 < S'(u), u > -b(p-1)\|u\|^{p+1}_{L^{p+1}}, \\ &= -b(p-1)\|u\|^{p+1}_{L^{p+1}} \neq 0. \end{aligned}$$

On the other hand $S'(u) = \lambda I'(u)$, this implies that

$$0 =< S'(u), u >= \lambda < I'(u), u > .$$

Since $< I'(u), u > \neq 0$, this implies

$$\lambda = 0.$$

Therefore the minimizer u_∞ verifies $S'(u_\infty) = 0$, so it is a solution of the ordinary differential equation (4.1.5). □

4.6.2 Anti-periodic case

4.6.2.1 Focusing case

Lemma 4.6.2. The minimum of (4.6.2) is finite.

Proof. Consider a minimizing sequence $(u_n) \subset H^1_{loc} \cap A_{\frac{T}{2}}$ for (4.6.2). We have $I(u_n) = 0$, therefore

$$S(u_n) = S(u_n) - \frac{1}{p+1} I(u_n) = \left(\frac{1}{2} - \frac{1}{p+1}\right) \left(\|\partial_x u_n\|^2_{L^2} - a\|u_n\|^2_{L^2}\right). \quad (4.6.4)$$

We will distinguish between two cases whether $a < 0$ or $a > 0$. In the first case, as in the periodic case, we can directly conclude by contradiction with the minimizing nature of (u_n) that it is bounded in $H^1_{loc} \cap A_{\frac{T}{2}}$. In the second case, we suppose that $a > 0$. Since $u_n \in A_{\frac{T}{2}}$, u_n must have 0 mean value. In that case u_n verifies the Poincaré-Wirtinger inequality:

$$\|u_n\|_{L^2} \leqslant \frac{T}{2\pi} \|\partial_x u_n\|_{L^2}.$$

Replacing in (4.6.4), we obtain that

$$S(u_n) \geqslant \left(\frac{1}{2} - \frac{1}{p+1}\right) \left(\frac{4\pi^2}{T^2} - a\right) \|u_n\|^2_{L^2}.$$

Then by the same arguments as in the first case we can prove that (u_n) is bounded in $H^1_{loc} \cap A_{\frac{T}{2}}$ if

$$a < \frac{4\pi^2}{T^2}.$$

Therefore up to a subsequence, (u_n) converges weakly in $H^1_{loc} \cap A_{\frac{T}{2}}$ and strongly in $L^2_{loc} \cap A_{\frac{T}{2}}$ and $L^{p+1}_{loc} \cap A_{\frac{T}{2}}$ towards $u_\infty \in H^1_{loc} \cap A_{\frac{T}{2}}$. By the weak convergence we have

$$\|u_\infty\|_{H^1} \leqslant \lim_{n\to\infty} \inf \|u_n\|_{H^1}.$$

If $a < 0$, by the equivalence of the norms we have

$$\|\partial_x u_\infty\|_{L^2}^2 - a\|u_\infty\|_{L^2}^2 \leqslant \lim_{n\to\infty} \inf \left(\|\partial_x u_n\|_{L^2}^2 - a\|u_n\|_{L^2}^2\right).$$

And if $a > 0$, by the strong convergence in $L^2_{loc} \cap A_{\frac{T}{2}}$ we also have the above inequality. Therefore

$$S(u_\infty) - \frac{1}{p+1} I(u_\infty) \leqslant \lim_{n\to\infty} \inf S(u_n).$$

On the other hand we have

$$\begin{aligned} I(u_\infty) &= \|\partial_x u_\infty\|_{L^2}^2 - a\|u_\infty\|_{L^2}^2 - \|u_\infty\|_{L^{p+1}}^{p+1} \\ &\leqslant \lim_{n\to\infty} \inf \left(\|\partial_x u_n\|_{L^2}^2 - a\|u_n\|_{L^2}^2\right) - \lim_{n\to\infty} \|u_n\|_{L^{p+1}}^{p+1} \\ &\leqslant \lim_{n\to\infty} I(u_n) = 0. \end{aligned}$$

Then

$$I(u_\infty) \leqslant 0,$$

and this implies that

$$S(u_\infty) \leqslant S(u_\infty) - \frac{1}{p+1} I(u_\infty) \leqslant \lim_{n\to\infty} \inf S(u_n).$$

As in the periodic case with the Figure 4.11 we prove that there exists $t_0 < 1$ such that $I(t_0 u_\infty) = 0$ and $S(t_0 u_\infty) \leqslant \lim_{n\to\infty} \inf S(u_n)$ which implies the existence of the minimizer. □

We now consider the following minimization problem:

$$\min \left\{ \left(\frac{1}{2} - \frac{1}{p+1}\right) \|v\|_{H^1}^2 : v \neq 0, I(v) \leqslant 0, v \in H^1_{loc} \cap A_{\frac{T}{2}} \right\}. \tag{4.6.5}$$

We have the following lemma.

Lemma 4.6.3. The minimization problems (4.6.2) and (4.6.5) share the same minimizer. Moreover when p is an odd integer the minimizer is real and it is a solution of (4.1.5).

Proof. Let

$$m_1 := \min\{S(u) : u \in H^1_{loc} \cap A_{\frac{T}{2}}, u \neq 0, I(u) = 0\},$$

and

$$m_2 := \min\{\left(\frac{1}{2} - \frac{1}{p+1}\right) \|v\|_{H^1}^2 : v \in H^1_{loc} \cap A_{\frac{T}{2}}, v \neq 0, I(v) \leqslant 0\}.$$

We will prove that $m_1 = m_2$. Let u be such that m_1 is reached. Hence $I(u) = 0$. We have

$$m_1 = S(u) = S(u) - \frac{1}{p+1} I(u) = \left(\frac{1}{2} - \frac{1}{p+1}\right) \|u\|_{H^1}^2 \geqslant m_2.$$

Let u be such that m_2 is reached. Then $I(u) \leqslant 0$. We will prove that $I(u) = 0$. By contradiction, we suppose that $I(u) < 0$. As we can see in Figure 4.11 there exists $t_0 < 1$ such that $I(t_0 u) = 0$. Therefore we have

$$\left(\frac{1}{2} - \frac{1}{p+1}\right) \|t_0 u\|_{H^1}^2 \leqslant \left(\frac{1}{2} - \frac{1}{p+1}\right) \|u\|_{H^1}^2 = m_2,$$

which gives the contradiction. Thus $I(u) = 0$. That being the case, we have

$$m_2 = \left(\frac{1}{2} - \frac{1}{p+1}\right) \|u\|_{H^1}^2 = S(u) \geqslant m_1.$$

Hence $m_1 = m_2$. On the other hand from Lemma 4.5.1 of the Fourier rearrangement inequality, we conclude that if p is an odd integer, then there exists $\tilde{u} \in H^1_{loc} \cap A_{\frac{T}{2}}$ such that:

$$\tilde{u}(x) \in \mathbb{R}, \quad \|\tilde{u}\|_{L^2} = \|u\|_{L^2}, \quad \|\partial_x \tilde{u}\|_{L^2} = \|\partial_x u\|_{L^2}, \quad \|\tilde{u}\|_{L^{p+1}} \geqslant \|u\|_{L^{p+1}}.$$

Hence the minimizer is real. Moreover as in the periodic case the minimizer is a solution of (4.1.5) and this concludes the proof. □

4.7 Spectral stability around the constant

This section is concerned with the spectral stability of the constant solution for the nonlinear Schrödinger equation. We begin by examining the linearization of the equation around the constant solution in the general case. In particular, we focus on the triple power nonlinearity case and we establish conditions under which the constant solution is spectrally stable.

Given a standing wave $u(t,x) = e^{i\omega t}\phi(x)$ solution to (4.1.1), we consider the linearization of (4.1.1) around this solution: if $u(t,x) = (\phi_0 + h(t,x))e^{i\omega t}$ then h verifies

$$i\partial_t h - Lh - N(h) = 0,$$

where L denotes the linear part and N the non linear part. We have

$$u_t = (\partial_t h + i\omega(\phi_0 + h))e^{i\omega t}$$

and

$$u_{xx} = h_{xx} e^{i\omega t}.$$

In the general case the nonlinearity $f : \mathbb{C} \to \mathbb{C}$ is defined for any $z \in \mathbb{C}$ by $f(z) = g(|z|^2)z$ with $g \in C^0([0, +\infty), \mathbb{R}) \cap C^1((0, +\infty), \mathbb{R})$. Let

$$G : t \to g(|\phi + th|^2)(\phi + th).$$

We suppose that $\phi \in \mathbb{R}$, we have

$$\begin{aligned}\frac{\partial G}{\partial t}_{|t=0} &= hg(\phi^2) + 2\phi^2 Re(h)g'(\phi^2) \\ &= (g(\phi^2) + 2\phi^2 g'(\phi^2))Re(h) + ig(\phi^2)Im(h) = f'(\phi)Re(h) + i\frac{f(\phi)}{\phi}Im(h).\end{aligned}$$

We know that u is a solution of (4.1.1), therefore h verifies the following equation

$$h_t = ih_{xx} - i\omega h + if'(\phi)Re(h) - \frac{f(\phi)}{\phi}Im(h) + N(h),$$

where $N(h)$ holds in all of the nonlinear terms. We separate h into real and imaginary parts and let $h = h_R + ih_I$, hence we have:

$$\begin{pmatrix} h_R \\ h_I \end{pmatrix}_t = L \begin{pmatrix} h_R \\ h_I \end{pmatrix} + N(h)$$

where

$$L = \begin{pmatrix} 0 & -\partial_{xx}(.) + \omega - \frac{f(\phi)}{\phi} \\ \partial_{xx}(.) - \omega + f'(\phi) & 0 \end{pmatrix}.$$

For the triple power case where $f(u) = |u|u - \gamma|u|^2u + |u|^3u$ we have the following lemma.

Lemma 4.7.1. Let $\theta = \frac{2k\pi}{T}$. For a given value of θ, there exists a constant γ^* such that if $\gamma > \gamma^*$, then the determinant of the linearization of the nonlinear Schrödinger equation around the constant solution is positive. As a consequence, the eigenvalues of the linearization are purely imaginary, and the constant solution is spectrally stable. The value of γ^* depends on θ and the specific form of the nonlinear term in the equation.

Proof. We have

$$|u|u = (\phi_0 + h)^{\frac{3}{2}}(\phi_0 + \bar{h})^{\frac{1}{2}}e^{i\omega t}, \quad |u|^2u = (\phi_0 + h)^2(\phi_0 + \bar{h})e^{i\omega t},$$

$$|u|^3u = (\phi_0 + h)^{\frac{5}{2}}(\phi_0 + \bar{h})^{\frac{3}{2}}e^{i\omega t}.$$

Hence we have

$$\begin{pmatrix} h_R \\ h_I \end{pmatrix}_t = L \begin{pmatrix} h_R \\ h_I \end{pmatrix} + N(h)$$

where

$$L = \begin{pmatrix} 0 & -\partial_{xx}(.) + \omega - \phi_0 + \gamma\phi_0^2 - \phi_0^3 \\ \partial_{xx}(.) - \omega + 2\phi_0 - 3\gamma\phi_0^2 + 4\phi_0^3 & 0 \end{pmatrix}.$$

As the perturbations are periodic, using the Fourrier variable we have

$$\hat{L} = \begin{pmatrix} 0 & -\left(\frac{2ik\pi}{T}\right)^2 + \omega - \phi_0 + \gamma\phi_0^2 - \phi_0^3 \\ \left(\frac{2ik\pi}{T}\right)^2 - \omega + 2\phi_0 - 3\gamma\phi_0^2 + 4\phi_0^3 & 0 \end{pmatrix}.$$

The characteristic polyniomal of $\hat{L}$ is given by

$$P(\lambda) = \lambda^2 + det(\hat{L}),$$

where

$$det(\hat{L}) = -\left(\left(\frac{2ik\pi}{T}\right)^2 - \omega + 2\phi_0 - 3\gamma\phi_0^2 + 4\phi_0^3\right) \cdot \left(-\left(\frac{2ik\pi}{T}\right)^2 + \omega - \phi_0 + \gamma\phi_0^2 - \phi_0^3\right).$$

We are interested in whether the entire spectrum of L lies on the imaginary axis, in which case, we say the periodic wave u is spectrally stable. If there exists at least one eigenvalue λ such that $Re(\lambda) > 0$ then the solution is spectrally unstable. Therefore if $det(\hat{L})$ is positive then the eigenvalues of $\hat{L}$ are purely imaginary and we have the spectral stability. As $\theta = \frac{2k\pi}{T}$, we have

$$det(\hat{L}) = \left(\theta^2 + \omega - 2\phi_0 + 3\gamma\phi_0^2 - 4\phi_0^3\right)\left(\theta^2 + \omega - \phi_0 + \gamma\phi_0^2 - \phi_0^3\right).$$

If $\phi_0 = 0$ then $det(\hat{L}) = (\theta^2+\omega)^2 > 0$. Moreover we know that ϕ_0 is a solution of (4.1.5), therefore as we suppose that ϕ_0 is a real constant we have

$$-\omega\phi_0 + \phi_0^2 - \gamma\phi_0^3 + \phi_0^4 = 0.$$

Hence if $\phi_0 \neq 0$ we have $\omega = \phi_0 - \gamma\phi_0^2 + \phi_0^3$ which gives

$$det(\hat{L}) = \theta^2\left(\theta^2 + \omega - 2\phi_0 + 3\gamma\phi_0^2 - 4\phi_0^3\right).$$

Replacing ω as a function of ϕ_0 we obtain

$$det(\hat{L}) = \theta^2\left(2\phi_0\gamma + \theta^2 - 3\phi_0^3 - \phi_0\right).$$

We can see that $2\phi_0\gamma + \theta^2 - 3\phi_0^3 - \phi_0$ is linear and increasing in γ. If we fix θ and ϕ_0, then there exists a γ^* depending on θ such that $det(\hat{L}) > 0$ if $\gamma > \gamma^*$. □

Bibliography

[1] Milton Abramowitz and Irene A. Stegun. *Handbook of mathematical functions with formulas, graphs, and mathematical tables*. Vol. 55. National Bureau of Standards Applied Mathematics Series. U.S. Government Printing Office, Washington, D.C., 1964, pp. xiv+1046.

[2] Robert A. Adams. *Sobolev spaces*. Vol. 65. Pure and Applied Mathematics. New York-London: Academic Press, 1975.

[3] G.P. Agrawal. *Nonlinear fiber optics*. Optics and Photonics. Academic Press, 2007. ISBN: 9780123695161.

[4] Nail Akhmediev, Adrian Ankiewicz, and Roger Grimshaw. "Hamiltonian-versus-energy diagrams in soliton theory". In: *Physical Review E* 59.5 (1999), p. 6088.

[5] A. Ambrosetti and P. H. Rabinowitz. "Dual variational methods in critical point theory and applications". In: *J. Funct. Anal.* 14 (1973), pp. 349–381.

[6] Szulkin Andrzej and Weth Tobias. "The method of Nehari manifold". In: *Handbook of nonconvex analysis and applications* 597632 (2010).

[7] Jaime Angulo Pava. "Nonlinear stability of periodic traveling wave solutions to the Schrödinger and the modified Korteweg-de Vries equations". In: *J. Differential Equations* 235.1 (2007), pp. 1–30. ISSN: 0022-0396. DOI: 10.1016/j.jde.2007.01.003.

[8] Jaime Angulo Pava and César A. Hernández Melo. "On stability properties of the cubic-quintic Schrödinger equation with δ-point interaction". In: *Commun. Pure Appl. Anal.* 18.4 (2019), pp. 2093–2116. ISSN: 1534-0392. DOI: 10.3934/cpaa.2019094.

[9] Jaime Angulo Pava, César A. Hernández Melo, and Ramón G. Plaza. "Orbital stability of standing waves for the nonlinear Schrödinger equation with attractive delta potential and double power repulsive nonlinearity". In: *J. Math. Phys.* 60.7 (2019), pp. 071501, 23. ISSN: 0022-2488. DOI: 10.1063/1.5097417.

[10] Xavier Antoine, Weizhu Bao, and Christophe Besse. "Computational methods for the dynamics of the nonlinear Schrödinger/Gross-Pitaevskii equations". In: *Comput. Phys. Commun.* 184.12 (2013), pp. 2621–2633. ISSN: 0010-4655. DOI: 10.1016/j.cpc.2013.07.012.

[11] Paolo Antonelli and Boris Shakarov. "Stability of Cnoidal Waves for the Damped Nonlinear Schr\" odinger Equation". In: *arXiv preprint arXiv:2212.02195* (2022).

[12] Fabrice B'ethuel, Philippe Gravejat, Jean-Claude Saut, and Didier Smets. "Orbital stability of the black soliton to the Gross-Pitaevskii equation". In: *Indiana University Mathematics Journal* 57 (2008), pp. 2611–2642.

[13] Weizhu Bao and Qiang Du. "Computing the ground state solution of Bose-Einstein condensates by a normalized gradient flow". In: *SIAM J. Sci. Comput.* 25.5 (2004), pp. 1674–1697. ISSN: 1064-8275. DOI: 10.1137/S1064827503422956.

[14] Jacopo Bellazzini, Luigi Forcella, and Vladimir Georgiev. "Ground state energy threshold and blow-up for NLS with competing nonlinearities". In: *arXiv preprint arXiv:2012.10977* (2020).

[15] H. Berestycki and T. Cazenave. "Instabilité des états stationnaires dans les équations de Schrödinger et de Klein-Gordon non linéaires". In: *C. R. Acad. Sci. Paris* 293.9 (1981), pp. 489–492.

[16] H. Berestycki, T. Gallouët, and O. Kavian. "Équations de champs scalaires euclidiens non linéaires dans le plan". In: *C. R. Acad. Sci. Paris* 297 (1983), pp. 307–310.

[17] H. Berestycki and P.-L. Lions. "Nonlinear scalar field equations. I. Existence of a ground state". In: *Arch. Rational Mech. Anal.* 82.4 (1983), pp. 313–345. ISSN: 0003-9527. DOI: 10.1007/BF00250555.

[18] H. Berestycki and P.-L. Lions. "Nonlinear scalar field equations. II. Existence of infinitely many solutions". In: *Arch. Rational Mech. Anal.* 82.4 (1983), pp. 347–375. ISSN: 0003-9527.

[19] Christophe Besse. "A relaxation scheme for the nonlinear Schrödinger equation". In: *SIAM Journal on Numerical Analysis* 42.3 (2004), pp. 934–952.

[20] Christophe Besse, Romain Duboscq, and Stefan Le Coz. "Gradient flow approach to the calculation of stationary states on nonlinear quantum graphs". English. In: *Ann. Henri Lebesgue* 5 (2022), pp. 387–428. ISSN: 2644-9463. DOI: 10.5802/ahl.126.

[21] Nathaniel Bottman, Bernard Deconinck, and Michael Nivala. "Elliptic solutions of the defocusing NLS equation are stable". In: *J. Phys. A* 44.28 (2011), pp. 285201, 24. ISSN: 1751-8113. DOI: 10.1088/1751-8113/44/28/285201.

[22] Nabile Boussaïd and Andrew Comech. *Nonlinear Dirac equation: Spectral stability of solitary waves*. Vol. 244. American Mathematical Soc., 2019.

[23] Rémi Carles, Christian Klein, and Christof Sparber. "On soliton (in-)stability in multi-dimensional cubic-quintic nonlinear Schrödinger equations". 21 pages. 2020.

[24] T. Cazenave. *Semilinear Schrödinger equations*. Vol. 10. Courant Lecture Notes in Mathematics. New York: New York University / Courant Institute of Mathematical Sciences, 2003.

[25] T. Cazenave and P.-L. Lions. "Orbital stability of standing waves for some nonlinear Schrödinger equations". In: *Comm. Math. Phys.* 85.4 (1982), pp. 549–561. ISSN: 0010-3616.

[26] S. Coleman, V. Glaser, and A. Martin. "Action minima among solutions to a class of Euclidean scalar field equations". In: *Comm. Math. Phys.* 58.2 (1978), pp. 211–221.

[27] Mathieu Colin and Masahito Ohta. "Stability of solitary waves for derivative nonlinear Schrödinger equation". In: 23 (2006), pp. 753–764.

[28] Mathieu Colin and Tatsuya Watanabe. "On the existence of Ground states for a nonlinear Klein-Gordon-Maxwell type system". In: *Funkcialaj Ekvacioj* 61.1 (2018), pp. 1–14.

[29] Andrew Comech and Dmitry Pelinovsky. "Purely nonlinear instability of standing waves with minimal energy". In: *Comm. Pure Appl. Math.* 56.11 (2003), pp. 1565–1607.

[30] T. Dauxois and M. Peyrard. *Physics of Solitons*. Cambridge: Cambridge University Press, 2006.

[31] Stephan De Bièvre, François Genoud, and Simona Rota Nodari. "Orbital stability: analysis meets geometry". In: *Nonlinear optical and atomic systems*. Vol. 2146. Lecture Notes in Math. Springer, Cham, 2015, pp. 147–273. DOI: 10.1007/978-3-319-19015-0_3.

[32] Stephan De Bièvre and Simona Rota Nodari. "Orbital Stability via the Energy–Momentum Method: The Case of Higher Dimensional Symmetry Groups". In: *Archive for Rational Mechanics and Analysis* 231.1 (2019), pp. 233–284. DOI: 10.1007/s00205-018-1278-5.

[33] P. G. Drazin and R. S. Johnson. *Solitons: an introduction*. Cambridge Texts in Applied Mathematics. Cambridge: Cambridge University Press, 1989, pp. xii+226. ISBN: 0-521-33389-X.

[34] Erwan Faou and Tiphaine Jézéquel. "Convergence of a normalized gradient algorithm for computing ground states". In: *IMA J. Numer. Anal.* 38.1 (2018), pp. 360–376. ISSN: 0272-4979. DOI: 10.1093/imanum/drx009.

[35] Gadi Fibich. *The nonlinear Schrödinger equation*. Vol. 192. Applied Mathematical Sciences. Springer, Cham, 2015, pp. xxxii+862. ISBN: 978-3-319-12747-7; 978-3-319-12748-4. DOI: 10.1007/978-3-319-12748-4.

[36] Noriyoshi Fukaya and Masayuki Hayashi. "Instability of algebraic standing waves for nonlinear Schrödinger equations with double power nonlinearities". In: *Trans. Amer. Math. Soc.* 374.2 (2021), pp. 1421–1447. ISSN: 0002-9947. DOI: 10.1090/tran/8269.

[37] R. Fukuizumi. "Stability and instability of standing waves for nonlinear Schrödinger equations". PhD thesis. Tohoku Mathematical Publications 25, June 2003.

[38] Thierry Gallay and Mariana Hărăgus. "Orbital stability of periodic waves for the nonlinear Schrödinger equation". In: *J. Dynam. Differential Equations* 19.4 (2007), pp. 825–865. ISSN: 1040-7294. DOI: 10.1007/s10884-007-9071-4.

[39] Thierry Gallay and Mariana Hărăguş. "Stability of small periodic waves for the nonlinear Schrödinger equation". In: *J. Differential Equations* 234.2 (2007), pp. 544–581. ISSN: 0022-0396. DOI: 10.1016/j.jde.2006.12.007.

[40] Thierry Gallay and Dmitry Pelinovsky. "Orbital stability in the cubic defocusing NLS equation: II. The black soliton". In: *J. Differential Equations* 258.10 (2015), pp. 3639–3660. ISSN: 0022-0396. DOI: 10.1016/j.jde.2015.01.019.

[41] François Genoud, Boris A. Malomed, and Rada M. Weishäupl. "Stable NLS solitons in a cubic-quintic medium with a delta-function potential". In: *Nonlinear Anal.* 133 (2016), pp. 28–50. ISSN: 0362-546X. DOI: 10.1016/j.na.2015.11.016.

[42] R. T. Glassey. "On the blowing up of solutions to the Cauchy problem for nonlinear Schrödinger equations". In: *J. Math. Phys.* 18.9 (1977), pp. 1794–1797.

[43] Manoussos Grillakis, Jalal Shatah, and Walter Strauss. "Stability theory of solitary waves in the presence of symmetry. I". In: *J. Funct. Anal.* 74.1 (1987), pp. 160–197. ISSN: 0022-1236. DOI: 10.1016/0022-1236(87)90044-9.

[44] Manoussos Grillakis, Jalal Shatah, and Walter Strauss. "Stability theory of solitary waves in the presence of symmetry. II". In: *J. Func. Anal.* 94.2 (1990), pp. 308–348.

[45] Zihua Guo, Cui Ning, and Yifei Wu. "Instability of the solitary wave solutions for the generalized derivative nonlinear Schrödinger equation in the critical frequency case". In: *Math. Res. Lett.* 27.2 (2020), pp. 339–375. ISSN: 1073-2780. DOI: 10.4310/mrl.2020.v27.n2.a2.

[46] Stephen Gustafson, Stefan Le Coz, and Tai-Peng Tsai. "Stability of periodic waves of 1D cubic nonlinear Schrödinger equations". In: *Appl. Math. Res. Express. AMRX* 2 (2017), pp. 431–487. ISSN: 1687-1200.

[47] Masayuki Hayashi. "Potential well theory for the derivative nonlinear Schrödinger equation". In: *Analysis & PDE* 14.3 (2021), pp. 909–944.

[48] Nakao Hayashi and Tohru Ozawa. "On the derivative nonlinear Schrödinger equation". In: *Phys. D* 55.1-2 (1992), pp. 14–36. ISSN: 0167-2789. DOI: 10.1016/0167-2789(92)90185-P.

[49] I.D. Iliev and K.P. Kirchev. "Stability and instability of solitary waves for one-dimensional singular Schrödinger equations". In: *Differential and Integral Equations* 6 (1993), pp. 685–703.

[50] T. Ivey and S. Lafortune. "Spectral stability analysis for periodic traveling wave solutions of NLS and CGL perturbations". In: *Phys. D* 237.13 (2008), pp. 1750–1772. ISSN: 0167-2789. DOI: 10.1016/j.physd.2008.01.017.

[51] L. Jeanjean. "On the existence of bounded Palais-Smale sequences and application to a Landesman-Lazer-type problem set on $\mathbf{R}^N$". In: *Proc. Roy. Soc. Edinburgh Sect. A* 129.4 (1999), pp. 787–809.

[52] Perla Kfoury, Stefan Le Coz, and Tai-Peng Tsai. "Analysis of stability and instability for standing waves of the double power one dimensional nonlinear Schrödinger equation". In: 360 (2022), pp. 867–892.

[53] Perla Kfoury, Stefan Le Coz, and Tai-Peng Tsai. *Stability-of-standing-waves-of-the-double-power-1D-NLS*. https://github.com/perlakfoury/Stability-of-standing-waves-of-the-double-power-1D-NLS. 2021.

[54] Stefan Le Coz. "Standing waves in nonlinear Schrödinger equations". In: *Analytical and numerical aspects of partial differential equations* (2009), pp. 151–192.

[55] Stefan Le Coz, Yvan Martel, and Pierre Raphaël. "Minimal mass blow up solutions for a double power nonlinear Schrödinger equation". In: *Rev. Mat. Iberoam.* 32.3 (2016), pp. 795–833.

[56] Stefan Le Coz and Yifei Wu. "Stability of Multisolitons for the Derivative Nonlinear Schrödinger Equation". In: *International Mathematics Research Notices* 2018.13 (2018), pp. 4120–4170. DOI: 10.1093/imrn/rnx013.

[57] Mathieu Lewin and Simona Rota Nodari. "The double-power nonlinear Schrödinger equation and its generalizations: uniqueness, non-degeneracy and applications". In: *Calculus of Variations and Partial Differential Equations* 59.6 (2020), pp. 1–49.

[58] Fei Justina Liu, Tai-Peng Tsai, and Ian Zwiers. "Existence and stability of standing waves for one dimensional NLS with triple power nonlinearities". English. In: *Nonlinear Anal., Theory Methods Appl., Ser. A, Theory Methods* 211 (2021). Id/No 112409, p. 34. ISSN: 0362-546X. DOI: 10.1016/j.na.2021.112409.

[59] Masaya Maeda. "Stability and instability of standing waves for 1-dimensional nonlinear Schrödinger equation with multiple-power nonlinearity". In: *Kodai Math. J.* 31.2 (2008), pp. 263–271. ISSN: 0386-5991. DOI: 10.2996/kmj/1214442798.

[60] Masaya Maeda. "Stability of bound states of Hamiltonian PDEs in the degenerate cases". In: *J. Funct. Anal.* 263.2 (2012), pp. 511–528. ISSN: 0022-1236. DOI: 10.1016/j.jfa.2012.04.006.

[61] M. Ohta. "Instability of standing waves for the generalized Davey-Stewartson system". In: *Ann. Inst. H. Poincaré Phys. Théor.* 62.1 (1995), pp. 69–80.

[62] Masahito Ohta. "Instability of bound states for abstract nonlinear Schrödinger equations". In: *J. Funct. Anal.* 261.1 (2011), pp. 90–110. ISSN: 0022-1236. DOI: 10.1016/j.jfa.2011.03.010.

[63] Masahito Ohta and Takahiro Yamaguchi. "Strong instability of standing waves for nonlinear Schrö-dinger equations with double power nonlinearity". In: *SUT J. Math.* 51.1 (2015), pp. 49–58. ISSN: 0916-5746.

[64] A Pankov. "Gap solitons in periodic discrete nonlinear Schrodinger equations II: A generalized Nehari manifold approach". In: *Discrete and Continuous Dynamical Systems* 19.2 (2007), p. 419.

[65] S. I. Pohožaev. "On the eigenfunctions of the equation $\Delta u + \lambda f(u) = 0$". In: *Soviet Math. Dokl.* 6 (1965), pp. 1408–1411.

[66] G Rowlands. "On the stability of solutions of the non-linear Schrödinger equation". In: *IMA Journal of Applied Mathematics* 13.3 (1974), pp. 367–377.

[67] Walter A. Strauss. "Existence of solitary waves in higher dimensions". In: *Comm. Math. Phys.* 55.2 (1977), pp. 149–162. ISSN: 0010-3616.

[68] Catherine Sulem and Pierre-Louis Sulem. *The nonlinear Schrödinger equation*. Vol. 139. Applied Mathematical Sciences. Self-focusing and wave collapse. New York: Springer-Verlag, 1999, pp. xvi+350. ISBN: 0-387-98611-1.

[69] Phan Tin. "Instability of algebraic standing waves for nonlinear Schrödinger equations with triple power nonlinearities". In: *Complex Variables and Elliptic Equations* (2022), pp. 1–18. DOI: 10.1080/17476933.2022.2146104.

[70] Phan Van Tin. "On the derivative nonlinear Schrödinger equation on the half line with Robin boundary condition". In: *J. Math. Phys.* 62.8 (2021), Paper No. 081502, 24. ISSN: 0022-2488. DOI: 10.1063/5.0049337.

[71] Michael I. Weinstein. "Modulational stability of ground states of nonlinear Schrödinger equations". In: *SIAM J. Math. Anal.* 16 (1985), pp. 472–491.

[72] Michael I. Weinstein. "Nonlinear Schrödinger equations and sharp interpolation estimates". In: *Comm. Math. Phys.* 87.4 (1982/83), pp. 567–576. ISSN: 0010-3616.

[73] Yifei Wu. *Instability of the standing waves for the nonlinear Klein-Gordon equations in one dimension*. 2018. arXiv: 1705.04216 [math.AP].

[74] Guoping Zhang and Alexander Pankov. "Standing waves of the discrete nonlinear Schrödinger equations with growing potentials." In: *Communications in Mathematical Analysis* 5.2 (2008).

Etude des ondes périodiques et stationnaires pour l'équation de Schrödinger non linéaire

Résumé: La thèse s'intéresse à l'étude des ondes périodiques et stationnaires pour l'équation de Schrödinger non linéaire unidimensionnelle. La première partie de la thèse se concentre sur la stabilité orbitale des ondes stationnaires pour l'équation de Schrödinger non linéaire à double puissance. Dans cette thèse, nous fournissons une image de stabilité complète pour le problème en utilisant le critère de pente de Grillakis, Shatah et Strauss. Les principaux nouveaux ingrédients de notre approche sont une reformulation de la pente et le calcul explicite de la valeur de la pente dans le cas de la fréquence zéro. Nous avons fourni des expériences numériques pour compléter nos résultats théoriques. Dans la deuxième partie de la thèse, nous étudions les solutions quasi-périodiques pour l'équation de Schrödinger cubique non-linéaire. Nous utilisons une approche variationnelle pour étudier les solutions quasi-périodiques, en minimisant l'énergie à masse et moment fixes en utilisant la méthode du flux de gradient avec normalisation discrète : à chaque pas de temps, nous évoluons dans la direction du gradient de l'énergie et renormalisons la masse et le moment du résultat. Nous établissons un lien entre les minimiseurs de l'énergie et les solutions de l'équation différentielle ordinaire. La dernière partie étend le travail sur le cas cubique à une non-linéarité plus générale et fournit des caractérisations variationnelles pour ce cas. La thèse dans son ensemble, contribue à la compréhension de la dynamique des équations de Schrödinger non linéaires, en mettant l'accent sur l'étude des ondes périodiques et stationnaires. Nous utilisons une combinaison de méthodes analytiques, numériques et variationnelles pour fournir une compréhension plus profonde du comportement des équations et de leurs solutions.

Study of periodic and standing waves for the nonlinear Schrödinger equation

Abstract: The thesis focuses on the study of periodic and standing waves for the one dimensional nonlinear Schrödinger equation. The first part of the thesis focuses on the orbital stability of standing waves for the double power nonlinear Schrödinger equation. In this thesis we provide a complete stability picture for the problem using the slope criterion of Grillakis, Shatah and Strauss. The main new ingredients in our approach are a reformulation of the slope and the explicit calculation of the slope value in the zero-frequency case. We provided numerical experiments to complement our theoretical results. In the second part of the thesis, we study the quasi-periodic solutions for the cubic nonlinear Schrödinger equation. We use a variational approach to study the quasi-periodic solutions by minimizing the energy at fixed mass and momentum, using the method of the gradient flow with discrete normalization:at each step of time, we evolve in the direction of the gradient of the energy and renormalize the mass and the momentum of the outcome. We establish a connection between the minimizers of the energy and the solutions of the ordinary differential equation. The final part extends the work on the cubic case to a more general nonlinearity and provides variational characterizations for this case. Overall, the thesis contributes to the understanding of the dynamics of nonlinear Schrödinger equations, with a focus on the study of periodic and standing waves. We use a combination of analytical, numerical, and variational methods to provide a deeper understanding of the behavior of the equations and their solutions.